FEMA 440
IMPROVEMENT OF NONLINEAR STATIC SEISMIC ANALYSIS PROCEDURES

Prepared by:

ATC

Applied Technology Council (ATC-55 Project)

201 Redwood Shores Parkway, Suite 240
Redwood City, California 94065

Prepared for:

Department of Homeland Security
Federal Emergency Management Agency

Washington, D.C.

June, 2005

Notice

Any opinions, findings, conclusions, or recommendations expressed in this publication do not necessarily reflect the views of the Applied Technology Council (ATC) or the Federal Emergency Management Agency (FEMA). Additionally, neither ATC, DHS, FEMA, nor any of their employees makes any warranty, expressed or implied, nor assumes any legal liability or responsibility for the accuracy, completeness, or usefulness of any information, product, or process included in this publication. Users of information from this publication assume all liability arising from such use.

Forward

One of the primary goals of the Department of Homeland Security's Federal Emergency Management Agency (FEMA) and the National Earthquake Hazards Reduction Program (NEHRP) is to encourage design and building practices that address the earthquake hazard and minimize the resulting damage. This document, *Improvement of Nonlinear Static Seismic Analysis Procedures* (FEMA 440), reaffirms FEMA's ongoing efforts to improve the seismic safety of new and existing structures in this country.

The primary goal of this project was the evaluation and improvement of the nonlinear static procedures (NSPs) contained in the *Prestandard and Commentary for Seismic Rehabilitation of Buildings* (FEMA 356) and in the Applied Technology Council ATC-40 report, *Seismic Evaluation and Retrofit of Concrete Buildings*, and the development of guidance on when and how each methodology should be used to avoid conflicting answers. FEMA initiated this project with ATC based on reports of discrepancies between the two NSP methodologies. However, in the course of this project, several improvements to both procedures were also identified and we thought it in the best interests of the earthquake engineering community to capture those improvements as part of this state-of-the-art resource document.

There are some potential differences between this document and other FEMA-sponsored products, such as the FEMA 356-based *Standard for the Seismic Rehabilitation of Existing Buildings* currently being developed by the American Society of Civil Engineers (ASCE-41) and FEMA's *HAZUS* standardized loss estimation methodology, which uses the procedures of ATC-40 in its fragility functions. Some of this document's recommendations concerning NSPs could bias selection of analysis procedures to linear static procedures (LSPs) unless similar modifications are also made to the LSPs. These differences are primarily for short-period structures, and should not affect the ongoing use of those current products. This document is a resource guide to capture the current state of the art for improved understanding of NSPs and to generate future improvements to those products, and as such, should not take precedence over those products.

Looking ahead, FEMA is already funding ATC to perform additional studies of the cyclic and in-cycle stiffness and strength degradation nonlinear models and their impact on response and response stability. Future FEMA-funded ATC studies will focus on the differences between linear and nonlinear design for short-period buildings and on soil-structure interaction. The results of these studies should be available within the next four years, within the time frame for submittal to a future update of ASCE 41.

FEMA is proud to have sponsored the development of this resource document through ATC. We are particularly grateful for work done by Project Director Craig Comartin, the Project Management Committee, the Project Review Panel, the Project Focus Groups and Working Groups, and all of the other contributors who made this document possible. FEMA also wishes to acknowledge the National Science Foundation (NSF) for their funding provided through the Pacific Earthquake Engineering Research Center (PEER) for the investigation of short-period building response and soil-structure interaction. We also wish to acknowledge the NSF funding of the research of Andrew Guyader on equivalent linearization and the NATO science fellowship from the Scientific Research and Technical Council of Turkey that partially funded research by Sinan Akkar. This project is an excellent example of the interagency cooperation that is made possible through the NEHRP. All of the individuals involved in this project are listed at the end of this document, and FEMA gratefully appreciates their involvement. This product would not have been possible without their dedication and professionalism.

Federal Emergency Management Agency

Preface

Knowledgeable engineers have long recognized that the response of buildings to strong ground shaking caused by earthquakes results in inelastic behavior. Until recently, most structural analysis techniques devised for practical application relied on linear procedures to predict the seismic behavior of buildings. With the publication of the ATC-40 Report, *Seismic Evaluation and Retrofit of Concrete Buildings*, in 1996, the FEMA 273 Report, *Guidelines for the Seismic Rehabilitation of Buildings*, in 1997, and the FEMA 356 Report, *Prestandard and Commentary for the Seismic Rehabilitation of Buildings* (which replaced FEMA 273), in 2000, nonlinear static analysis procedures became available to engineers providing efficient and transparent tools for predicting seismic behavior of structures.

Both the ATC-40 and FEMA 356 documents present similar performance-based engineering methods that rely on nonlinear static analysis procedures for prediction of structural demands. While procedures in both documents involve generation of a "pushover" curve to predict the inelastic force-deformation behavior of the structure, they differ in the technique used to calculate the inelastic displacement demand for a given ground motion. The FEMA 356 document uses the Coefficient Method, whereby displacement demand is calculated by modifying elastic predictions of displacement demand. The ATC-40 Report details the Capacity-Spectrum Method, whereby modal displacement demand is determined from the intersection of a capacity curve, derived from the pushover curve, with a demand curve that consists of the smoothed response spectrum representing the design ground motion, modified to account for hysteretic damping effects.

The publication of the above cited documents resulted in the widespread use of these two methods, and engineers have since reported that the two procedures often give different estimates for displacement demand for the same building. Hence the Applied Technology Council (ATC) proposed to the Federal Emergency Management Agency (FEMA) in 2000 that a study be conducted to determine the reasons for differing results and to develop guidance for practicing engineers on improved application of these two methods. FEMA agreed to fund the investigation, and in October 2000, ATC commenced a project to provide guidance for improved applications of these two widely used inelastic seismic analysis procedures (ATC-55 Project).

The ATC-55 Project had two objectives: (1) the development of practical recommendations for improved prediction of inelastic structural response of buildings to earthquakes (i.e., guidance for improved application of inelastic analysis procedures) and (2) the identification of important issues for future research. Intended outcomes of the project included:

1. Improved understanding of the inherent assumptions and theoretical underpinnings of existing and proposed updated inelastic analysis procedures.
2. Recognition of the applicability, limitations, and reliability of various procedures.
3. Guidelines for practicing engineers to apply the procedures to new and existing buildings.
4. Direction for researchers on issues for future improvements of inelastic analysis procedures.

The project was conducted in three phases over a 3-year time span. Phase 1 consisted of the assembly and refinement of important issues relating to the improvement of inelastic seismic analysis procedures. Activities included (1) the solicitation of input from researchers and practicing engineers, and (2) the development of study models of typical buildings to stimulate discussion, facilitate analytical studies, and provide example applications. Phase 2 consisted of analytical studies to explore selected key issues, the generation of written discussions on important topics, and the development of examples of the application of inelastic analysis procedures. This phase also included assembly of guidelines for the improved practical implementation of the procedures. Phase 3 consisted of the report development process, under which this document was drafted, reviewed, and finalized.

This report (FEMA 440) is the final and principal product of the ATC-55 Project. The document has three specific purposes: (1) to provide guidance directly applicable to the evaluation and design of actual structures by engineering practitioners; (2) to facilitate a basic conceptual understanding of underlying principles as well as the associated capabilities and limitations of the procedures; and (3) to provide additional detailed information used in the development of the document for future reference and use by researchers and others.

A wide variety of personnel participated in the project. The project was conducted under the direction of ATC Senior Consultant Craig Comartin, who served as Project Director. Technical and management direction were provided by a Project Management Committee consisting of Craig Comartin (Chair), Christopher Rojahn (Ex-Officio member), Ronald O. Hamburger, William T. Holmes, Wilfred D. Iwan, Jack P. Moehle and Jonathan Stewart. A Project Review Panel, identified by ATC with input from FEMA, provided overview and guidance; this Panel consisted of Anthony B. Court (ATC Board Representative), Leonard Joseph, Daniel Shapiro, Steve Sweeney, Chia-Ming Uang, and Michael Valley.

The Project Management Committee created four Focus Groups to assist in developing findings on the following specific subtopics: (1) displacement modification; (2) equivalent linearization; (3) multi-degree-of-freedom effects; and (4) response of short-period buildings, with a specific focus on soil-structure interaction. The purpose of the Focus Groups was to gather fresh perspective from qualified sources that were not directly responsible for the project planning or the resulting recommendations. Focus Group participants reviewed draft materials developed by the project team. They then attended a one-day meeting with representative members of the Project Management Committee and the project team members responsible for the subject materials. The meetings allowed for a constructive discussion of the subject in general and critical feedback – positive and negative – on the draft materials. Focus Group members were also afforded an opportunity to comment on the final draft of materials related to their area of expertise. It is important to note that Focus Group members were not asked to endorse the project process or the recommendations in documents developed as part of the ATC-55 Project. These remain the responsibility of ATC and the Project Management Committee.

Each Focus Group consisted of three members. John Hooper, Gregory A. MacRae, and Stephen A. Mahin were members of the Focus Group on Displacement Modification. The Focus Group on Equivalent Linearization consisted of Terrance Paret, Graham Powell, and Andrew S. Whittaker. Anil K. Chopra, Jon A. Heintz, and Helmut Krawinkler served on the Focus Group on Multi-Degree-of-Freedom Effects, and Jacobo Bielak, Gregory L. Fenves, and James Malley served on the Focus Group on Soil-structure Interaction.

Detailed work on the project was carried out by several Working Groups appointed by the Project Management Committee. The Phase 1 Project Working Group consisted of Joseph R. Maffei (Group Leader), Mark Aschheim, Maureen Coffey, and Mason T. Walters. The Phase 2 Project Working Group consisted of Sinan Akkar, Mark Aschheim, Andrew Guyader, Mehmet Inel, Eduardo Miranda, Junichi Sakai, Jorge Ruiz-Garcia, Tjen Tjhin and Tony Yang. Peter N. Mork produced and formatted the electronic files from which this report was printed.

The affiliations of the project personnel identified above are provided in the list of Project participants.

The Applied Technology Council gratefully acknowledges the cooperation, insight and patience provided by the FEMA Project Officer, Michael Mahoney, and the FEMA Technical Monitor, Robert D. Hanson. ATC also gratefully acknowledges the National Science Foundation (NSF)for supplemental funding provided through the Pacific Earthquake Engineering Research Center to conduct the investigation of the response of short-period buildings, soil-structure-foundation interaction, and application of the proposed methods. NSF also provided funding for the research of Andrew Guyader on equivalent linearization. A NATO science fellowship from the Scientific Research and Technical Council of Turkey provided partial support for research by Sinan Akkar.

Christopher Rojahn
ATC Executive Director

Executive Summary

This document records in detail an effort to assess current nonlinear static procedures (NSP) for the seismic analysis and evaluation of structures. In addition, the document presents suggestions that were developed to improve these procedures for future application by practicing engineers. The elements of work included several analytical studies to evaluate current procedures and to test potential improvements. An extensive review of existing pertinent technical literature was compiled. A survey of practicing engineers with experience in applying nonlinear static procedures was also conducted. Expert practitioners and researchers in appropriate fields worked together to develop the proposed improvements presented in this document. The context for the work was provided by two existing documents, the FEMA 356 *Prestandard and Commentary for the Seismic Rehabilitation of Buildings,* and the ATC-40 report, *Seismic Evaluation and Retrofit of Concrete Buildings*, each of which contain procedures for nonlinear static analysis. These procedures were both evaluated and suggestions for improvement are made for each. Not all of the portions of the two current documents (FEMA 356 and ATC-40) were evaluated. Conclusions regarding the relative accuracy or technical soundness of these documents should not be inferred beyond the specific material and discussions contained in this document.

1. Overview of Inelastic Seismic Analysis Procedures

Nonlinear static procedures are one type of inelastic analysis that can be used to estimate the response of structures to seismic ground shaking. The differences between the various approaches relate to the level of detail of the structural model and the characterization of the seismic ground shaking. Detailed structural models can often be simplified into equivalent multi-degree-of-freedom (MDOF) models; or, in some cases, single-degree-of-freedom (SDOF) oscillator models, as with nonlinear static procedures. The most detailed characterizations of seismic ground motion are actual ground motion records that comprise accelerations, velocities, and displacements expected at the ground surface at a specific site. A simplification can be made by representing the effects ground motion has in the frequency domain with response spectra that plot maximum response of an elastic SDOF oscillator as a function of period. This is the type of characterization normally used for nonlinear static procedures.

The discussion provided in Chapter 2 includes basic descriptions of the two nonlinear static procedures that currently are used in practice. FEMA 356 utilizes a displacement modification procedure (Coefficient Method) in which several empirically derived factors are used to modify the response of a single-degree-of-freedom model of the structure assuming that it remains elastic. The alternative Capacity-Spectrum Method of ATC-40 is actually a form of equivalent linearization. This technique uses empirically derived relationships for the effective period and damping as a function of ductility to estimate the response of an equivalent linear SDOF oscillator.

2. Evaluation of Current Nonlinear Static Procedures

In practice, the current procedures can result in estimates of maximum displacement that are significantly different from one another. This has caused concern on the part of practicing engineers. One of the major objectives of the project was to ascertain the reason for these differences and to try to correct both procedures to produce similar results. Chapter 3 documents a comprehensive evaluation of both current procedures. The basic technique was to develop a series of nonlinear single-degree-of-freedom oscillators of varying period, strength, and hysteretic behavior. These were subjected to ground motion representing different site soil conditions. The resulting database of approximately 180,000 predictions of maximum displacement was used as a benchmark to judge the accuracy of the approximate nonlinear static procedures. This was accomplished by comparing the estimates for each oscillator from both nonlinear static procedures to the results of the nonlinear response history analyses. Differences in the two estimates were compiled and compared in a statistical study.

3. Strength Degradation

The results of the evaluation of the nonlinear static procedures suggest that both procedures would benefit from greater clarity with respect to the different types of possible degradation in structures subject to seismic shaking. This is particularly critical for degradation in strength. Chapter 4 presents a discussion of the differences between the consequences of strength loss within a single cycle of deformation (in-cycle) and that which occurs in subsequent cycles (cyclic). In-cycle strength degradation, including that associated with P-Δ

effects, can lead to dynamic instability. To account for this, a limitation on the strength of a structure is suggested for use with nonlinear static procedures. The limit is a function of the period of the structure and the post-elastic stiffness characteristics as modified for in-cycle strength degradation. If the structure has less strength than the limit, nonlinear dynamic analysis is recommended.

4. Improved Procedures for Displacement Modification

Based on the evaluation of nonlinear static procedures, Chapter 5 proposes modifications to the Coefficient Method of FEMA 356. The suggestions relate primarily to the coefficients themselves. Improved relationships for coefficients C_1 and C_2 are proposed. It is also suggested that the coefficient C_3 be replaced with a limitation on minimum strength as suggested in the previous section.

5. Improved Procedures for Equivalent Linearization

Chapter 6 presents the results of an effort to improve the practical application of equivalent linearization procedures. The resulting suggestions focus upon improved estimates of equivalent period and damping. This chapter also includes an optional adjustment to generate a modified acceleration-displacement response spectrum (MADRS) that does intersect the capacity spectrum at the Performance Point. Similar to the current ATC-40 procedure, the effective period and damping are both dependent on ductility and consequently an iterative or graphical technique is required to calculate the Performance Point. Several options are outlined in Chapter 6. In application, the improved procedures are similar to the current ATC-40 Capacity-Spectrum Method.

6. Evaluation and Comparison of Improved Nonlinear Static Procedures

The improved procedures were evaluated in an independent study. This study, summarized in Chapter 7, utilized nine elastic-perfectly-plastic oscillators with three different periods and three different strengths. These were subjected to thirteen ground motions for class C sites. Estimates of maximum displacements were calculated utilizing both current procedures and the proposed improved procedures.

This study was not comprehensive enough to make broad general conclusions. However, a number of key observations can be made:

- The improved procedures do not exhibit large differences between displacement modification and equivalent linearization approaches.
- The improved procedures also produced more accurate estimates of displacements when compared to response history analysis (also known as time-history analysis) results than those produced by the current nonlinear procedures.
- Improved procedures also seem to work well, at least for the case that was studied, in estimating maximum displacement response in conjunction with a design spectrum.
- The results of the evaluation of the improved nonlinear procedures illustrate the dispersion of results from nonlinear response history analysis using design level ground motions.

7. Soil-Structure Interaction Effects

Chapter 8 presents procedures to incorporate soil-structure interaction (SSI) into nonlinear static analyses. The objective is to replace the judgmental limits with rational technical justifications for reducing seismic demand. These SSI techniques address the following issues.

- radiation and material damping in supporting soils;
- response reduction resulting from structure embedment in the ground (i.e., full and partial basements); and
- incoherent ground-motion input to buildings with relatively large plan dimensions.

The basic principles used for the development of the SSI procedures for damping in Chapter 8 have been included in the FEMA 368 *NEHRP Recommended Provisions for Seismic Regulations for New Buildings and Other Structures* (BSSC, 2000)[1] for the linear analysis and design of new buildings for a number of years. They have been adapted for use with inelastic procedures. Both the damping and ground motion procedures are applicable to both the displacement modification and equivalent linearization forms of nonlinear static analysis.

1.Superseded in 2003 with the FEMA 450 *Recommended Provisions for Seismic Regulations for New Buildings and Other Structures.*

8. Multiple-Degree-of Freedom Effects

Chapter 9 reviews the accuracy and practical implications of the requirements of ATC-40 and FEMA 356 related to MDOF effects including:

1. current options for load vectors, and
2. the conversion of a MDOF pushover curve to an equivalent SDOF system.

The results of a comprehensive study of five example buildings that examines the differences in response predicted using various options compared to a common nonlinear dynamic analyses benchmark are also summarized. The results are consistent with previous research. Practical implications are:

- Nonlinear static procedures generally provide reliable estimates of maximum floor and roof displacements.
- Nonlinear static procedures are not particularly capable, however, of accurate prediction of maximum story drifts, particularly within flexible structures.
- Nonlinear static procedures are very poor predictors of story forces, including shears and overturning moments.
- The use of the first mode load vector is suggested due to the relatively good displacement estimates made with this assumption.
- Multi-mode pushover analysis consisting of the use of multiple load vectors proportional to the mode shapes of the structure and combining them statistically shows promise in producing better estimates in inter-story drifts over the heights of the buildings.
- The provisions of FEMA 356 as to when higher modes are to be considered significant are not particularly reliable.
- Specific limitations as to when nonlinear static procedures produce reliable results are elusive.
- As a result of the study it was observed that, in many cases, a single time history response of a multi-degree-of-freedom model gave better indications of drifts and story forces than any of the approximate single-degree-of-freedom estimates.

9. Important Future Developments

The proposed improvements to nonlinear static analysis procedures in this document will lead to better results in practice. Nonetheless, not all of the shortcomings of NSP's have been addressed. In developing the improvements a number of important observations about the need for future develop and improvement of inelastic seismic analysis procedures have emerged. These include the need for additional developmental work on:

1. Nonlinear Modeling for Cyclic and In-Cycle Degradation of Strength and Stiffness
2. Soil and Foundation Structure Interaction
3. Nonlinear Multi-Degree of Freedom Simplified Modeling

10. Application Example

Chapter 10 includes an example application of the recommended nonlinear static analysis procedures on an example building. The application example includes a flowchart describing the implementation process, along with building plans, calculations, and commentary. The example illustrates both the displacement modification and the equivalent linearization procedures to estimate the maximum displacement of a building model.

Table of Contents

List of Figures

List of Tables

1. Introduction

This report documents the results of a project for the Department of Homeland Security's Federal Emergency Management Agency (FEMA) by the Applied Technology Council (ATC) to evaluate and improve the application of simplified inelastic analysis procedures for use with performance-based engineering methods for seismic design, evaluation, and upgrade of buildings. Chapters 1 through 9 summarize the developmental efforts and results in concise language to facilitate application of the project findings in practice. Chapter 10 contains a summary and a practical application example using the improved procedures. Supporting information describing the project findings in detail are provided in the appendices.

This document has been published in two formats: (1) a printed version, which summarizes the developmental efforts and project findings and includes the application example (Chapters 1 through 10), and (2) a complete version of the report on CD-ROM (inside back cover), which includes all of the material in the printed version plus six appendices containing project results and findings. The printed version of the report is relatively brief to facilitate use by design professionals.

1.1 Background

During the past decade, significant progress has been made in performance-based engineering methods that rely on nonlinear static analysis procedures (NSPs). In 1996, ATC published the ATC-40 report, *Seismic Evaluation and Retrofit of Concrete Buildings*, which was developed with funding from the California Seismic Safety Commission. In a larger project funded by FEMA, ATC (under contract to the Building Seismic Safety Council) prepared the FEMA 273 *Guidelines for the Seismic Rehabilitation of Buildings*, and the companion FEMA 274 *Commentary*, which were published in 1997 by FEMA. Soon thereafter, the American Society of Civil Engineers (ASCE) prepared the FEMA 356 report, *Prestandard and Commentary for the Seismic Rehabilitation of Buildings* (the successor to FEMA 273/274*)*, which was published by FEMA in 2000. All of these documents present similar approaches. FEMA 273 and FEMA 356 use a procedure known as the Coefficient Method, and ATC-40 details the Capacity-Spectrum Method. The two approaches are essentially the same when it comes to generating a "pushover" curve to represent the inelastic force-deformation behavior of a building. They differ, however, in the technique used to calculate the inelastic displacement demand for a given representation of ground motion.

The development of this report was instigated by several factors. The use of NSPs in engineering practice has accelerated since the publication of ATC-40 and FEMA 356. Consequently, there is valuable information available on the practical application of these inelastic analysis procedures. In addition to experience with the initial application of these performance-based methods by practicing professionals, ongoing research promises important modifications, improvements, and alternatives to current NSPs.

There has also been a large national investment in performance-based engineering, because of the tangible prospect of vastly improving seismic design practices. The future effective use of performance-based engineering depends on the continued development of reliable and credible inelastic analysis procedures.

The intent of the ATC-55 project has been to gather the results of practical experience and relevant research and to develop guidance for improving the application of nonlinear static analysis procedures to both existing and new structures.

1.2 Project Purpose and Scope

The purpose of the ATC-55 project was to evaluate current NSPs, as described in FEMA 356 and ATC-40 and to develop improvements where feasible. The primary objectives were:

- to improve understanding of the inherent assumptions and theoretical underpinnings of existing and proposed new simplified analysis procedures;
- to recognize the applicability, limitations, and reliability of various procedures;
- to develop guidelines for practicing engineers on how to apply the procedures to new and existing buildings; and
- to provide direction for researchers on issues to consider for future improvements of simplified inelastic analysis procedures.

Project activities also were guided by the fact that engineers and researchers have similar concerns with

respect to inelastic analysis procedures. Some of the more prominent issues considered are listed below.

- In some cases, different nonlinear static procedures produce significantly different results for the same building model and ground motion representation.
- Current procedures for addressing the degradation of stiffness and strength in structures are ambiguous and unclear.
- The predicted response of short-period structures seems to be extreme when compared with observed performance.
- Since they are based on single-degree-of-freedom (SDOF) approximations, nonlinear static procedures may not reliably predict important response parameters for some multi-degree-of-freedom (MDOF) structures.

1.3 Report Scope, Organization and Contents

The document is intended to be useful from the practical, educational, and archival standpoints. Its fundamental purpose is to provide guidance that can be used directly by engineering practitioners. From an educational perspective, the report is intended to facilitate a basic conceptual understanding of underlying principles, as well as the associated capabilities and limitations of the procedures, so that practicing structural engineers can apply the procedures appropriately. Finally, the archival aspect recognizes that the development of inelastic procedures will continue, and that it is important to record detailed information from the project for future reference and use.

The scope of the evaluation of inelastic analysis procedures and the development of recommendations for improvement, as presented in this document, focus on nonlinear static procedures (NSPs). In light of the concerns identified by practicing engineers and researchers, the document specifically addresses the following questions:

- How well do current NSPs predict maximum global displacement (elastic plus inelastic)?
- How well do current NSPs predict effects arising from the multiple-degree-of-freedom (MDOF) response of structures?
- What modifications might be incorporated into NSPs to improve accuracy and to reduce uncertainty associated with the first two questions?

The initial phase of the project, during early 2001, focused on the identification and refinement of important issues related to the improvement of inelastic seismic analysis procedures. Activities included the solicitation of input from researchers (see Appendix A.) and practicing engineers (see Appendix B.). This information was used to formulate a plan for the subsequent phases of the project, comprising the evaluation of current procedures and the development of proposed improvements.

Several analytical efforts formed the basis for the evaluation of current procedures and the development of improvements. The first tested the accuracy of the Coefficient Method of FEMA 356 and the Capacity-Spectrum Method of ATC-40 in predicting global displacement demands, when compared to response-history analysis of SDOF oscillators. This effort is described in Chapter 3, with detailed results provided in Appendix C.

During evaluations of both the Coefficient Method and Capacity-Spectrum Method, it became evident that important clarifications regarding strength degradation are applicable to both NSP approaches. This issue is addressed in Chapter 4.

Improved procedures for use with the Coefficient Method are described in Chapter 5. Improved procedures for use with the Capacity-Spectrum Method, are described in Chapter 6. Supplementary information and data on the equivalent linearization approach are provided in Appendix D.

Chapter 7 describes an independent analysis that was implemented to test the accuracy of the procedural improvements described in Chapters 5 and 6. Comparisons with results using the original procedures are provided.

For many years, researchers have observed that the predicted inelastic displacement response of oscillators, with periods in excess of about 1 second, is often very similar to the predicted displacement response of elastic oscillators having the same period. This has led to the so-called “equal displacement approximation.” Researchers have also recognized that the predicted inelastic response of oscillators with short periods, less than approximately 0.5 seconds, are often significantly larger than the predicted response of elastic structures of the same period, particularly if the structures are both very stiff and very weak. When this principle is applied using nonlinear analysis techniques to the performance

evaluation of small, stiff buildings, such as those that comprise much of the building inventory in the United States, very poor performance and extreme damage is often predicted. This has created a paradox, in that such buildings have generally been observed to experience limited damage in past earthquakes. Several factors contribute to this conflict between predicted and observed performance of such structures, including:

- models used to predict performance of such structures commonly neglect many elements that contribute to their strength;
- fixed base models used to predict structural response neglect foundation flexibility, resulting in predictions of smaller periods than that of the actual structures;
- stiff buildings will experience small displacements even at large ductility demand and thus may experience only limited damage; and
- in addition to foundation flexibility, other soil-structure interaction effects can significantly reduce the response of some stiff structures to ground shaking.

In part, these effects can be addressed by more accurate analytical models that incorporate all structural and nonstructural elements significant to structural response as well as the flexibility of foundations. Soil-structure interaction effects are of particular importance. Chapter 8 describes analysis techniques for SSI effects that have been adapted for use with nonlinear static procedures and detailed supporting information on soil-structure interaction is provided in Appendix E.

Multi-degree-of-freedom effects are addressed in Chapter 9, which summarizes a comprehensive analysis of five example buildings to illustrate the application and limitations of simplified techniques to account for MDOF effects within current NSPs. Details are provided in Appendix F.

Finally, Chapter 10 comprises a complete summary of the results of the efforts and the suggested improvements from a practical perspective. Chapter 10 concludes with a detailed example application of the suggested improved procedures to a building structure.

2. Overview of Inelastic Seismic Analysis Procedures

Practicing engineers use inelastic analysis procedures for the seismic evaluation and design of upgrades of existing buildings and other structures, as well as design of new construction. The practical objective of inelastic seismic analysis procedures is to predict the expected behavior of the structure in future earthquake shaking. This has become increasingly important with the emergence of performance-based engineering (PBE) as a technique for seismic evaluation and design (ATC, 1996; BSSC, 2000). PBE uses the prediction of performance to inform decisions regarding safety and risk. For this purpose, PBE characterizes performance primarily in terms of expected damage to structural and nonstructural components and contents. Since structural damage implies inelastic behavior, traditional design and analysis procedures that use linear elastic techniques can predict performance only implicitly. By contrast, the objective of inelastic seismic analysis procedures is to directly estimate the magnitude of inelastic deformations and distortions.

The generic process of inelastic analysis is similar to conventional linear procedures in that the engineer develops a model of the building or structure, which is then subjected to a representation of the anticipated seismic ground motion (see Figure 2-1). The results of analysis are predictions of engineering demand parameters within the structural model that are subsequently used to determine performance based on acceptance criteria. The engineering demand parameters normally comprise global displacements (e.g., roof or other reference point), story drifts, story forces, component distortions, and component forces.

There are several basic inelastic analysis procedures that differ primarily on the types of structural models used for analysis and the alternatives for characterizing seismic ground shaking.

2.1 Structural Modeling

Detailed structural models for inelastic analysis are similar to linear elastic finite-element (component) models (see Figure 2-2). The primary difference is that

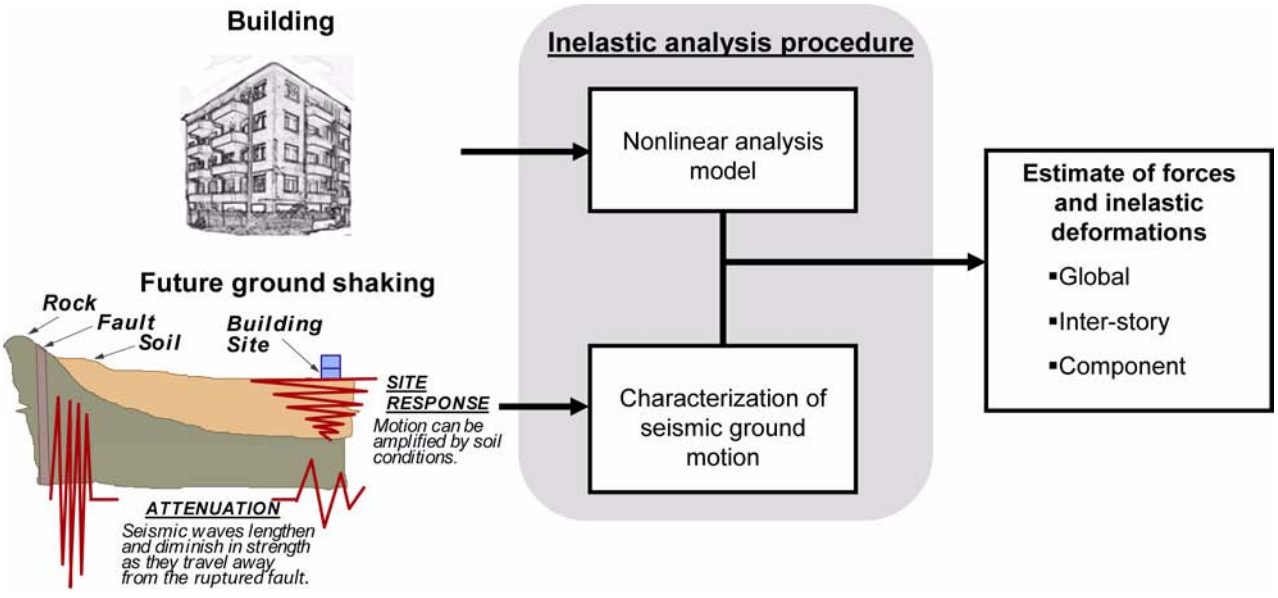

Figure 2-1 Schematic depiction of the use of inelastic analysis procedures to estimate forces and inelastic deformations for given seismic ground motions and a nonlinear analysis model of the building.

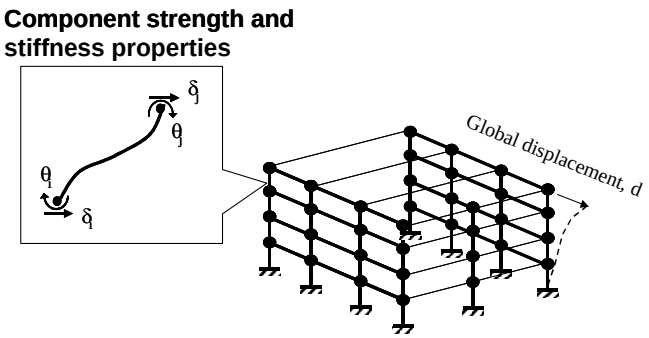

Figure 2-2 Schematic of a detailed 3-dimensional inelastic structural model developed from component properties.

the properties of some or all of the components of the model include post-elastic strength and deformation characteristics in addition to the initial elastic properties. These are normally based on approximations derived from test results on individual components or theoretical analyses (see Figure 2-3). Information of this type is tabulated in ATC-40 and FEMA 356. In many instances, it is important to include the structural and geotechnical components of the foundation in the analysis model.

As detailed as these models may be, they inevitably introduce approximations and associated uncertainties into the analysis process. In most instances with inelastic analysis, it is preferable to base the model on the best estimate of the expected properties of the structure. In this manner, the overall analysis results in the estimate of central values (e.g., median or mean) of engineering demand parameters with minimum bias. Subsequently, the engineer may decide on the appropriate interpretation of the results in light of all the uncertainties involved and the specific decision in question.

In some instances, engineers simplify detailed structural models into *equivalent multi-degree-of-freedom* models. These can be used to consolidate properties into what have been termed “fish bone” models (see Figure 2-4a). In some cases, the model can simplified further. For example, when rotational coupling among various vertical flexural elements is negligible (e.g., cantilever shear walls or braced frames) or when story shear mechanisms are anticipated (e.g., strong beam/weak column frames) a “stick” model can be used (see Figure 2-4b and c). Often, substructuring techniques are helpful in developing simplified models. The purpose of the simplified models is to reduce computational and data management efforts. More importantly, they can also provide an improved visualization tool for the engineer. The negative aspect to simplified models is that they introduce additional approximations and uncertainty into the analysis.

Another important simplification to detailed structural models is what have become known as “pushover” or “capacity” curves. These curves form the basis of nonlinear static procedures discussed below. They are generated by subjecting a detailed structural model to one or more lateral load patterns (vectors) and then increasing the magnitude of the total load to generate a nonlinear inelastic force-deformation relationship for the structure at a global level (see Figure 2-5). The load vector is usually an approximate representation of the relative accelerations associated with the first mode of vibration for the structure. In the Coefficient Method of FEMA 356, the global parameters are normally base shear and roof displacement. For the Capacity-Spectrum Method of ATC-40, these are transformed to spectral acceleration and spectral displacement. Nonlinear static procedures use these force-deformation relationships to represent the behavior of a simple *single-degree-of-freedom* (SDOF) oscillator.

2.2 Characterization of Seismic Ground Motion

When an earthquake occurs, the amplitude, phasing, and frequency content of the shaking depend strongly on source characteristics (e.g., magnitude, rupture mechanism, fault plane orientation with respect to site). In addition, the characteristics of shaking are affected by attenuation that occurs as seismic waves propagate through rock from the source to the site and by local site effects. Site characteristics that may be important include potential 3-D basin structure, dynamic properties of relatively shallow sediments, and surface topography. The source, attenuation, and site effects, which are depicted schematically in the left frame of Figure 2-6, affect the character of ground shaking as expressed by *ground motion records* (i.e., plots of the acceleration, velocity and displacement of a point on the ground surface as a function of time (center frame in Figure 2-6)).

Ground motion records can be used to define *elastic response spectra* (right frame in Figure 2-6), which comprise a relationship of the maximum response

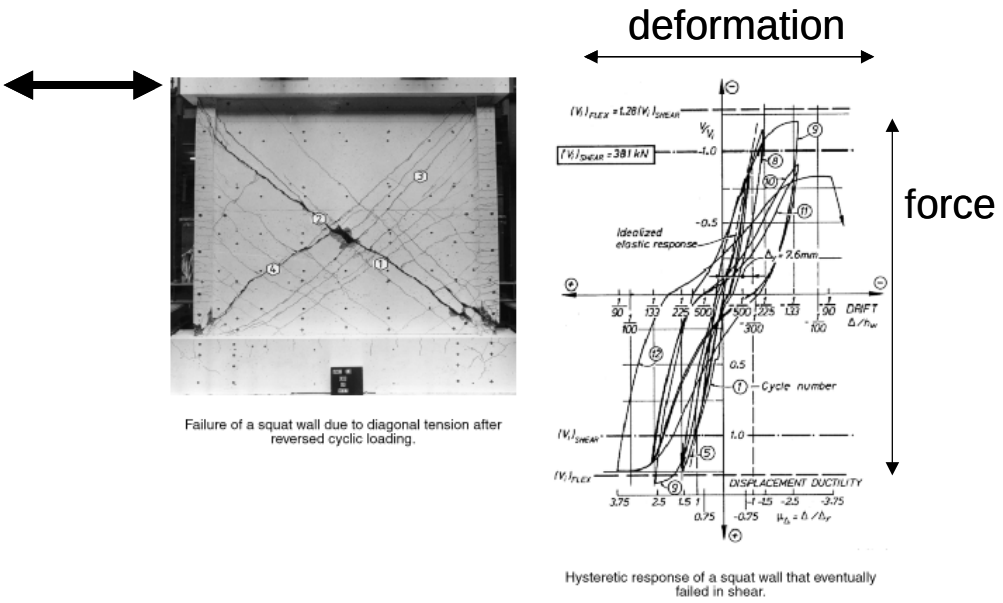

a) Hysteretic force-deformation behavior from tests

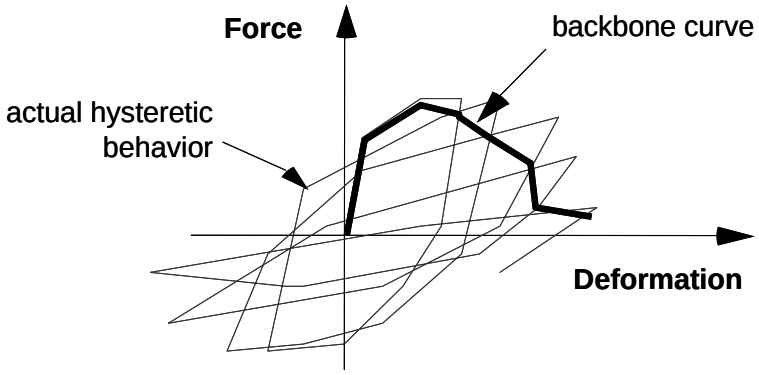

b) Backbone representation of hysteretic behavior

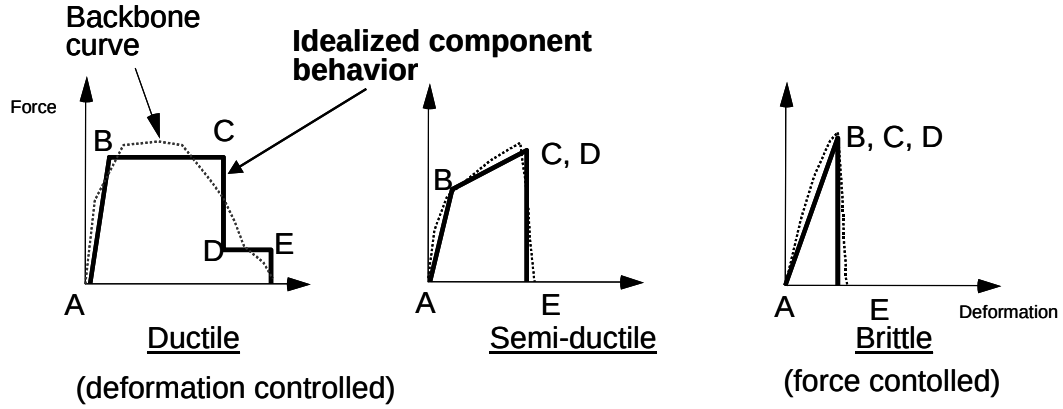

c) Idealized properties for analysis models

Figure 2-3 Schematic depictions illustrating how inelastic component strength and stiffness properties from test data are used to create idealized force-deformation relationships.

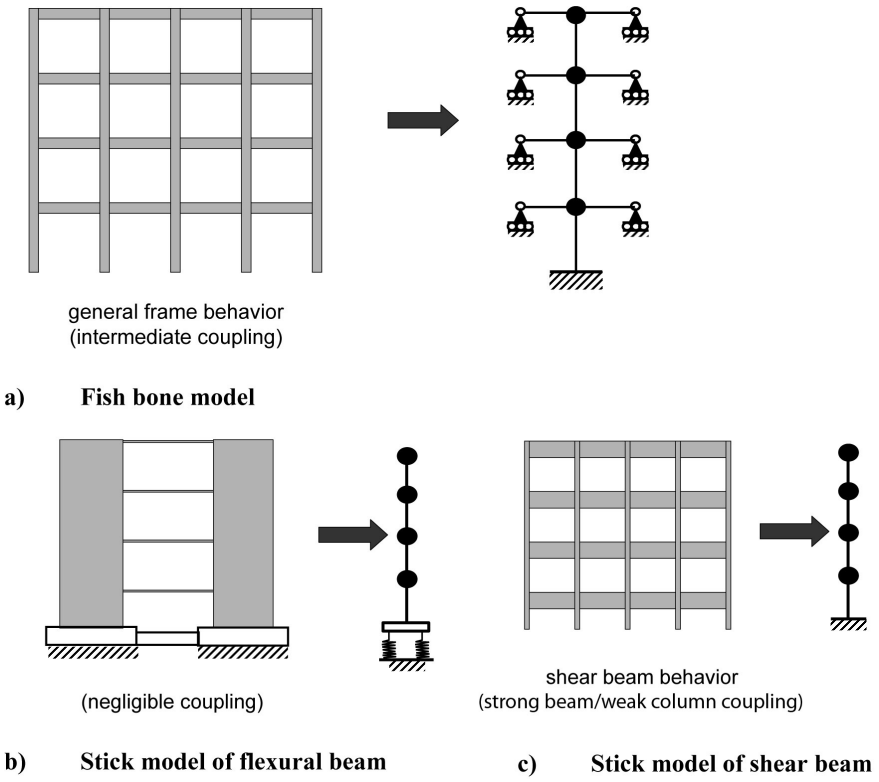

Figure 2-4 Forms of simplified equivalent multiple-degree-of-freedom models.

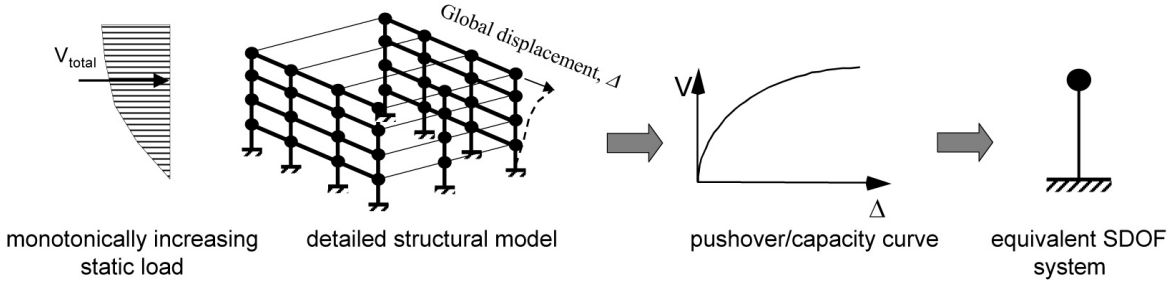

Figure 2-5 Schematics depicting the development of an equivalent SDOF system from a pushover/capacity curve.

(acceleration, velocity, and displacement) over the entire response-history record of a single-degree-of-freedom oscillator and the frequency, or more commonly the period, of the oscillator, for a specified level of damping. Response spectral ordinates are commonly used to represent seismic demand for structural design. It should be noted that in this document, as in conventional structural engineering practice, pseudo-acceleration is used in place of actual spectral acceleration. The notation S_a actually represents the pseudo-acceleration.

The response spectrum for a single ground motion record is typically highly variable (jagged), depending on the assumed level of damping. For this reason, multiple records representative of a single source at a specified distance from the site and of a specified magnitude are often combined and smoothed, as implied in Figure 2-6. The results of this type of seismic

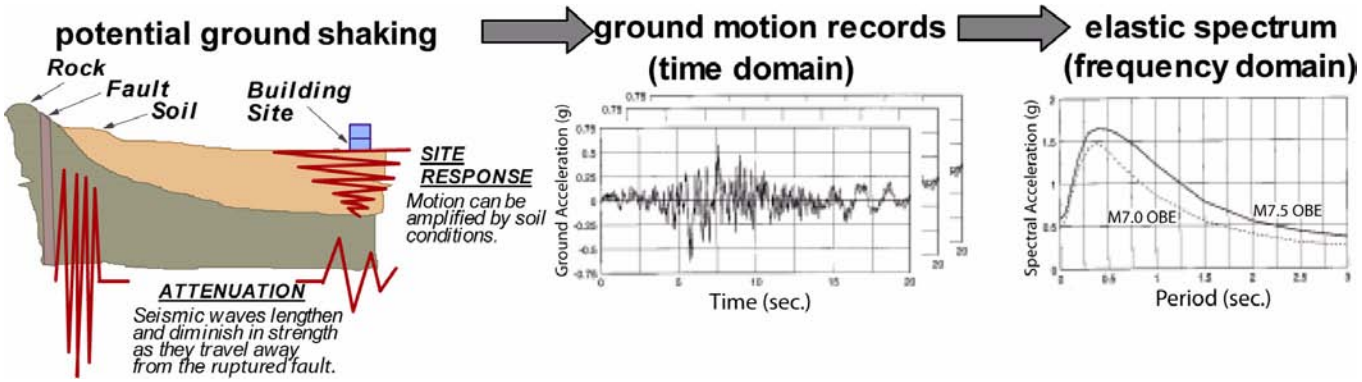

Figure 2-6 Factors affecting seismic ground motion and various ways to characterize ground motions graphically.

hazard analysis that provide an estimate of ground motion for a specified set of source and path parameters is a *deterministic spectrum*.

The level of uncertainty in source, path, and site effects associated with deterministic spectra is relatively poorly defined. These uncertainties are accounted for directly in probabilistic seismic hazard analyses that provide estimates of ground motion parameters (such as response spectral ordinates) with a specified probability of being exceeded within a specified time period. The analysis includes all earthquakes (magnitudes and faults) that potentially could cause significant seismic shaking at a given site. When response spectral ordinates for a range of periods are evaluated for a specified probability of being exceeded, the result is an *equal-hazard spectrum*.

Modern standards and guidelines (FEMA 356, ATC-40, and the *NEHRP Recommended Provisions for New Buildings*), allow the use of approximate *design spectra* that represent a simplification of equal-hazard spectra on a location-specific basis. Design spectra have standardized shapes, and can be evaluated based on nationally mapped values of spectral accelerations for short and long periods.

Deterministic spectra, equal-hazard spectra, and design spectra commonly exhibit smooth shapes with respect to period in contrast with the highly variable (jagged) shape of actual ground motion spectral records (particularly for low levels of damping). Structural response to an actual ground motion record is likely to be sensitive to the complex nature of the resulting spectrum. This uncertainty is not eliminated by the use of smooth spectra.

2.3 Options for Inelastic Analysis

Various combinations of structural model types and characterizations of seismic ground motion define a number of options for inelastic analysis. The selection of one option over another depends on the purpose of the analysis, the anticipated performance objectives, the acceptable level of uncertainty, the availability of resources, and the sufficiency of data. In some cases, applicable codes and standards may dictate the analysis procedure.

The primary decision is whether to choose inelastic procedures over more *conventional linear elastic analysis*. In general, linear procedures are applicable when the structure is expected to remain nearly elastic for the level of ground motion of interest or when the design results in nearly uniform distribution of nonlinear response throughout the structure. In these cases, the level of uncertainty associated with linear procedures is relatively low. As the performance objective of the structure implies greater inelastic demands, the uncertainty with linear procedures increases to a point that requires a high level of conservatism in demand assumptions and/or acceptability criteria to avoid unintended performance. Inelastic procedures facilitate a better understanding of actual performance. This can lead to a design that focuses upon the critical aspects of the building, leading to more reliable and efficient solutions.

Nonlinear dynamic analysis using the combination of ground motion records with a detailed structural model theoretically is capable of producing results with relatively low uncertainty (see Figure 2-7). In nonlinear dynamic analyses, the detailed structural model subjected to a ground-motion record produces estimates of component deformations for each degree of freedom in the model. Higher-level demands (element

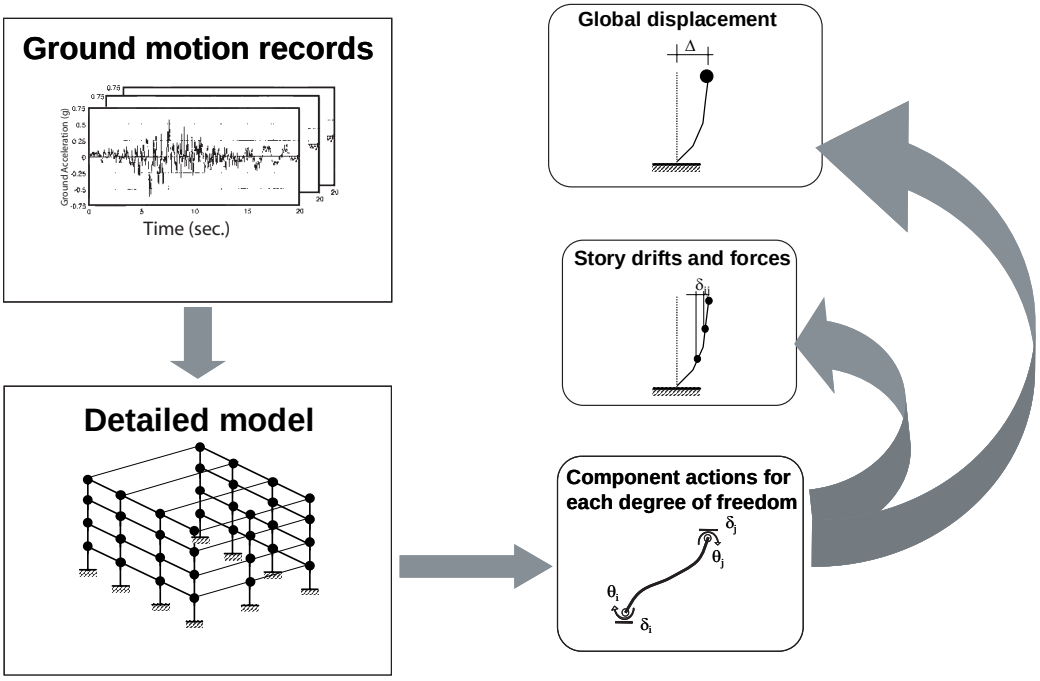

Figure 2-7 Flow chart depicting the nonlinear dynamic analysis process. Note that component actions are used to determine higher-level effects, such as story drifts and roof displacement, Δ.

distortions, story drifts, roof displacement) derive directly from the basic component actions, as illustrated in Figure 2-7. There is still uncertainty with the detailed models, associated primarily with the lack of data on actual component behavior, particularly at high ductilities. In addition, the variability of ground motion results in significant dispersion in engineering demand parameters. This is illustrated in Figure 2-8, which depicts results from a series of nonlinear dynamic analyses for increasingly larger intensities of ground shaking (Vamvatsikos and Cornell, 2002). At each level of intensity, the multiple time histories produce a distribution of results in terms of a selected engineering demand parameter. Note that the dispersion increases with higher shaking intensity and with greater elasticity.

Simplified nonlinear dynamic analysis with equivalent multi-degree-of-freedom models also use ground motion records to characterize seismic demand. However, these techniques produce engineering demand parameters above the basic component level only. For example, a "stick" model produces story displacements or drifts. The engineer can estimate corresponding component actions using the assumptions that were originally the basis of the simplified model. Thus the uncertainty associated with the component actions in the simplified model is greater than those associated with the detailed model.

Simplified nonlinear dynamic analysis with equivalent single-degree-of-freedom (SDOF) models are a further simplification using ground motion records to characterize seismic shaking (see Figure 2-9). The result of the analysis is an estimate of global displacement demand. It is important to recognize that the resulting lower-level engineering demands (e.g., story drifts, component actions) are calculated from the global displacement using the force-deformation relationship for the oscillator. In contrast to the use of the more detailed model (see Figure 2-7), they are directly related to the assumptions, and associated uncertainties, made to convert the detailed structural model to an equivalent SDOF model in the first place. This adds further to the overall uncertainty associated with the simplified nonlinear dynamic analysis. Note that if the SDOF model is subjected to multiple time histories a statistical representation of response can be generated.

Nonlinear static procedures (NSPs) convert MDOF models to equivalent SDOF structural models and represent seismic ground motion with response spectra as opposed to ground-motion records (see Figure 2-10). They produce estimates of the maximum global displacement demand. Story drifts and component actions are related subsequently to the global demand parameter by the pushover or capacity curve that was

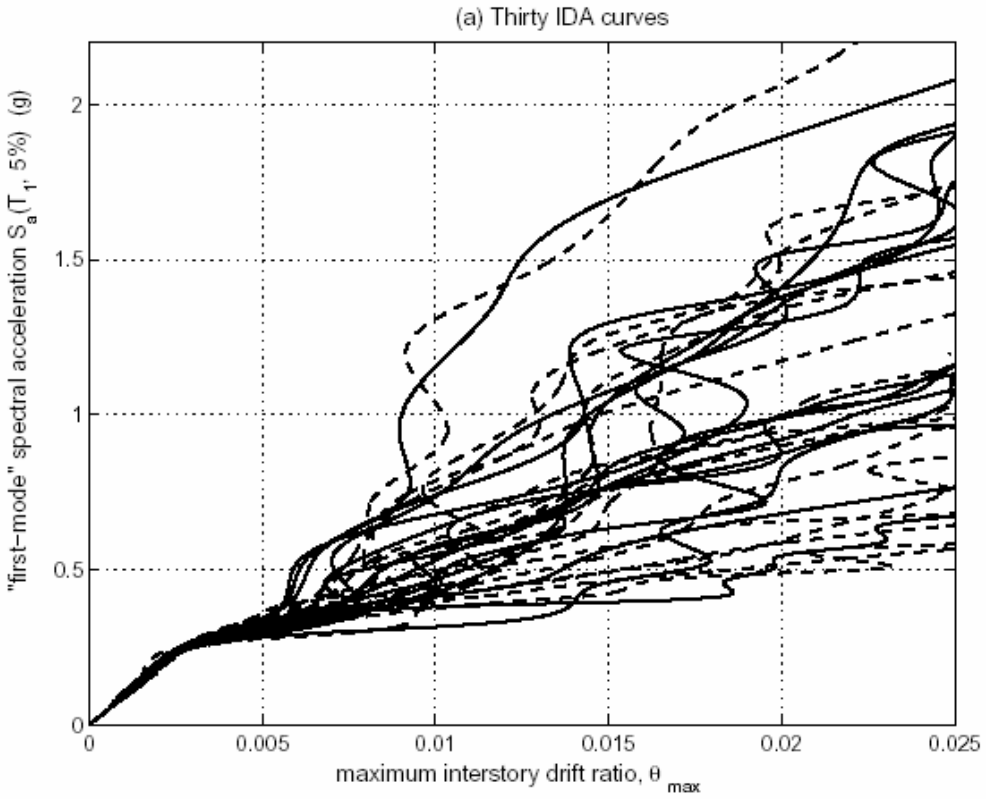

Figure 2-8 Incremental dynamic analysis study for thirty ground motion records for a 5-story steel braced frame (Vamvatsikos and Cornell, 2002)

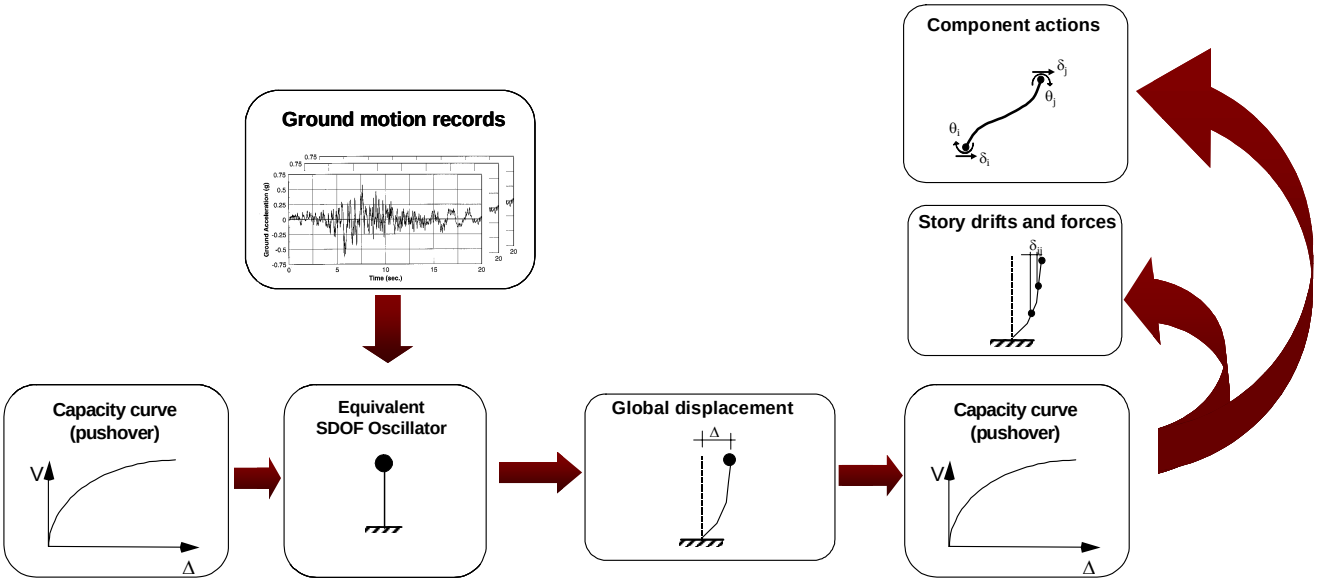

Figure 2-9 Flow chart depicting simplified SDOF nonlinear analysis process. Note that component actions are estimated from global displacement demand using the pushover curve.

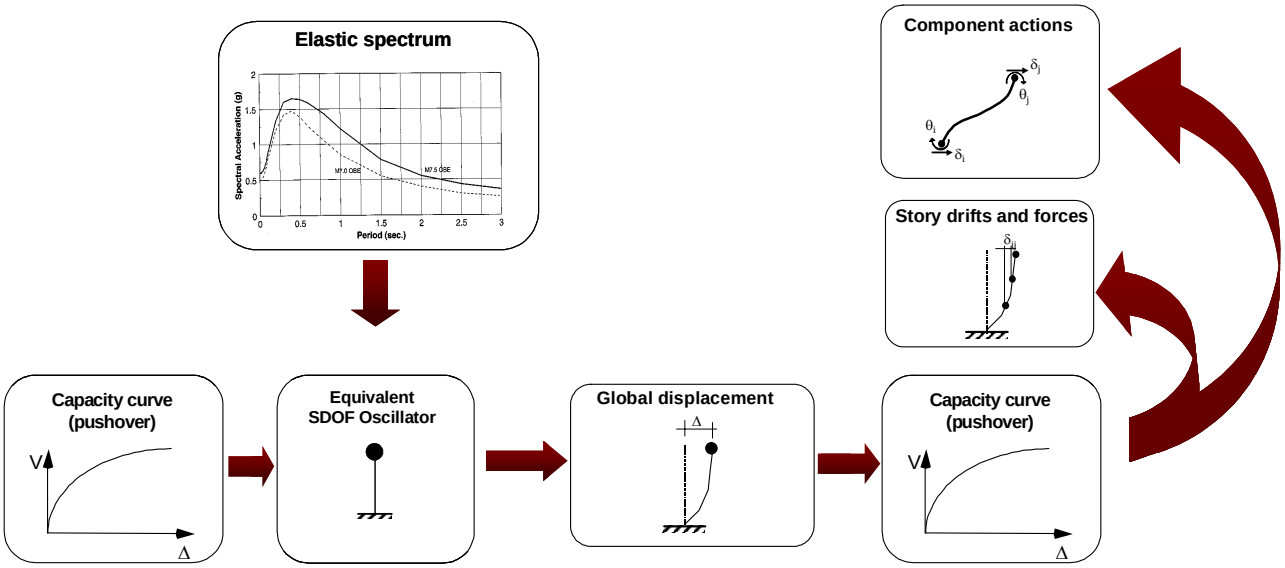

Figure 2-10 Flow chart depicting the process followed in nonlinear static procedures. Note that component actions are based on global displacement demand and a pushover/capacity curve.

used to generate the equivalent SDOF model. This is similar to simplified nonlinear dynamic analyses using SDOF models. In contrast to the use of simplified dynamic analyses using multiple ground motion records, the use of nonlinear static procedures implies greater uncertainty due to the empirical procedures used to estimate the maximum displacement. This is true even if spectra representative of the multiple ground motion records are used in the nonlinear static analysis.

Figure 2-11 summarizes the relationship among the normal options for inelastic seismic analysis procedures with respect to the type of structural model and characterization of ground motion. Also noted in the figure is the relative uncertainty associated with each option. The actual uncertainty inherent in any specific analysis depends on a number of considerations. Nonlinear dynamic analyses can be less uncertain than other techniques if the nonlinear inelastic properties of the components in the detailed structural model are accurate and reliable. If the component properties are poorly characterized, however, the results might not be an improvement over other alternatives. Some analysis options are better than others, depending on the parameter of interest. For example, with simplified dynamic analyses, a SDOF oscillator can be subjected to a relatively large number of ground motion records to provide a good representation of the uncertainty associated with global displacement demand due to the variability of the ground motion. On the other hand, if the engineer is comfortable with the estimate of maximum global displacement from a nonlinear static procedure, a multi-mode pushover analysis might provide improved estimates of inter-story drift that would not necessarily be available from the simplified SDOF dynamic analyses.

2.4 Current Nonlinear Static Procedures

Nonlinear static procedures are popular with practicing engineers, as demonstrated by the voluntary state-of-practice internet query results in Appendix B. Two options are used predominantly. Equivalent linearization techniques are based on the assumption that the maximum total displacement (elastic plus inelastic) of a SDOF oscillator can be estimated by the elastic response of an oscillator with a larger period and damping than the original. These procedures use estimates of ductility to estimate effective period and damping. The Coefficient Method is fundamentally a displacement modification procedure that is presented in FEMA 356. Alternatively, displacement modification procedures estimate the total maximum displacement of the oscillator by multiplying the elastic response, assuming initial linear properties and damping, by one or more coefficients. The coefficients are typically derived empirically from series of nonlinear response-history analyses of oscillators with varying periods and strengths.

A form of equivalent linearization known as the Capacity-Spectrum Method is documented in ATC-40. Other variations and versions of these two procedures

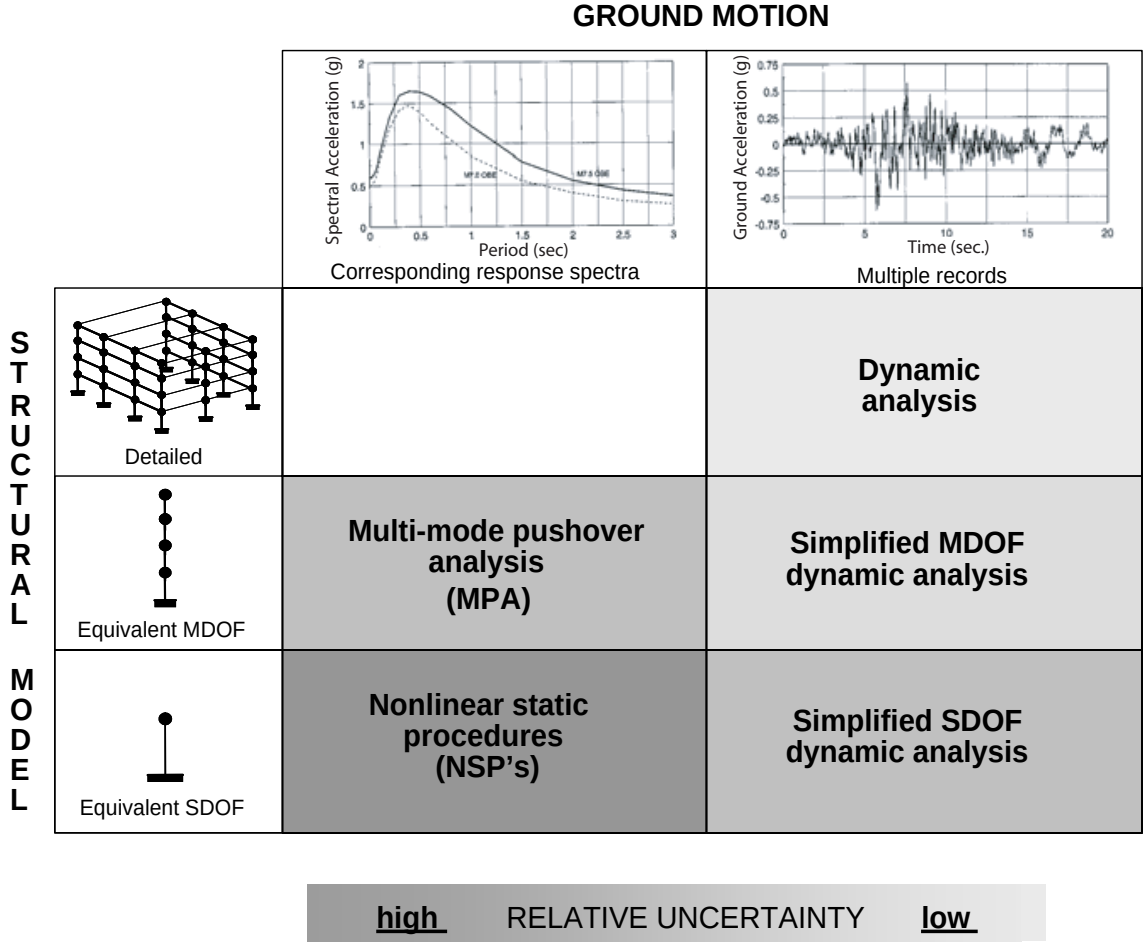

Figure 2-11 Matrix depicting possible inelastic seismic analysis procedures for various structural models and ground-motion characterizations along with trends of uncertainty in the result.

have been suggested (see Appendices A and B), but all are related fundamentally to either displacement modification or equivalent linearization. Both approaches use nonlinear static analysis (pushover analysis) to estimate the lateral force-deformation characteristics of the structure. In both procedures the global deformation (elastic and inelastic) demand on the structure is computed from the response of an equivalent single-degree-of-freedom system having the load-deformation properties determined from the pushover analysis. They differ, however, in the technique used to estimate the maximum deformation demand (elastic and inelastic).

2.4.1 The Coefficient Method of Displacement Modification from FEMA 356

The Coefficient Method is the primary nonlinear static procedure presented in FEMA 356. This approach modifies the linear elastic response of the equivalent SDOF system by multiplying it by a series of coefficients C_0 through C_3 to generate an estimate of the maximum global displacement (elastic and inelastic), which is termed the target displacement. The process begins with an idealized force-deformation curve (i.e., pushover curve) relating base shear to roof displacement (see Figure 2-12). An effective period, T_e, is generated from the initial period, T_i, by a graphical procedure that accounts for some loss of stiffness in the transition from elastic to inelastic behavior. The effective period represents the linear stiffness of the equivalent SDOF system. When plotted on an elastic response spectrum representing the seismic ground motion as peak acceleration, S_a, versus period, T, the effective period identifies a maximum acceleration response for the oscillator. The assumed damping, often five percent, represents a level that might be expected for a typical structure responding in the elastic range.

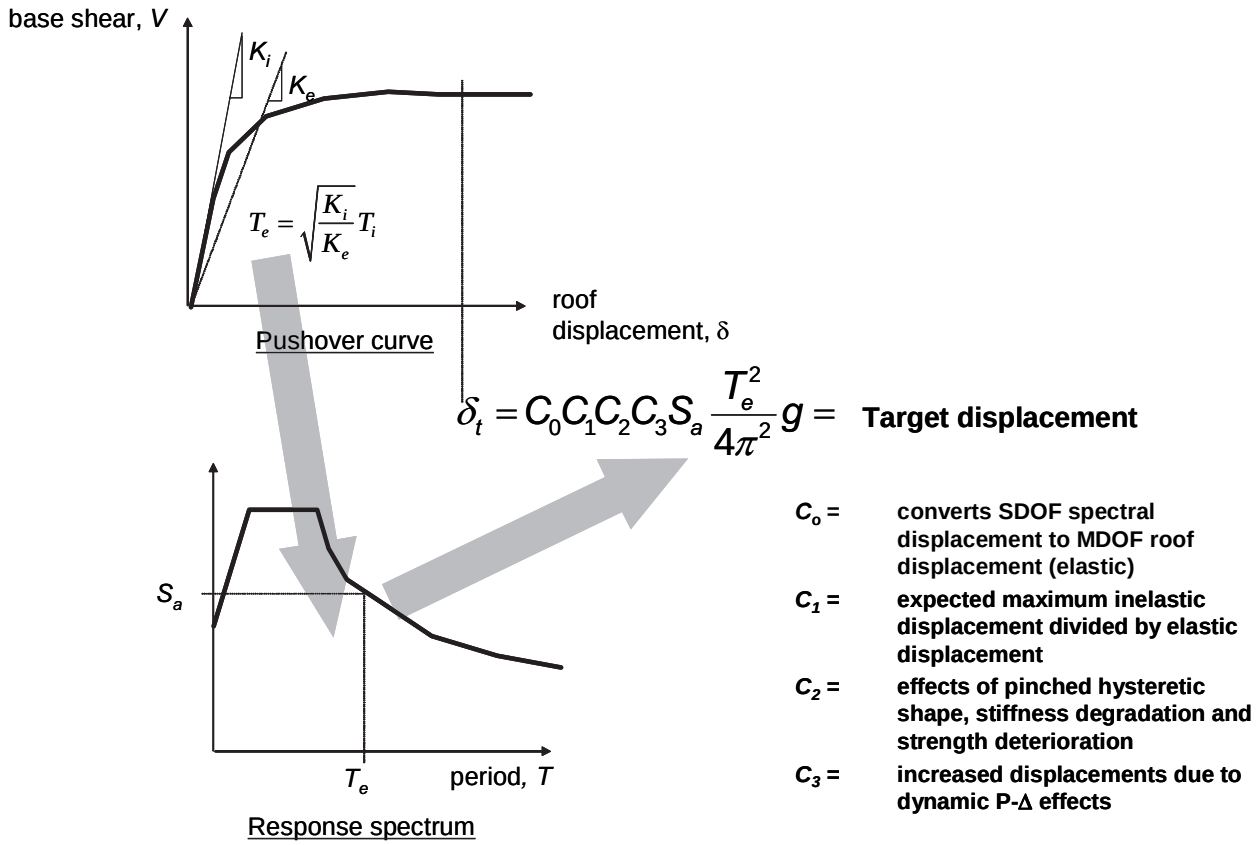

Figure 2-12 Schematic illustrating the process by which the Coefficient Method of displacement modification (per FEMA 356) is used to estimate the target displacement for a given response spectrum and effective period, T_e.

The peak elastic spectral displacement is directly related to the spectral acceleration by the relationship

$$S_d = \frac{T_{eff}^2}{4\pi^2} S_a . \qquad (2\text{-}1)$$

The coefficient C_0 is a shape factor (often taken as the first mode participation factor) that simply converts the spectral displacement to the displacement at the roof. The other coefficients each account for a separate inelastic effect.

The coefficient C_1 is the ratio of expected displacement (elastic plus inelastic) for a bilinear inelastic oscillator to the displacement for a linear oscillator. This ratio depends on the strength of the oscillator relative to the response spectrum and the period of the SDOF system, T_e. The coefficient C_2 accounts for the effect of pinching in load-deformation relationships due to degradation in stiffness and strength. Finally, the coefficient C_3 adjusts for second-order geometric nonlinearity (P-Δ) effects. The coefficients are empirical and derived primarily from statistical studies of the nonlinear response-history analyses of SDOF oscillators and adjusted using engineering judgment. The coefficients are described in greater detail in Chapter 3.

2.4.2 Capacity-Spectrum Method of Equivalent Linearization in ATC-40

The basic assumption in equivalent linearization techniques is that the maximum inelastic deformation of a nonlinear SDOF system can be approximated from the maximum deformation of a linear elastic SDOF system that has a period and a damping ratio that are larger than the initial values of those for the nonlinear system. In the Capacity-Spectrum Method of ATC-40, the process begins with the generation of a force-deformation relationship for the structure. This process is virtually identical to that for the Coefficient Method of FEMA 356, except that the results are plotted in acceleration-

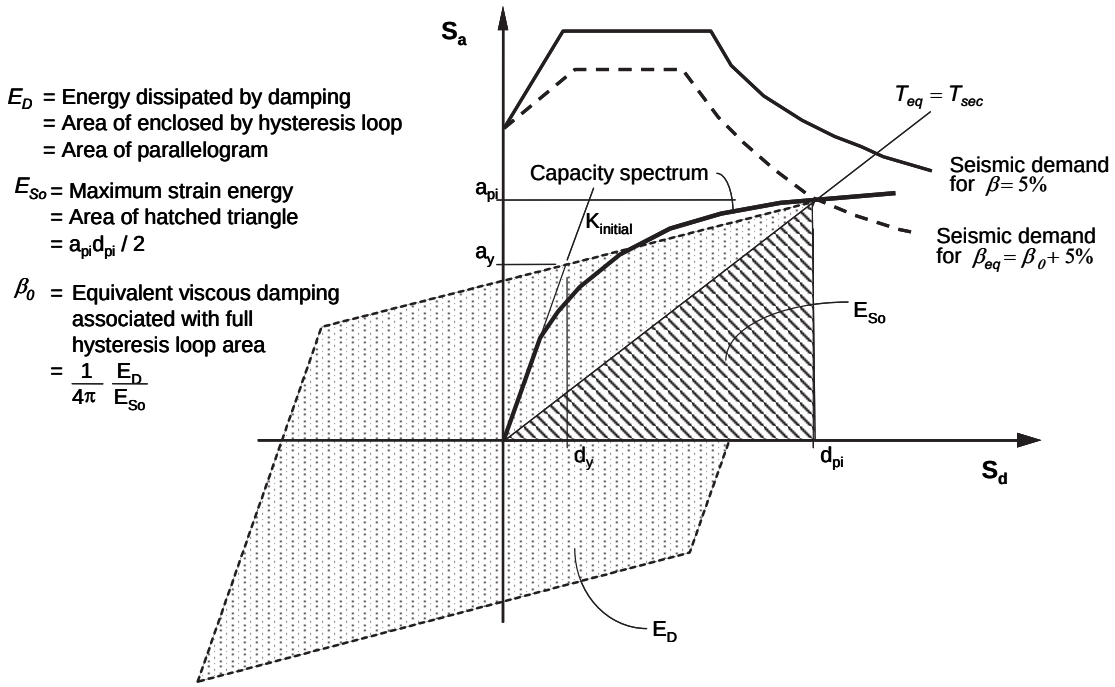

Figure 2-13 Graphical representation of the Capacity-Spectrum Method of equivalent linearization, as presented in ATC-40.

displacement response spectrum (ADRS) format (see Figure 2-13). This format is a simple conversion of the base-shear-versus-roof-displacement relationship using the dynamic properties of the system, and the result is termed a capacity curve for the structure. The seismic ground motion is also converted to ADRS format. This enables the capacity curve to be plotted on the same axes as the seismic demand. In this format, period can be represented as radial lines emanating from the origin.

The Capacity-Spectrum Method of equivalent linearization assumes that the equivalent damping of the system is proportional to the area enclosed by the capacity curve. The equivalent period, T_{eq}, is assumed to be the secant period at which the seismic ground motion demand, reduced for the equivalent damping, intersects the capacity curve. Since the equivalent period and damping are both a function of the displacement, the solution to determine the maximum inelastic displacement (i.e., performance point) is iterative. ATC-40 imposes limits on the equivalent damping to account for strength and stiffness degradation. These limits are reviewed in greater detail in Chapter 3.

3. Evaluation of Current Nonlinear Static Procedures

3.1 Introduction

This chapter summarizes the results of studies to assess the ability of current approximate nonlinear static procedures to estimate the maximum displacement of inelastic structural models. Initial studies evaluated both the Coefficient Method of FEMA 356 and the Capacity-Spectrum Method of ATC-40.

The use of NSPs (nonlinear static procedures) has accelerated in the United States since the publication of ATC-40, FEMA 273/274 and FEMA 356 documents. As a consequence there is valuable information available on the practical application of these inelastic analysis procedures (see Appendix B, "Summary of Practice using Inelastic Analysis Procedures"). Various researchers and practicing engineers have found that, in some cases, different inelastic analysis methods give substantially different estimates for displacement demand for the same ground motion and same SDOF oscillator (Aschheim et al., 1998; Chopra and Goel 1999a,b, 2000; Albanessi et al., 2000; Kunnath and Gupta, 2000; Lew and Kunnath, 2000; Yu et al, 2001; Zamfirescu and Fajfar, 2001; MacRae and Tagawa, 2002). The disparities in displacement predictions highlight the need for comparison and further study of these different approaches (see Appendix A, "Summary of Research on Inelastic Analysis Procedures").

The objective of this evaluation was to study the accuracy of the approximate methods described in ATC-40 and FEMA 356 for estimating the maximum displacement demand of inelastic single-degree-of-freedom (SDOF) systems. This global displacement is a spectral displacement, termed the Performance Point in ATC-40. It is the roof displacement, termed the Target Displacement in FEMA 356. In particular, this study was aimed at identifying and quantifying the errors in these procedures when applied to SDOF systems. For this purpose, approximate total displacements computed with ATC-40 and with FEMA 356 were compared with the results of nonlinear response-history analyses of SDOF oscillators. The nonlinear response-history analyses are "exact" for the assumptions made for the properties of the oscillator (damping ratio and type of hysteretic behavior) and for the particular ground motion record. Thus these results are a useful benchmark to evaluate the approximate procedures.

Of particular interest is the extent to which the approximate methods might tend to overestimate or underestimate displacement demands (introduce bias) and the spectral regions or strength levels for which these biases are likely to occur. Errors were quantified through statistical analyses. A large number of SDOF systems (with a wide range of periods of vibration, lateral strengths, and hysteretic behavior) were subjected to a relatively large number of recorded earthquake ground motions. Ground motions included near-fault and far-fault records representative of site conditions ranging from rock to very soft soil. However, it is recognized that there may be some situations that deviate from those used in this investigation. Caution should be used when extrapolating the results presented in this evaluation for ground motions and site conditions that differ substantially.

Section 3.2 describes the period of vibration, damping ratio, lateral strength, and hysteretic behavior of the SDOF systems that were considered in this investigation. This section also describes the types and characteristics of the recorded ground motion records that were used as well as the error measures computed in this study. Section 3.3 describes the evaluation of the simplified inelastic analysis procedure in ATC-40 to estimate the maximum displacement of inelastic systems using equivalent linearization. Section 3.4 provides a corresponding evaluation of the simplified analysis procedure in FEMA 356. In particular, this chapter provides an evaluation of coefficients C_1, C_2 and C_3 in this method. Finally, Section 3.5 summarizes the dynamic response of nonlinear elastic, or rocking, oscillators. A complete compilation of the evaluation study data is provided in Appendix C, "Supplemental Data on the Evaluation of Current Procedures."

3.2 Evaluation Procedures

3.2.1 Hysteretic Characteristics

SDOF systems with initial periods of vibration between 0.05 s and 3.0 s were used in this investigation. A total of 50 periods of vibration were considered (40 periods between 0.05 s and 2.0 s, equally spaced at 0.05 s, and 10 periods between 2.0 s and 3.0 s, equally spaced at 0.1 s intervals). The initial damping ratio, β, was assumed to be equal to 5% for all systems.

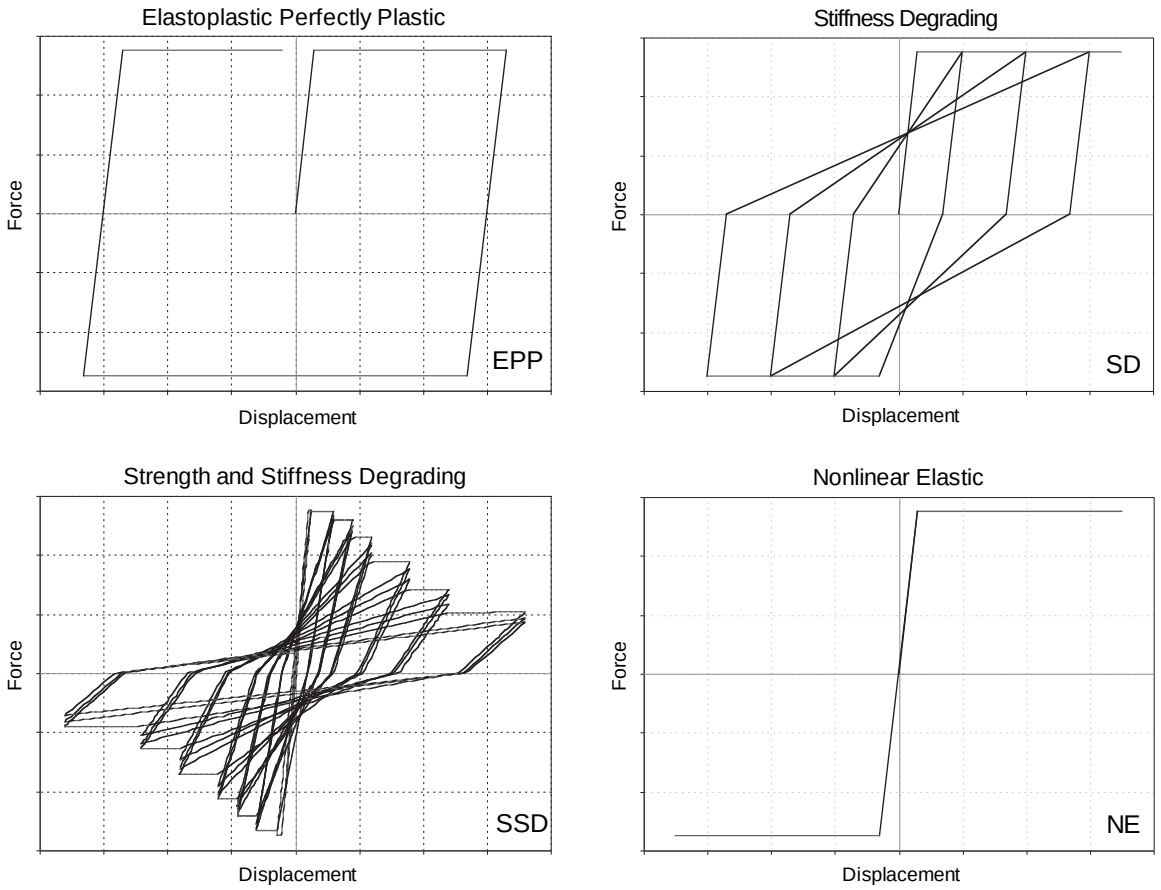

Figure 3-1 Basic hysteretic models used in the evaluation of current procedures: elastic perfectly plastic (EPP); stiffness-degrading (SD); strength and stiffness degrading (SSD), and nonlinear elastic (NE).

In this study the lateral strength is normalized by the strength ratio *R*, which is defined as

$$R = \frac{mS_a}{F_y} \tag{3-1}$$

where m is the mass of the SDOF oscillator, S_a is the spectral acceleration ordinate corresponding to the initial period of the system, and F_y is the lateral yield strength of the system. The numerator in Equation 3-1 represents the lateral strength required to maintain the system elasticity, which sometimes is also referred to as the elastic strength demand. *Note that this R-factor is not the same as the response-modification coefficient conventionally used for design purposes.* This *R*-factor is the design *R*-factor divided by the overstrength factor, omega sub-zero. This is discussed on page 105 of FEMA 450-2, *NEHRP Recommended Provisions for Seismic Regulations for New Buildings and Other Structures, Part 2: Commentary* (BSSC, 2003). Nine levels of normalized lateral strength were considered, corresponding to R = 1, 1.5, 2, 3, 4, 5, 6, 7 and 8.

Four different hysteretic behaviors were used in this study (see Figure 3-1):

- The *elastic perfectly plastic (EPP)* model is used as a reference model. This model has been used widely in previous investigations and therefore it represents a benchmark to study the effect of hysteretic behavior. Furthermore, recent studies have shown that this is a reasonable hysteretic model for steel beams that do not experience lateral or local buckling or connection failure (Foutch and Shi, 1998).
- The *stiffness-degrading (SD)* model corresponds to the modified-Clough model, as originally proposed by Clough (1966) and as modified by Mahin and Lin (1983). This model was originally proposed as

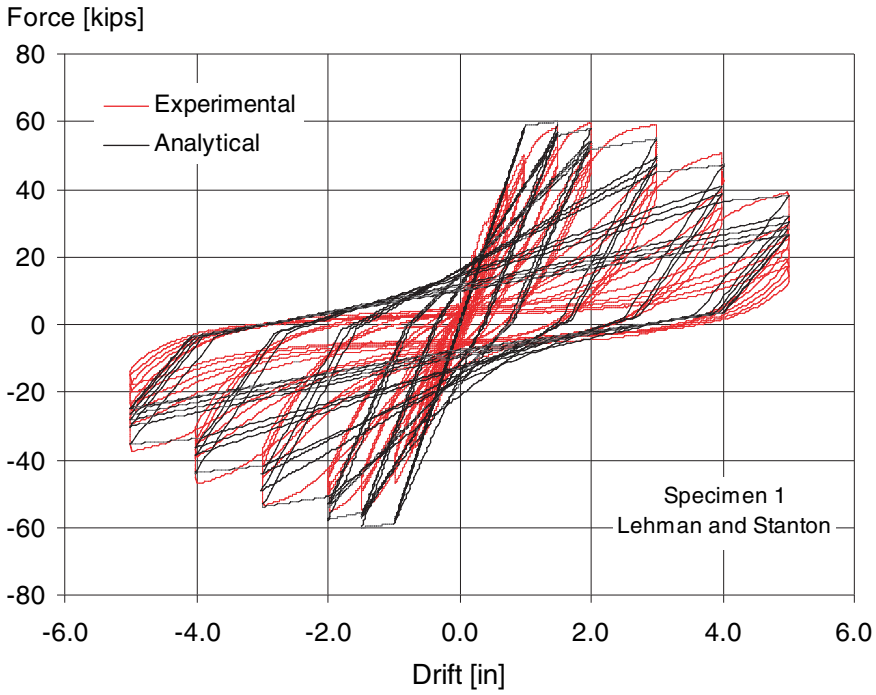

Figure 3-2 Comparison of experimental results (after Lehman et al., 2000) with the hysteretic response computed with the SSD model.

representative of well detailed and flexurally controlled reinforced concrete structures in which the lateral stiffness decreases as the level of lateral displacement increases.

- The *strength and stiffness-degrading (SSD)* model is aimed at approximately reproducing the hysteretic behavior of structures in which lateral stiffness and lateral strength decrease when subjected to cyclic reversals. In this model, the amount of strength and stiffness degradation is a function of the maximum displacement in previous cycles as well as a function of the hysteretic energy dissipated. This model is similar to the three-parameter model implemented in IDARC (Kunnath et al., 1992). When properly calibrated, this model can reproduce the response of poorly detailed reinforced concrete structures relatively well. An example is shown in Figure 3-2, in which the load-deformation relationship of a poorly detailed beam-column joint tested at the University of Washington (Lehman et al., 2000) is compared with the response computed with the SSD model. A single set of parameters representing severe strength and stiffness degradation was used for this model. The type of degradation that is captured by this model only includes cyclic degradation. Note that the post-elastic stiffness in any cycle is always equal to zero or greater. Thus, the strength never diminishes in the current cycle of deformation. The degradation of strength occurs in subsequent cycles (or half-cycles) of deformation. Oscillators that have in-cycle negative post-elastic stiffnesses and in-cycle degradation of strength can be prone to dynamic instability. They are covered in Section 3.4.4 and in Chapter 4.
- The *nonlinear elastic (NE)* model unloads on the same branch as the loading curve and therefore exhibits no hysteretic energy dissipation. This model approximately reproduces the behavior of pure rocking structures. Most instances of rocking in real structures are a combination of this type of behavior with one of the other hysteretic types that include hysteretic energy losses.

In summary, the combinations of period of vibration, lateral strength, and hysteretic behavior represent a total of 1,800 different SDOF systems.

3.2.2 Earthquake Ground Motions

A total of 100 earthquake ground motions recorded on different site conditions were used in this study. Ground motions were divided into five groups with 20 accelerograms in each group. The first group consisted of earthquake ground motions recorded on stations located on rock with average shear wave velocities between 760 m/s (2,500 ft/s) and 1,525 m/s (5,000 ft/s).

These are representative of site class B, as defined by the *NEHRP Recommended Provisions for Seismic Regulations for New Buildings and Other Structures, Part I, Provisions* (BSSC, 2000)[1]. The second group consisted of records obtained on stations on very dense soil or soft rock with average shear wave velocities between 360 m/s (1,200 ft/s) and 760 m/s, while the third group consisted of ground motions recorded on stations on stiff soil with average shear wave velocities between 180 m/s (600 ft/s) and 360 m/s. These are consistent with site class C and D respectively. The fourth group corresponds to ground motions recorded on very soft soil conditions with shear wave velocities smaller than 180 m/s, which can be classified as site class E. Finally, the fifth group corresponds to 20 ground motions influenced by near-field forward-directivity effects. Detailed listings of the ground motions are presented in Appendix C.

3.2.3 Error Measures and Statistical Study

The maximum displacement of each inelastic SDOF system was estimated with the simplified inelastic procedures in ATC-40 and FEMA 356 when subjected to each of the ground motions. The maximum displacement of each inelastic SDOF system was then computed using nonlinear response-history analyses. The maximum displacement is defined as the maximum of the absolute value of the displacement response. A total of 180,000 nonlinear response-history analyses were run as part of this investigation. In this study, the results computed with nonlinear response-history analyses are the benchmark maximum displacements, $(\Delta_i)_{ex}$. The maximum displacements estimated with simplified inelastic procedures of ATC-40 and FEMA 356 are the approximate maximum displacements, $(\Delta_i)_{app}$ of the inelastic system. It should be noted that the nonlinear response-history analyses are "exact" only for the SDOF oscillator with the assumed properties and for the particular ground motion. The uncertainty of the modeling assumptions with respect to the actual building is not included in either the nonlinear response-history analyses or the approximate analyses. The nonlinear response-history results are a convenient benchmark.

In order to evaluate the accuracy of these approximate procedures, an error measure was defined as the ratio of approximate, $(\Delta_i)_{app}$, to benchmark, $(\Delta_i)_{ex}$, maximum displacement as follows:

$$E_{T,R} = \left[\frac{(\Delta_i)_{\text{app}}}{(\Delta_i)_{\text{ex}}} \right]_{T,R} \tag{3-2}$$

This error measure was computed for each period of vibration T and each level of normalized lateral strength R. Values of $E_{T,R}$ larger than one indicate that the approximate method overestimates the maximum displacement of the SDOF system and values smaller than one indicate underestimation. A total of 320,000 individual errors were computed in this study.

In order to identify whether the approximate methods, on average, tend to overestimate or underestimate maximum displacements of inelastic systems, mean errors were computed as follows:

$$\bar{E}_{T,R} = \frac{1}{n} \sum_{i=1}^{n} \left(E_{T,R} \right)_i \tag{3-3}$$

where n is the number of records in each group of ground motions. Mean errors were computed for each hysteretic behavior type, each period of vibration (or for each normalized period of vibration as will be explained later) and each level of normalized lateral strength. Therefore, mean errors computed with Equation 3-3 do not allow for underestimations in a spectral region to be compensated by overestimations in another spectral region. Information on the bias for each period, for each type of hysteretic behavior, for each level of normalized lateral strength, and for each site class is retained.

The sample mean error computed with Equation 3-3 is an unbiased estimator of the mean error of the population. Therefore, it provides an estimate of the average error produced by the approximate methods. However, it provides no information on the dispersion of the error. In order to obtain a measure of the dispersion of the errors produced by the approximate methods, the standard deviation of the error was computed as

$$\sigma_{T,R} = \sqrt{\frac{1}{n-1} \sum_{i=1}^{n} \left[\left(E_{T,R} \right)_i - \bar{E}_{T,R} \right]^2} \tag{3-4}$$

The square of the sample standard deviation of the error computed with Equation 3-4 is an unbiased estimator of the variance of the error in the population. The standard deviation of the error was computed for each period, for

1. Superseded in 2003 with the FEMA 450 *Recommended Provisions for Seismic Regulations for New Buildings and Other Structures.*

each type of hysteretic behavior, for each level of normalized lateral strength, and for each site class.

3.3 Evaluation of Capacity-Spectrum Method of ATC-40

3.3.1 Summary of the Approximate Method

The simplified inelastic analysis procedure in ATC-40, a version of the Capacity-Spectrum Method (CSM), is based on equivalent linearization. The basic assumption in equivalent linear methods is that the maximum displacement of a nonlinear SDOF system can be estimated from the maximum displacement of a linear elastic SDOF system that has a period and a damping ratio that are larger than those of the initial values for the nonlinear system. The elastic SDOF system that is used to estimate the maximum inelastic displacement of the nonlinear system is usually referred to as the equivalent or substitute system. Similarly, the period of vibration and damping ratio of the elastic system are commonly referred to as equivalent period and equivalent damping ratio, respectively.

The concept of equivalent viscous damping was first proposed by Jacobsen (1930) to obtain approximate solutions for the steady forced vibration of damped SDOF systems with linear force-displacement relationships but with damping forces proportional to the *n*th power of the velocity of motion when subjected to sinusoidal forces. In this pioneering study, the stiffness of the equivalent system was set equal to the stiffness of the real system and the equivalent viscous damping ratio was based on equating the dissipated energy per cycle of the real damping force to that of the equivalent damping force. Years later, the same author extended the concept of equivalent viscous damping to yielding SDOF systems (Jacobsen, 1960). Since then, there have been many methods proposed in the literature. Review of the earlier equivalent linear methods can be found in Jennings (1968), Iwan and Gates (1979), Hadjian (1982), Fardis and Panagiatakos (1996), while a review of some recent methods can be found in Miranda and Ruiz-García (2003). The Capacity Spectrum Method as documented in ATC-40 is based primarily on the work of Freeman et al. (1975).

In equivalent linear methods, the equivalent period is computed from the initial period of vibration of the nonlinear system and from the maximum displacement ductility ratio, μ. Similarly, the equivalent damping ratio is computed as a function of damping ratio in the nonlinear system and the displacement ductility ratio. The main differences among the many equivalent linear methods that are available in the literature stem primarily from the functions used to compute the equivalent period and equivalent damping ratio.

As discussed in Section 2.4.2, the Capacity-Spectrum Method according to ATC-40 uses the secant stiffness at maximum displacement to compute the effective period and relates effective damping to the area under the hysteresis curve (see Figure 2-13).These assumptions result in an equivalent period, T_{eq}, and equivalent damping ratio (referred to as effective viscous damping, β_{eq}, in ATC-40) given by

$$T_{eq} = T_0 \sqrt{\frac{\mu}{1+\alpha\mu-\alpha}} \tag{3-5}$$

$$\beta_{eq} = \beta_{eff} = 0.05 + \kappa \frac{2}{\pi} \frac{(\mu-1)(1-\alpha)}{\mu(1+\alpha\mu-\alpha)} \tag{3-6}$$

where T_0 is the initial period of vibration of the nonlinear system, α is the post-yield stiffness ratio and κ is an adjustment factor to approximately account for changes in hysteretic behavior in reinforced concrete structures. ATC-40 proposes three equivalent damping levels that change according to the hysteretic behavior of the system. Type A hysteretic behavior denotes structures with reasonably full hysteretic loops, similar to the EPP oscillator in Figure 3-1. The corresponding equivalent damping ratios take the maximum values. Type C hysteretic behavior represents severely degraded hysteretic loops (e.g., SSD), resulting in the smallest equivalent damping ratios. Type B hysteretic behavior is an intermediate hysteretic behavior between types A and C (e.g., SD). The value of κ decreases for degrading systems (hysteretic behavior types B and C). ATC-40 suggests an initial elastic viscous damping ratio (first term on the right hand side of Equation 3-6) of 0.05 (5%) for reinforced concrete buildings. The terms to the right of κ in Equation 3-6 represent the equivalent hysteretic viscous damping for an idealized bilinear system designated as β_0 in ATC-40 documentation. Table 3-1 shows the variation of κ with respect to β_0 for different hysteretic behaviors types.

The equivalent period in Equation 3-5 is based on a lateral stiffness of the equivalent system that is equal to the secant stiffness at the maximum displacement. It only depends on the displacement ductility ratio and the

Table 3-1 Variation of κ-Value in ATC-40

Hysteretic Behavior	β_0	κ
Type A	≤ 0.1625	1.0
	> 0.1625	$1.13 - 0.51 \times (\pi/2) \times \beta_0$
Type B	≤ 0.25	0.67
	> 0.25	$0.845 - 0.446 \times (\pi/2) \times \beta_0$
Type C	Any value	0.33

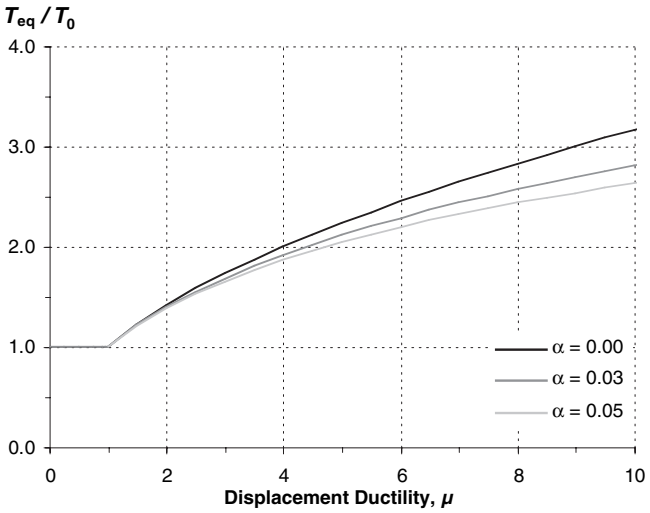

Figure 3-3 Variation of period shift based on secant stiffness.

post-yield stiffness ratio of the inelastic system. Figure 3-3 shows the variation of equivalent periods for different post-yield stiffness ratios for a wide range of displacement ductility ratios. The equivalent period becomes longer as the displacement ductility ratio increases and as the post-yield stiffness ratio decreases.

Figures 3-4 and 3-5 present the variation of κ and effective damping value, β_{eq}, with changes in the ductility ratio, respectively. The calculations were done assuming elastic perfectly plastic (EPP) behavior to represent a system that has full hysteretic loops (i.e., a non-degrading system). It can be seen that for structures with type A behavior (systems having full hysteretic loops), the κ value is 1.0 for displacement ductility ratios less than 1.3. For ductility ratios larger than 1.3, κ decreases up to a value of 0.77 at a displacement ductility ratio of 3.4 and remains constant at 0.77 for larger ductilities. Similarly, for structures with type B hysteretic behavior, the value of κ is constant and equal to 0.67 for displacement ductility ratios less than 1.6,

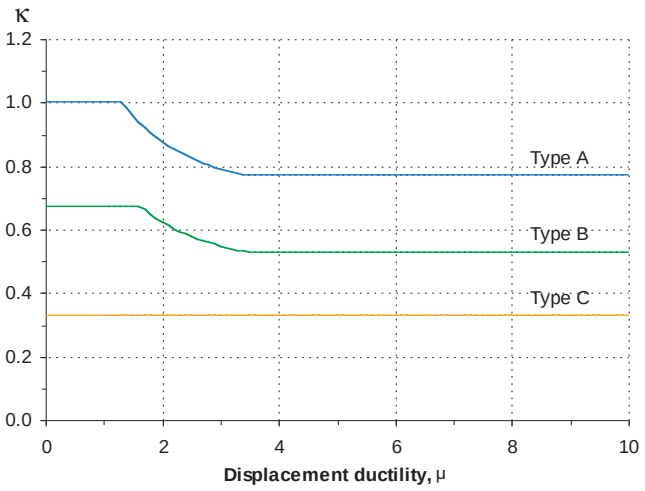

Figure 3-4 Variation of κ-factor with the displacement ductility ratio, μ.

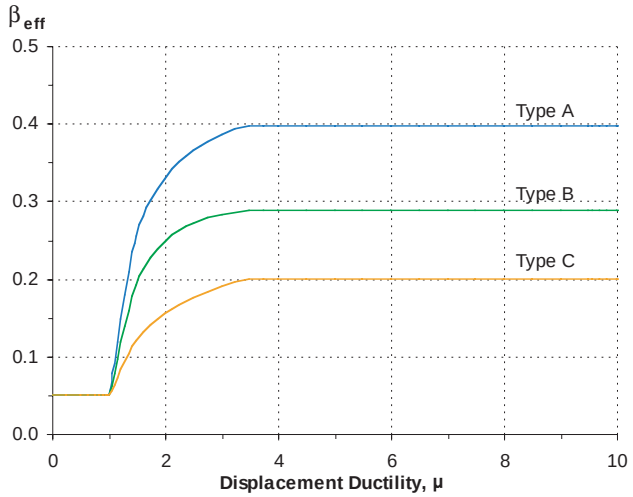

Figure 3-5 Variation of equivalent (effective) damping ratios with changes in the displacement ductility ratio, μ.

decreases to 0.53 for ductility ratio of 3.4, and remains constant for larger ductilities. For structures with type C hysteretic behavior, the κ factor is equal to 0.33 regardless of the level of ductility demand.

The equivalent damping ratio in the equivalent linear spectrum method documented in ATC-40 rapidly increases once the structures yields and remains constant for ductility ratios higher than 3.4. The maximum equivalent damping ratios for hysteretic behavior types A, B, and C are 0.40, 0.29 and 0.20, respectively. According to Equations 3-5 and 3-6, structures with hysteretic behaviors type B and C will

have much larger displacement demands because of the

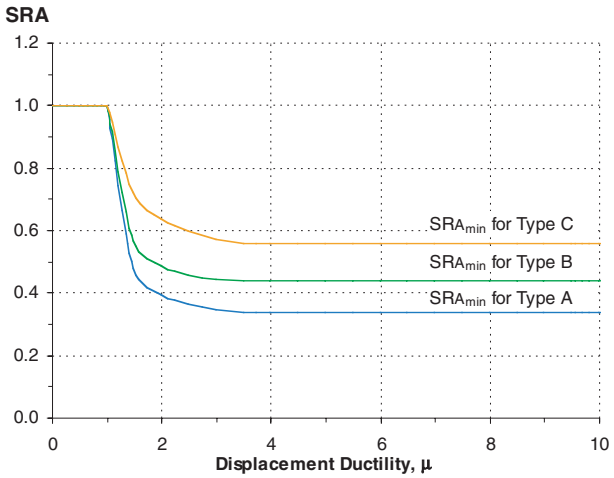

Figure 3-6 Variation of spectral reduction factors SRA for different hysteretic behaviors as a function of the displacement ductility ratio, μ.

reduced hysteretic energy dissipation capacity produced by narrower hysteretic loops.

When applied to design spectra, ATC-40 provides reduction factors to reduce spectral ordinates in the constant-acceleration region and constant-velocity region as a function of the effective damping ratio. These spectral reduction factors are given by

$$SR_A = \frac{3.21 - 0.68\ln\left(100\beta_{\text{eff}}\right)}{2.12} \qquad (3\text{-}7)$$

$$SR_V = \frac{2.31 - 0.41\ln\left(100\beta_{\text{eff}}\right)}{1.65} \qquad (3\text{-}8)$$

where β_{eff}, is the effective or equivalent damping ratio computed with Equation 3-6. SR_A is the spectral-reduction factor to be applied to the constant-acceleration region in the linear elastic design spectrum, and SR_V is the spectral reduction factor to be applied to the constant-velocity region (descending branch) in the linear elastic design spectrum. These spectral-reduction factors are shown in Figures 3-6 and 3-7. It can be seen that for displacement ductility demands larger than 3.4, the spectral ordinates no longer decrease. Consequently, the ATC-40 procedures impose limits on the amount of hysteretic damping-related reduction in spectral response that can be achieved. Table 3-2 shows these limiting values.

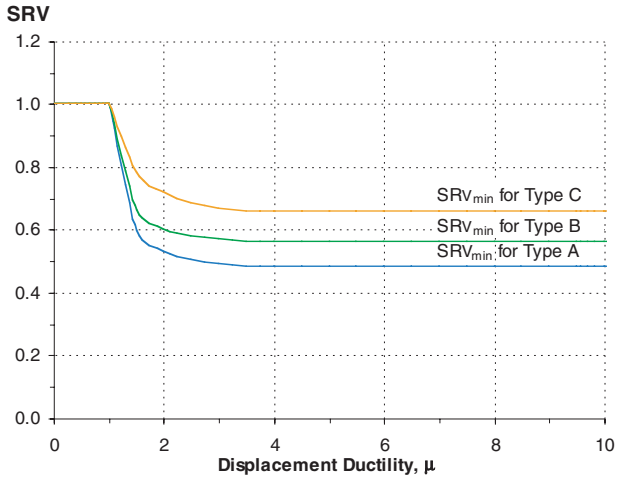

Figure 3-7 Variation of spectral reduction factors SRV for different hysteretic behaviors as a function of the displacement ductility ratio, μ.

Table 3-2 Minimum Allowable Spectral Reduction Factors for Displacement Ductility Ratios Larger than 3.4

Behavior Type	SR_A	SR_V
Type A	0.33	0.50
Type B	0.44	0.56
Type C	0.56	0.67

3.3.2 Iteration Procedures

Equivalent linearization equations, in general, require prior knowledge of the displacement ductility ratio in order to compute the equivalent period of vibration and equivalent damping ratio, μ, which are then needed to estimate the maximum inelastic displacement demand on a SDOF system when subjected to a particular ground motion. Specifically, in Equations 3-5 and 3-6, μ must be known in order to compute β_{eff} and T_{eq}. However, when evaluating a structure, the maximum displacement ductility ratio is not known. Consequently, iteration is required in order to estimate the maximum displacement.

ATC-40 describes three iterative procedures to reach a solution for the approximation. Procedures A and B are described as the most transparent and most convenient for programming, as they are based on an analytical method. Procedure C is a graphical method that is not convenient for spreadsheet programming. ATC-40 presents Procedure A as the most straightforward and

easy in application among the three procedures. In a recent study, Chopra and Goel (1999a,b, 2000) investigated the iteration methods implemented in ATC-40. By using various SDOF examples, they showed that Procedure A did not always converge when using actual earthquake spectra, as opposed to smooth design spectra. They also concluded that the displacement computed with Procedure B was unique and the same as that determined with Procedure A, provided that the latter converged. In a more recent study, Miranda and Akkar (2002) provide further discussion of the convergence issues in equivalent linearization procedures. They also note that equivalent linearization procedures can lead to multiple results for some specific earthquake ground motions.

An iteration procedure based on secant iteration that is guaranteed to converge was used for the evaluation study. As noted in the previous section, multiple equivalent linearization solutions may exist for actual ground motion records that were used for the study, as opposed to smoothed spectra normally used by engineers. For the purposes of this investigation, the first computed displacement encountered within 1% of the assumed displacement was taken as the approximate inelastic displacement without verifying whether this was the only possible solution.

3.3.3 Evaluation Using Ground Motion Records

In order to evaluate the Capacity-Spectrum Method when applied to structures with hysteretic behavior type A, approximate results were compared with response-history analysis (RHA) benchmark results computed with the EPP hysteretic model. Similarly, the approximate results computed for behavior type B were compared with RHA benchmark results of the stiffness degrading (SD) model, and the approximate results computed for behavior type C were compared with RHA benchmark results of the strength-and-stiffness-degrading (SSD) model. Mean errors corresponding to ground motions recorded in site class C and for hysteretic behaviors type A, B, and C are shown in Figure 3-8. Based on the complete results presented in Appendix C, it was found that the Capacity-Spectrum Method implemented in ATC-40 leads to very large overestimations of the maximum displacement for relatively short-period systems (periods smaller than about 0.5 s). Approximate maximum displacements in this period range can be, on average, larger than twice the RHA benchmark displacements. These large overestimations of displacement in the short-period range have also been reported previously for other

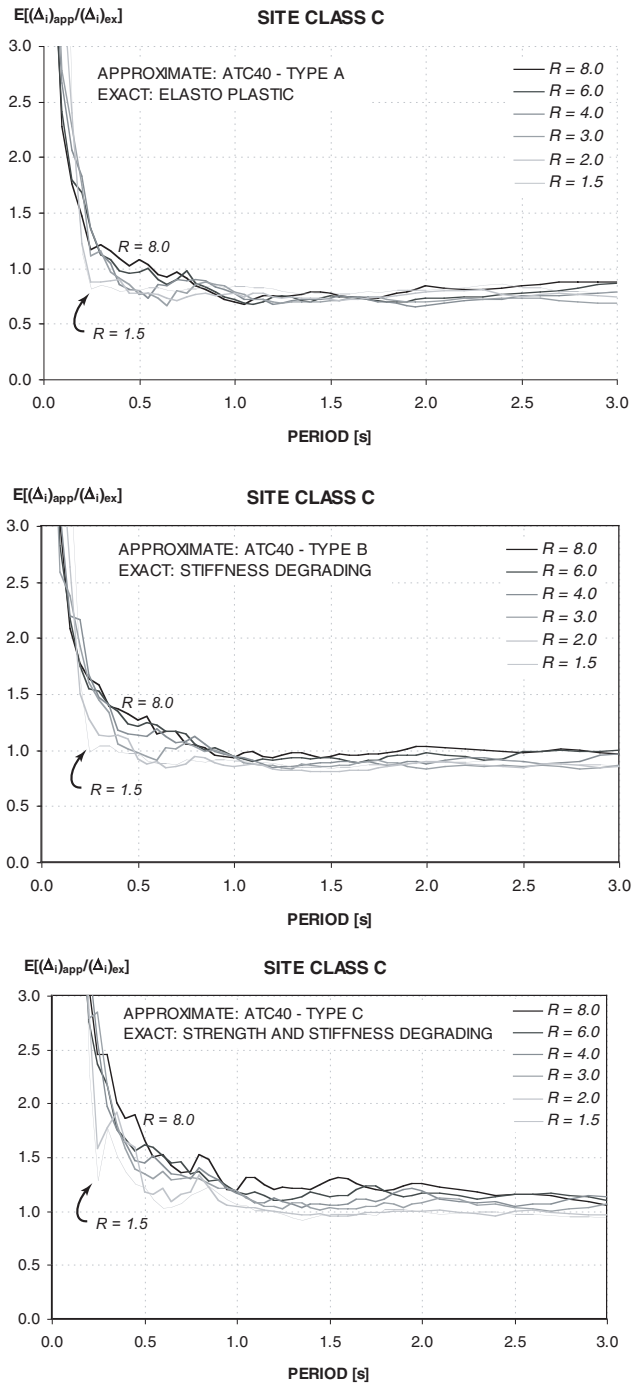

Figure 3-8 Mean error associated with the Capacity-Spectrum Method of ATC-40 for hysteretic behaviors types A, B, and C for site class C.

equivalent linearization methods that are based on secant stiffness (Miranda and Ruiz-García, 2003; Akkar and Miranda, 2005).

The complete results indicate that, for periods longer than about 0.6 s, ATC-40 behavior type A tends to underestimate the maximum displacements. Maximum displacements computed with the ATC-40 procedure are, on average, about 25% to 35% smaller than those computed with RHA using elasto-plastic systems. Underestimations are slightly smaller for site class B and slightly larger for site class D. Mean errors for ATC-40 behavior type A are not significantly influenced by changes in the normalized lateral strength *R*.

For systems with ATC-40 hysteretic behavior type B and periods longer than about 0.8 s, the Capacity-Spectrum Method tends to underestimate displacements compared with those of inelastic systems with stiffness-degrading (SD) models for site class B. Underestimations are small and tend to decrease as *R* increases. Average underestimations range from 5% to 25%. For site classes C and D, ATC-40 may underestimate or overestimate lateral deformation of systems with type B hysteretic behavior depending on the normalized lateral strength, *R*.

In the case of systems with hysteretic behavior type C, the approximate ATC-40 procedure tends to overestimate inelastic displacements for practically all periods when compared to those computed for inelastic systems with strength-and-stiffness-degrading (SSD) hysteretic models. Overestimations increase as *R* increases. The level of overestimation varies from one site class to another. Detailed information on the actual errors are contained in Appendix C.

Dispersion of the error is very large for periods smaller than about 0.5 s and is moderate and approximately constant for periods longer than 0.5 s. In general, dispersion increases as *R* increases. Mean errors computed with ground motions recorded on very soft soil sites or with near-fault ground motions are strongly influenced by the predominant period of the ground motion. Detailed results of dispersion for site classes B, C, and D and behavior types A, B, and C are also presented in Appendix C.

3.4 Evaluation of Coefficient Method (FEMA 356)

3.4.1 Summary of the Approximate Method

The determination of the target displacement in the simplified nonlinear static procedure (NSP) known as the displacement Coefficient Method is primarily described in the FEMA 356 document (Section 3.3.3.3.2). According to this document, the target displacement, δ_t, which corresponds to the displacement at roof level, can be estimated as

$$\delta_t = C_0 C_1 C_2 C_3 S_a \frac{T_e^2}{4\pi^2} g \tag{3-9}$$

where:

C_0 = Modification factor to relate spectral displacement of an equivalent SDOF system to the roof displacement of the building MDOF system. It can be calculated from

- the first modal participation factor,
- the procedure described in Section 3.3.3.2.3 in FEMA 356, or
- the appropriate value from Table 3.2 in FEMA 356.

C_1 = Modification factor to relate the expected maximum displacements of an inelastic SDOF oscillator with EPP hysteretic properties to displacements calculated for the linear elastic response.

$$C_1 = \begin{cases} 1.0 & \text{for } T_e \geq T_s \\ 1.0 + \dfrac{(R-1)T_s}{T_e} & \\ \dfrac{}{R} & \text{for } T_e < T_s \end{cases}$$

but not greater than the values given in Section 3.3.1.3.1 (Linear Static Procedure, LSP section) nor less than 1. Values of C_1 in Section 3.3.1.3.1 are

$$C_1 = \begin{cases} 1.5 \text{ for } T_e < 0.1 \text{ s} \\ 1.0 \text{ for } T_e \geq T_s \end{cases}$$

with linear interpolation used to calculate C_1 for the intermediate values of T_e.

The limit imposed on C_1 by Section 3.3.1.3.1 is often referred to as "C_1 *capping*."

C_2 = Modification factor to represent the effect of pinched hysteretic shape, stiffness degradation, and strength deterioration on the maxi-

mum displacement response. Values of C_2 for different framing systems and structural performance levels (i.e., immediate occupancy, life safety, and collapse prevention) are obtained from Table 3.3 of the FEMA 356 document. Alternatively, C_2 can take the value of one in nonlinear procedures.

C_3 = Modification factor to represent increased displacements due to dynamic *P-Δ* effects. For buildings with positive post-yield stiffness, C_3 is set equal to 1. For buildings with negative post-yield stiffness, values of C_3 are calculated using the following expression:

$$C_3 = 1.0 + \frac{|\alpha|(R-1)^{3/2}}{T_e} \qquad (3\text{-}10)$$

where:

T_e = Effective fundamental period of the building computed in accordance with section 3.3.3.2.5.

T_s = Characteristic period of the response spectrum, defined as the period associated with the transition from the constant-acceleration segment of the spectrum to the constant-velocity segment of the spectrum.

R = Ratio of elastic strength demand to calculated strength capacity.

S_a = Response spectrum acceleration, at the effective fundamental period and damping ratio of the building.

g = Gravitational acceleration.

3.4.2 Maximum Displacement Ratio (Coefficient C_1)

Coefficient C_1 is the ratio of the maximum displacement for inelastic response of a SDOF oscillator with non-degrading hysteretic behavior to the maximum displacement had the oscillator remained elastic. Figure 3-9 shows the variation of C_1 for site class B using a characteristic period T_s equal to 0.4 s. This characteristic period value is computed by applying the procedure described in Sections 1.6.1.5 and 1.6.2.1 of the FEMA 356 document. For the evaluation of the FEMA 356 Coefficient Method, this study utilized characteristic periods equal to 0.4 s,

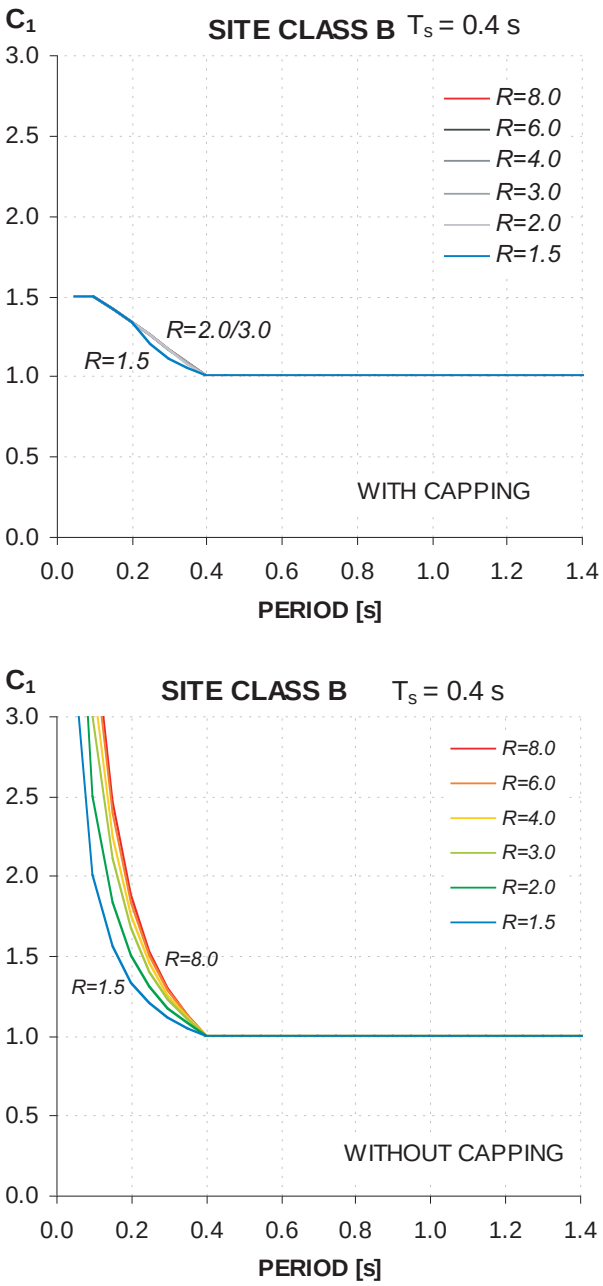

Figure 3-9 Comparison of coefficient C_1 in FEMA 356 with and without capping.

0.55 s, 0.6 s and 1.0 s for site classes B, C, D, and E, respectively. These characteristic periods are representative of the periods computed according to FEMA 356 when using large ground motion intensities for which the system is expected to behave nonlinearly. Figure 3-9 shows a comparison between the values of C_1 with the limitation (capping), as defined in FEMA 356 Section 3.3.3.3.2, and without the limitation.

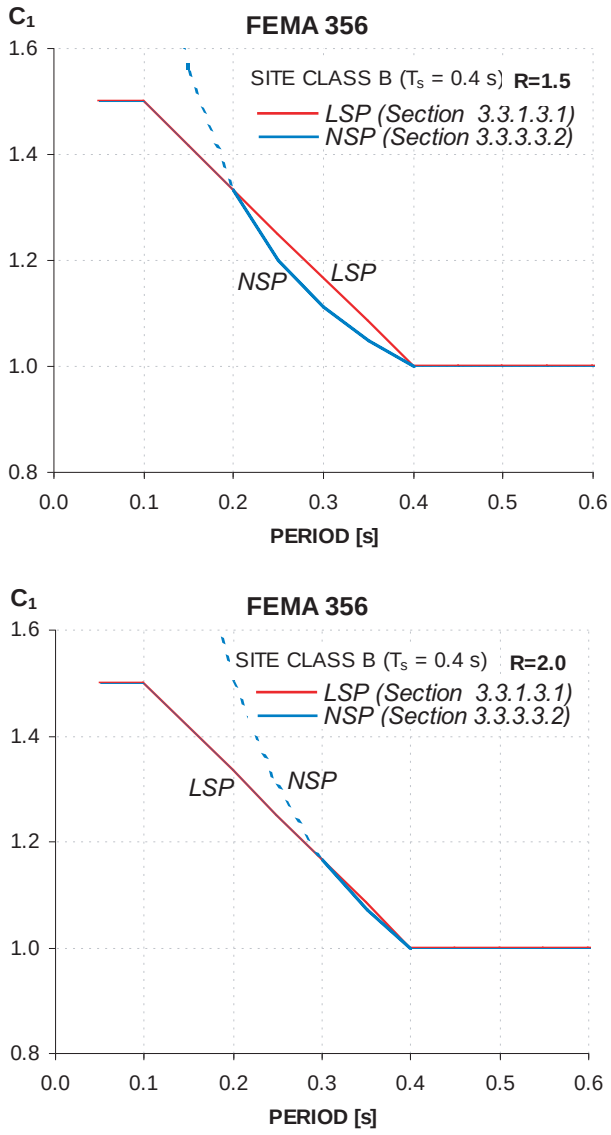

Figure 3-10 A close up view of the effect of the capping limitation of C_1 coefficient.

The most important observation that can be made from Figure 3-9 is that with the limitations on C_1 imposed by FEMA 356 for structures with short periods of vibration (often referred to as "capping"), the C_1 coefficient becomes independent of the lateral strength of the structure. This means that changes in R do not produce changes in lateral displacement demand. Figure 3-10 shows a close-up view of the C_1 coefficients for site class B as a function of period. For R = 1.5 (top graph) the equation specified in the NSP will control this coefficient for periods between 0.2 and 0.4 s, while for R = 2.0 (bottom graph) the NSP equation has only a minimal effect for periods between 0.3 and 0.4 s. For

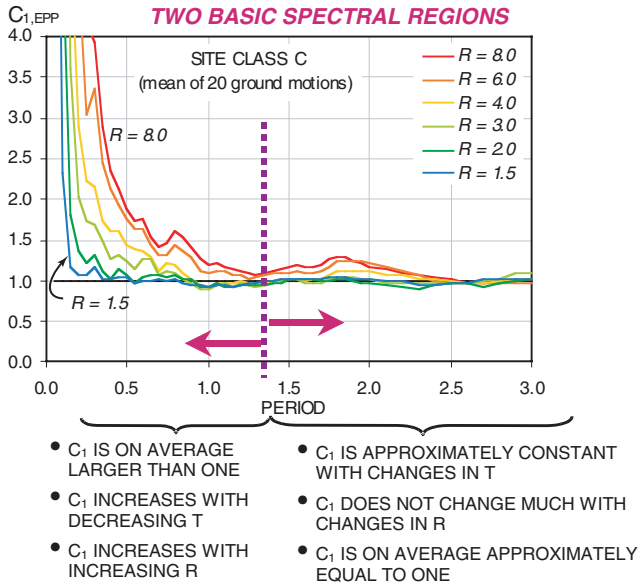

Figure 3-11 Variation of mean C_1 computed for the elastic perfectly plastic (EPP) model when subjected to ground motions recorded on site class C.

values of R approximately larger than 2.5, the capping equation will always control the value of C_1.

Mean values of the computed ratio of the maximum displacement for inelastic response of a SDOF oscillator with non-degrading hysteretic behavior, to the maximum displacement had the oscillator remained elastic when subjected to 20 ground motions recorded on site class C, is shown in Figure 3-11. It can be seen that this ratio is clearly different in two spectral regions. Based on this figure, the following observations can be made:

- For periods longer than about 1.0 s, the computed C_1 ratio is on average fairly insensitive to the level of strength (i.e., the value of C_1 does not change much with changes in R).
- In the long-period spectral region, the computed C_1 ratio is on average independent of the period of vibration (i.e., the value of C_1 does not change much with changes in T).
- The equal-displacement approximation is a relatively good approximation of the expected value of C_1 in the long-period spectral region (i.e., the value of C_1 is approximately equal to one when $T >$ 1.3).

- In the short-period region, inelastic displacements are on average larger than elastic displacements (i.e., C_1 is larger than one).
- In the short-period region, the value of C_1 is highly dependent (i.e., very sensitive) on the level of lateral strength. In general, C_1 increases as R increases (i.e., as the lateral strength decreases).
- In the short-period region, the value of C_1 is sensitive to changes in the period of vibration. In general, for a given R, a decrease in period produces an increase in C_1.
- The transition period dividing the region in which the equal-displacement approximation underestimates displacement, from the region in which this approximation applies (short- versus long-period region), increases as the lateral strength decreases (as R increases).

Figure 3-12 presents a comparison of mean values of coefficient C_1 generated from the nonlinear response-history analyses for site classes B, C, and D. The transition period dividing the region in which the equal-displacement approximation underestimates displacements, from the region in which this approximation is valid, increases as the site becomes softer. For site classes B and R smaller than 8, this period is approximately 1.0 s; for site class C it is approximately 1.1 s; and for site class D it is approximately 1.4 s.

Figure 3-13 compares mean values of the computed ratio of the maximum displacement for inelastic response of a SDOF oscillator with elasto-plastic hysteretic behavior to the maximum displacement had the oscillator remained elastic when subjected to 20 ground motions recorded on site B to the approximate coefficient C_1 specified in FEMA 356.

The FEMA 356 transition period, dividing the region in which the equal-displacement approximation underestimates displacements, from the region in which this approximation is valid, is shorter than that observed for the ground motions used in this study. For example, for site class B, the transition period in FEMA 356 is 0.4 s while results from nonlinear response-history analyses suggest that this period should be about twice as long. The transition periods that can be observed from these nonlinear response-history analyses in Figure 3-12 (approximately 1.0 s, 1.1 s and 1.4 s for site classes B, C and D, respectively) are all significantly longer than those specified in FEMA 356 (0.4 s, 0.55 s, 0.6 s, for site classes B, C, and D, respectively).

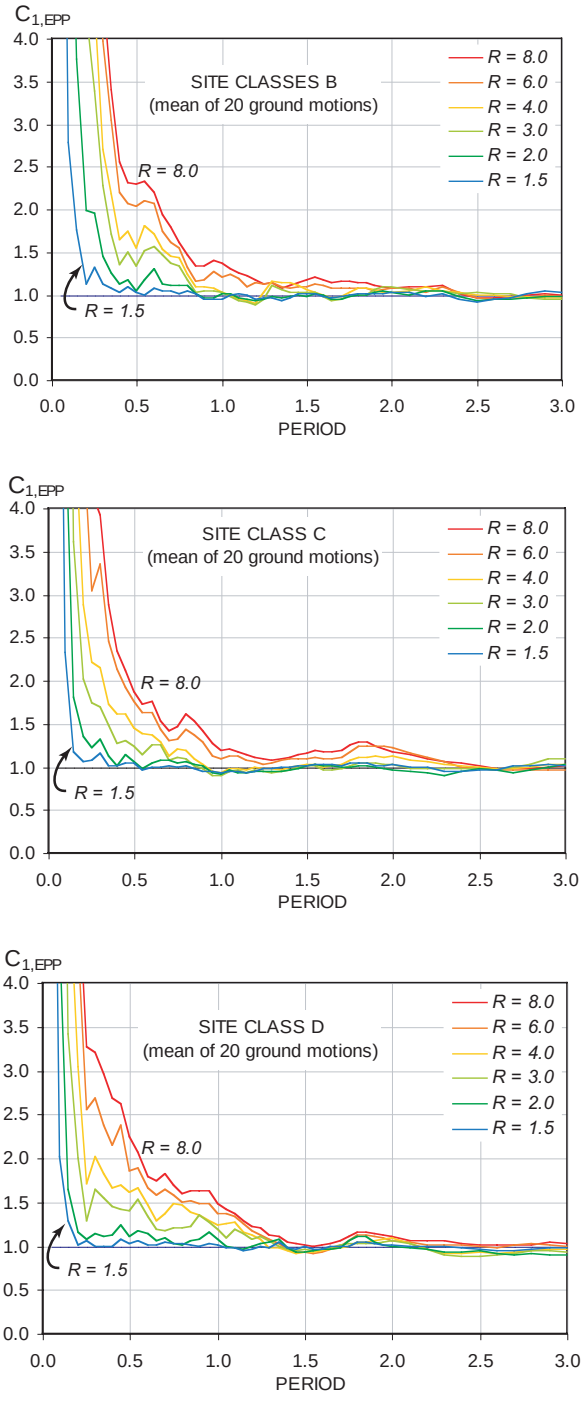

Figure 3-12 Mean coefficient C_1 for site classes B, C and D.

While results from nonlinear response-history analyses indicate a strong sensitivity of the computed C_1 ratio with changes in R for short periods, the capping in FEMA 356 practically eliminates this sensitivity to lateral strength. For example, mean inelastic displacement ratios computed from response-history analyses for a period of 0.3 s suggest that a change in R

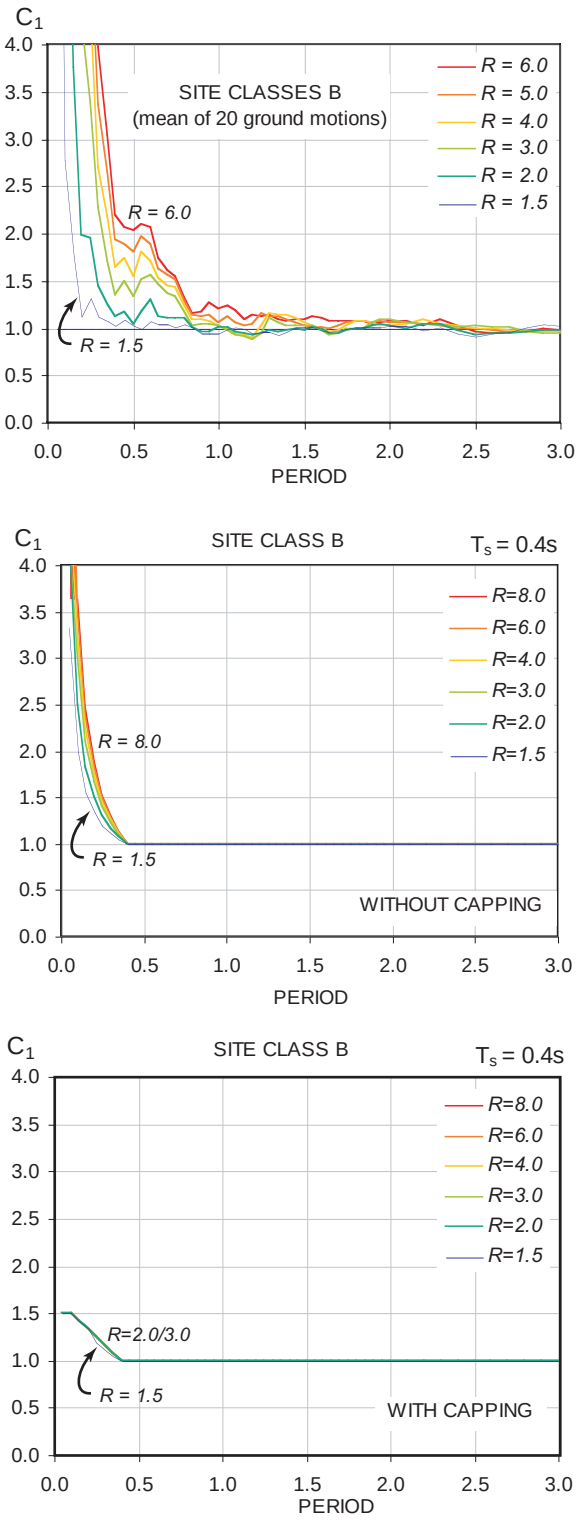

Figure 3-13 Comparison between the mean C_1 computed from nonlinear response-history analyses to C_1 in FEMA 356 (non-capped and capped).

from 2 to 8 almost triples the value of C_1, while the capped coefficient in FEMA 356 leads to the conclusion that the displacement of these systems is the same regardless of the lateral strength of the structure.

In the absence of the cap on C_1, the equation currently used in FEMA 356 to estimate this coefficient in section 3.3.3.3.2 does not capture the effect of changes in lateral strength on displacement demands. For example, for SDOF systems with periods of 0.3 s, one with $R = 2$ and the other with $R = 8$, the expression in FEMA 356 would indicate that the displacement demand in the weaker system would be only about 15% larger than the displacement demand in the stronger system, while response-history analyses indicate a much larger sensitivity to lateral strength.

Figure 3-14 shows inelastic displacement ratios computed for two ground motions recorded in very soft soil sites in the San Francisco Bay Area during the 1989 Loma Prieta earthquake. It can be seen that despite being in the same site class, the inelastic displacement ratios can be very different. For example, for a structure with a 1 s period and $R = 6$ at the Larkspur site C_1 can reach 2.8 (displacement for the inelastic oscillator 2.8 times larger than the maximum elastic), while at the Emeryville site it is 0.65 (displacement for the inelastic oscillator smaller than the maximum elastic). In order to obtain a better characterization of maximum displacement ratios, periods of vibration were normalized by the predominant period of the ground motion, as first proposed by Miranda (1991, 1993). The predominant period, T_g, of the ground motion is computed as the period of vibration corresponding to the maximum 5% damped relative-velocity spectral ordinate. Examples of the computation of T_g for these two recording stations are shown in Figure 3-15. The resulting inelastic displacement ratios are shown in Figure 3-16, where it can be seen that when the periods of vibration are normalized, a better characterization of displacement demands is obtained. As shown, inelastic displacement ratios at soft soil sites are characterized by values larger than one for normalized periods smaller than about 0.7, values smaller than one for normalized periods between 0.7 and 1.5 s, and values approximately equal to one for longer normalized periods.

Mean inelastic ratios computed for 20 ground motions for site class E are shown in Figure 3-17. The same trend observed in individual records is preserved for the mean. Additional information on inelastic displacement demands of structures on very soft soil can be found in Ruiz-García and Miranda (2004).

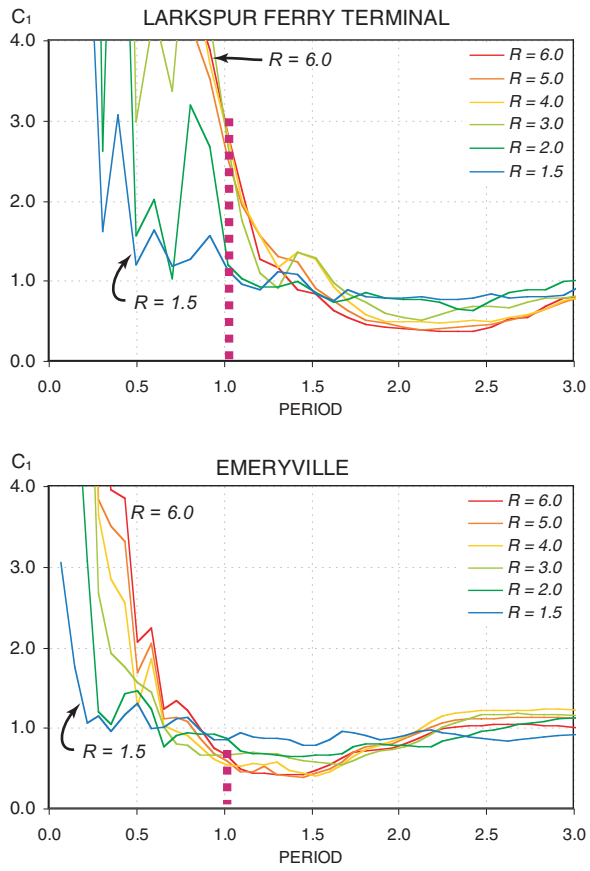

Figure 3-14 Variation of C_1 for two individual ground motions recorded on soft soil E.

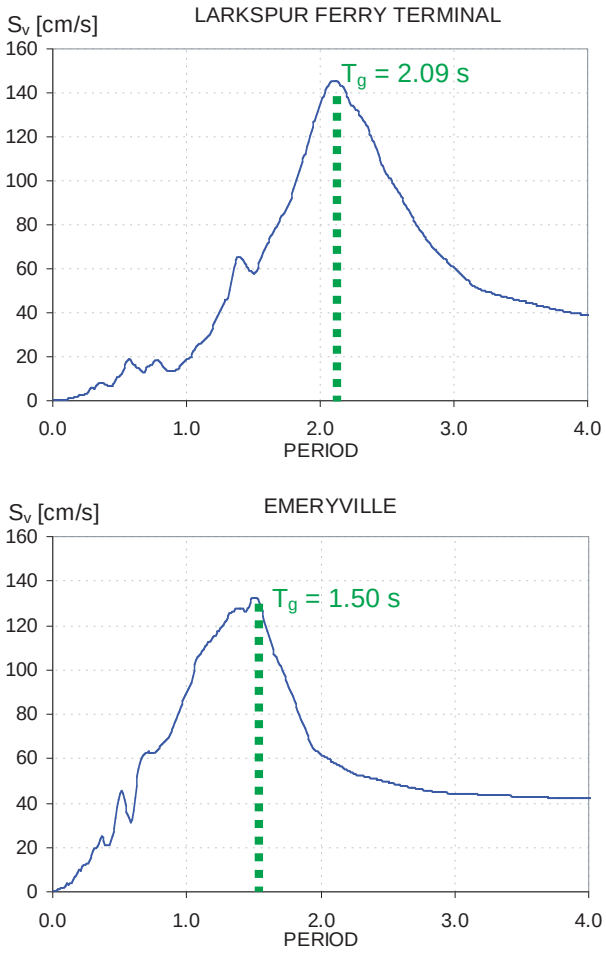

Figure 3-15 Predominant ground motion periods for the soft soil records obtained at Larkspur Ferry Terminal and Emeryville during the 1989 Loma Prieta earthquake.

Inelastic displacement ratios for near-fault ground motions influenced by forward directivity effects can be computed in an analogous manner by normalizing the periods of vibration by the pulse period, which was computed using the same procedure as for soft soils (refer to Figure 3-15).

The procedure described in Section 3.2 was used to calculate mean errors associated with the FEMA 356 specifications for the coefficient C_1 when compared with the nonlinear response-history benchmark. Figure 3-18 shows mean errors corresponding to maximum displacement demands computed using FEMA 356 with and without capping when subjected to ground motions recorded on site classes B and C. These mean errors correspond to displacements computed with $C_2 = C_3 = 1$, normalized by the benchmark displacement demands computed with an EPP hysteretic model. It can be seen that, in general, the results are very good for periods of vibration larger than 1.0, where the equal-displacement approximation provides acceptable results with only small overestimations.

In Figure 3-18, it is evident that for site class B and periods between 0.4 s and 1.0 s, the underestimation of the transition period leads to underestimation of maximum displacement. Underestimation increases as R increases. For example, for a period of 0.4 s, benchmark displacements are on average 1.8 times larger than approximate displacements for $R = 8$. Similar underestimations are produced for site class C.

For periods smaller than 0.4 s in the case of site class B, and for periods smaller than 0.55 s in the case of site class C, the use of capping on C_1 leads to large underestimation of displacements when R is larger than 2. When the capping is removed, in some cases large

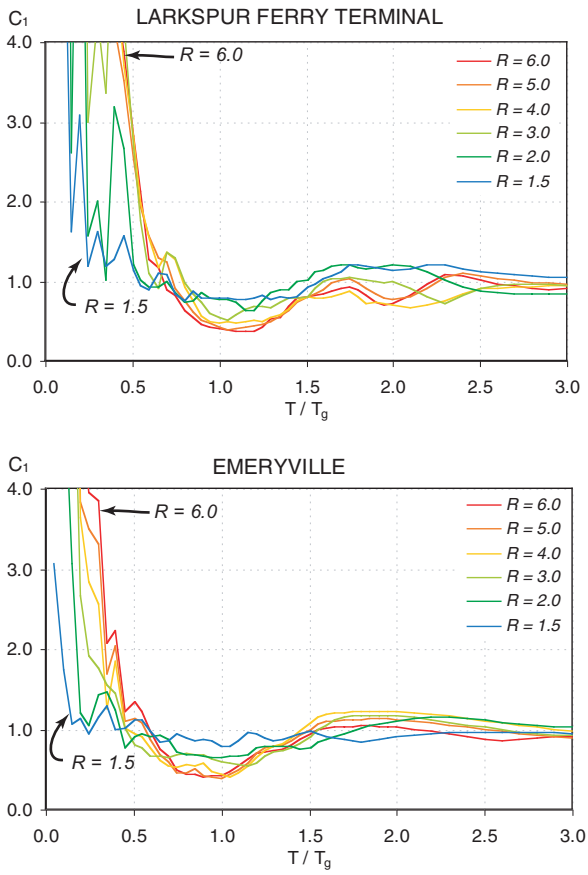

Figure 3-16 C_1 values of Larkspur Ferry Terminal and Emeryville soft soil records for normalized periods of vibration with respect to dominant ground motion periods of each record.

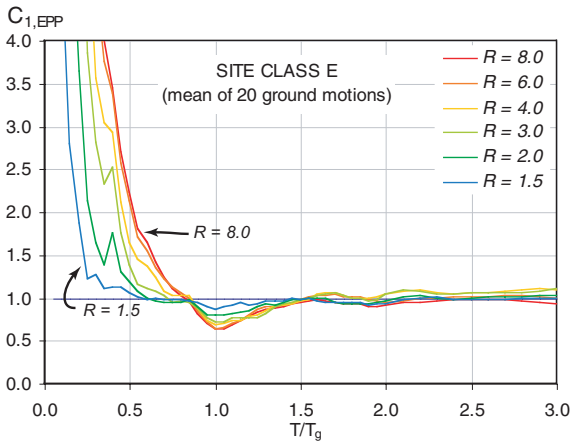

Figure 3-17 The variation of mean C_1 values for site class E.

underestimations of displacements are produced while in other cases large overestimations of displacements are computed. This suggests that the variation of C_1 with changes in period and lateral strength as specified in FEMA 356 could be improved.

3.4.3 *Degrading System Response (Coefficient C_2)*

The coefficient C_2 is a modification factor to represent the effect of pinched hysteretic shape, stiffness degradation, and strength deterioration on the maximum displacement response according to FEMA 356. Values of C_2 for implementation in FEMA 356 depend on the type of structural framing system and structural performance levels being considered (i.e., immediate occupancy, life safety, and collapse prevention). Values of coefficient C_2, computed according to Table 3-3 in FEMA 356, are shown in Figure 3-19.

Benchmark ratios of the maximum displacement demand were calculated by dividing the maximum displacement for the stiffness-degrading oscillator (SD) model by that for the EPP model when both were subject to actual ground motions. This ratio thus corresponds with the coefficient C_2. Mean ratios were calculated for the different site classes. An example for ground motions recorded on site class D is shown in Figure 3-20. With the exception of periods of vibration smaller than about 0.6 s, the maximum displacements of SD models are on average slightly smaller (3% to 12%) than that of the EPP systems. Although this may seem surprising considering the smaller hysteresis loops of the SD model, the results shown in this figure are consistent with previous investigations (Clough, 1966; Clough and Johnston, 1966; Chopra and Kan, 1973; Powell and Row, 1976; Riddel and Newmark, 1979; Mahin and Bertero, 1981; Gupta and Kunnath, 1998; Foutch and Shi, 1998; and Gupta and Krawinkler, 1998). The coefficient C_2 specified in FEMA 356, in contrast, increases lateral displacements in this period range.

For periods of vibration smaller than about 0.6 s, lateral displacement of SD systems are generally larger than those of non-degrading EPP systems. Differences increase with increasing R. This observation is similar to observations of several of the studies mentioned previously. Values of C_2 in the period range specified in FEMA 356 are generally higher than those computed for relatively strong SD systems ($R < 3$) but smaller than those computed for relatively weak SD systems.

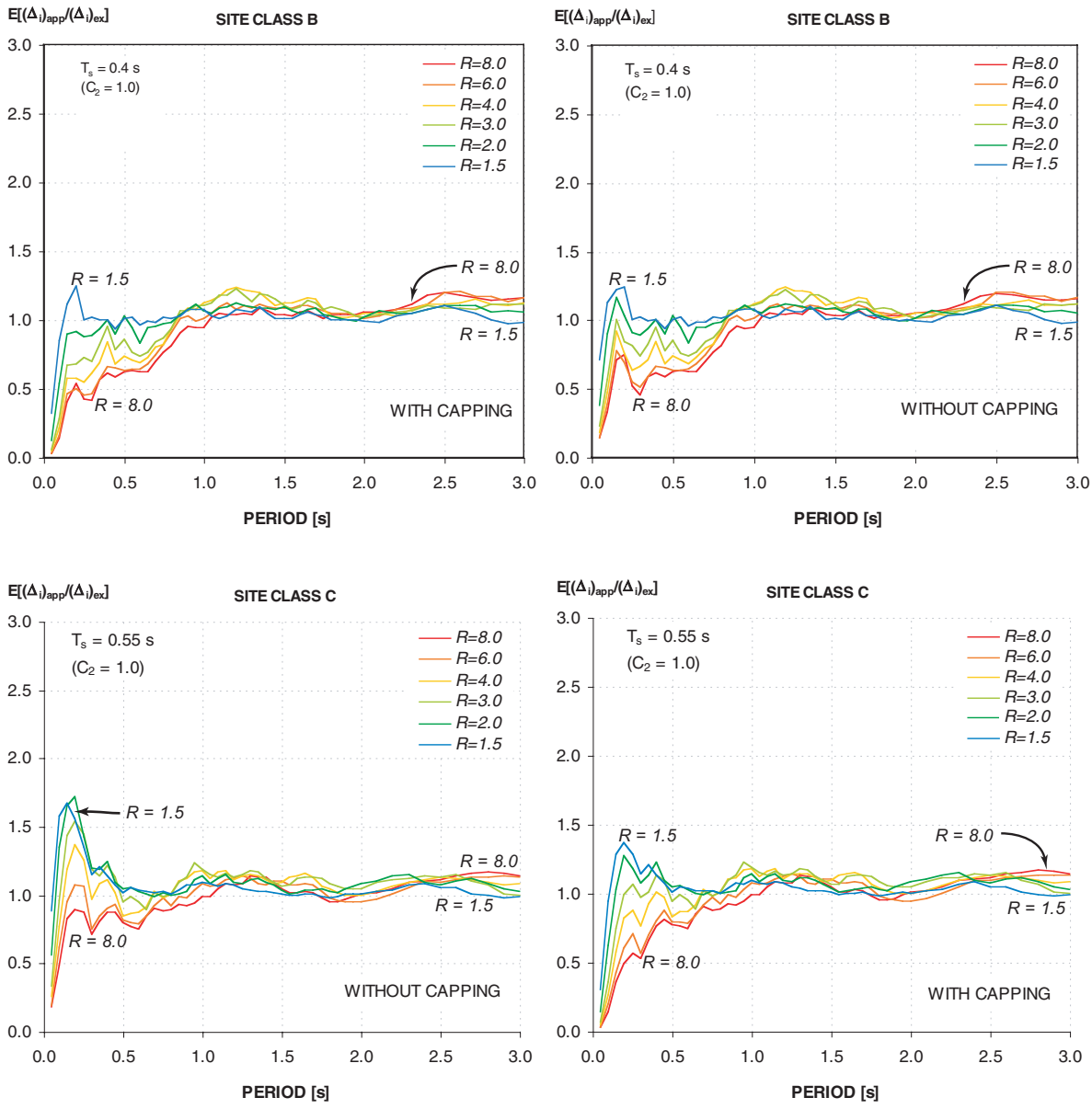

Figure 3-18 Mean error statistics of capped and not capped C_1 values for the ground motions recorded in site classes B and C, respectively.

Mean ratios of maximum displacements of strength-and-stiffness degrading (SSD) systems to those of EPP systems are shown in Figure 3-21, which shows very similar trends. However, in the case of periods shorter than 0.8 s, the increase in lateral displacement produced by SSD behavior is larger than that produced by stiffness degradation only. For periods longer than 0.8 s, the maximum displacement of SSD systems is on average equal to that of EPP systems. It should be noted that displacement ratios shown in Figures 3-20 and 3-21 only correspond to mean (average) values and that a very large uncertainty exists, particularly for periods smaller than 0.6 s.

Figure 3-22 presents mean errors calculated from the ratio of the displacements computed with FEMA 356 (with and without capping of C_1) for C_2 computed assuming a life safety structural performance level to the maximum displacements computed with nonlinear response-history analyses using the SD model. Results

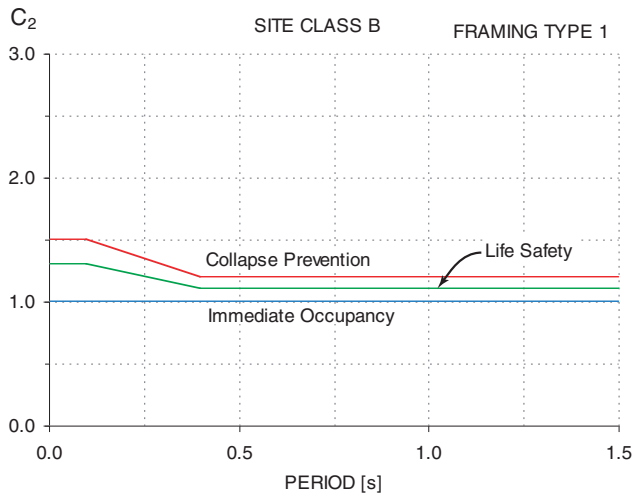

Figure 3-19 A sample variation of C_2 values in accordance with FEMA-356

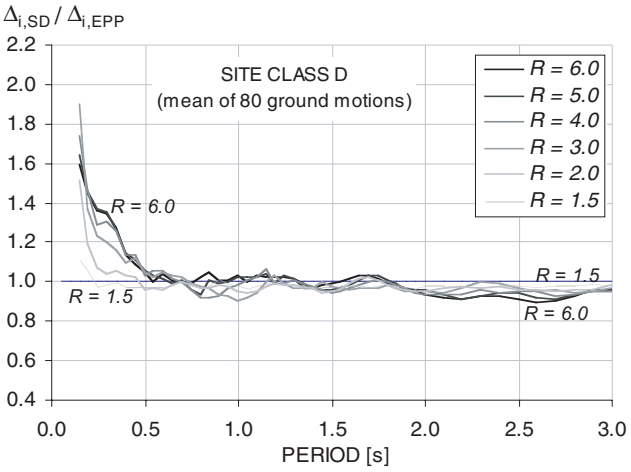

Figure 3-20 Mean displacement ratio of SD to EPP models computed with ground motions recorded on site class D.

presented in this figure are for site class B. For periods of vibration larger that 1.0 s, the simplified method in FEMA 356 overestimates displacements by about 25%. For short periods of vibration, maximum displacements tend to be overestimated for small values of *R* and underestimated for large values of *R*. This trend is more pronounced when capping is included.

Figure 3-23 presents mean errors calculated from the ratio of the displacements computed using C_1 and C_2 as determined from FEMA 356 to maximum displacements computed with nonlinear response-history analyses for the SSD model. Results in this case

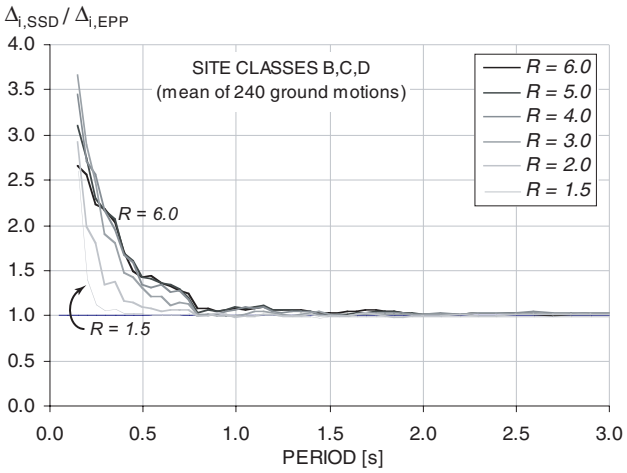

Figure 3-21 Mean displacement ratio of SSD to EPP models computed with ground motions recorded on site classes B, C, and D.

correspond to site class C. The trends are in general similar to those presented in Figure 3-22; however, in this case overestimations are larger and underestimations are smaller.

3.4.4 *P-Δ Effects (Coefficient C_3)*

The displacement modification factor C_3 is intended to account for increased displacements due to dynamic *P-Δ* effects. Displacement modification factors (C_3) computed using Equation 3-10 of FEMA 356 are shown in Figure 3-24. Displacement amplifications increase as the post-yield negative stiffness ratio α decreases (becomes more negative), as *R* increases, and as the period of vibration decreases.

In order to evaluate this coefficient, the model shown in Figure 3-25 was considered. Several studies have shown that systems with negative post-elastic stiffness may exhibit dynamic instability when subjected to earthquake ground motions (Jennings and Husid, 1968; Husid, 1969; Bernal 1987, 1992; MacRae, 1994; and Miranda and Akkar, 2003). An example from Miranda and Akkar (2003) is shown in Figure 3-26. In this figure, the ratio of maximum displacement of the system with negative post-yield stiffness to the maximum displacement in an elastic system is plotted for two systems with a period of 1.0 s as a function of *R* when subjected to a recorded earthquake ground motion. The darker line represents a system with relatively severe negative post-elastic stiffness, while the light line represents a system with more moderate negative post-elastic stiffness. It can be seen that in the system with moderate negative stiffness ($\alpha = -0.06$), *R*

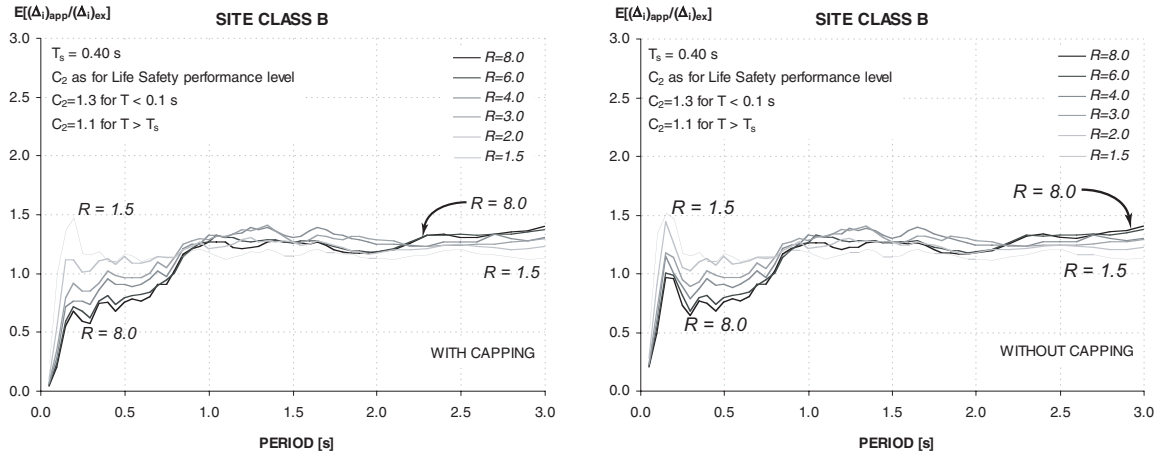

Figure 3-22 The mean error statistics associated with C_1 and C_2 assuming a Life Safety performance level in accordance with FEMA 356 for stiffness degrading (SD) systems.

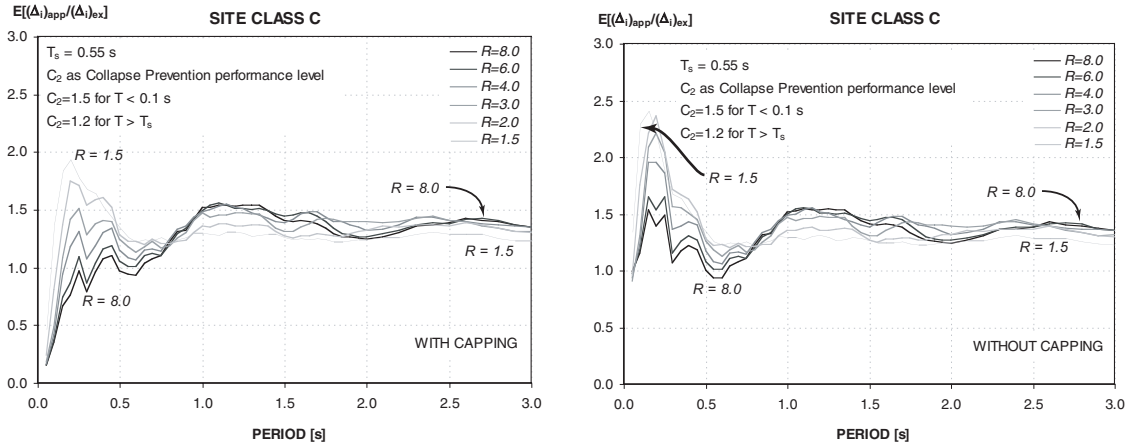

Figure 3-23 The mean error statistics associated with C_1 and C_2 assuming a Collapse Prevention performance level in accordance with FEMA 356 for stiffness and strength (SSD) degrading systems.

can be increased to approximately 4 without any significant increase in lateral displacement. Note that α is a ratio of the post-elastic stiffness to the elastic stiffness. Thus, a negative value of α indicates an effective decrease of strength with increasing displacement. If the lateral strength is further decreased (R is further increased), a large, abrupt increase in lateral displacements is produced, and soon after dynamic instability occurs. For the system with more severe negative stiffness ($\alpha = -0.21$), R can only be increased to about 1.8. From this and other similar data, it is clear that systems that may exhibit negative stiffness need to have a minimum lateral strength (an R smaller than a maximum critical value) in order to avoid collapse. Comparison of Figures 3-24 and 3-26 illustrates that this phenomenon is not adequately captured by coefficient C_3 in FEMA 356.

It should be noted that P-Δ effects are equivalent to a type of strength degradation that occurs in a single cycle (in-cycle) of vibratory motion. This differs from cyclic strength degradation that occurs in subsequent cycles modeled with the SSD type oscillator. These two types of strength degradation have different implications with respect to dynamic behavior. Further discussion of this subject is contained in Chapter 4.

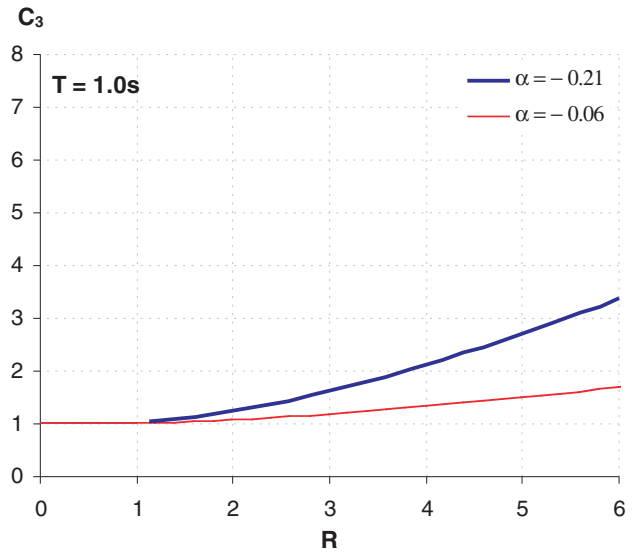

Figure 3-24 The variation of C_3 from FEMA 356 with respect to R for different negative post-elastic stiffness values.

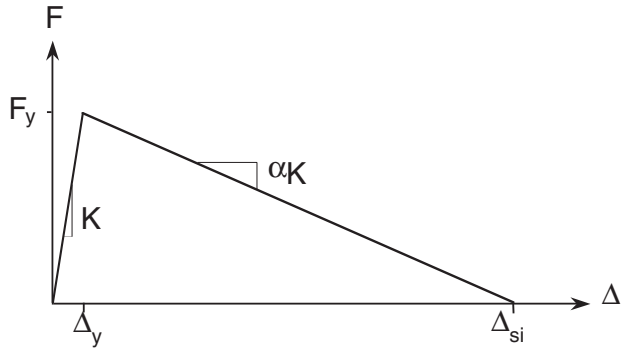

Figure 3-25 Bilinear system with in-cycle negative post-elastic stiffness due to *P-Δ* effects.

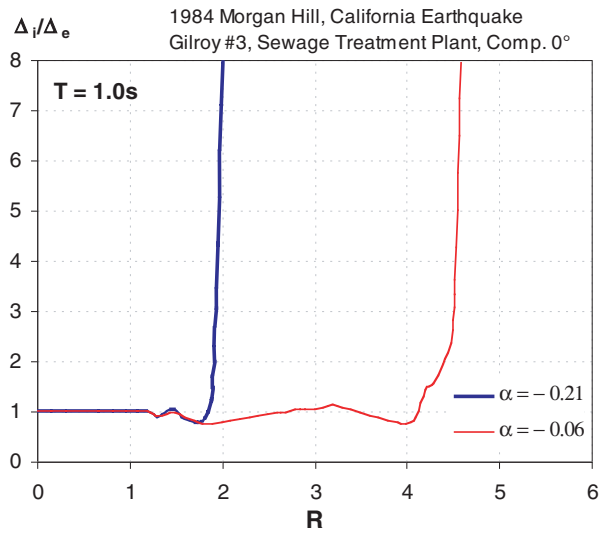

Figure 3-26 Displacement modification factors in SDOF that exhibit in-cycle negative post-yield stiffness.

3.5 Nonlinear Elastic Behavior

The results of the response-history analyses for the nonlinear elastic (NE) model are illustrated in Figure 3-27. Comparison with Figure 3-12 indicates that the maximum nonlinear elastic (NE) response is generally greater than the EPP. The difference varies with both period and strength and can exceed 40% in some cases. Neither ATC-40 nor FEMA 356 explicitly address nonlinear elastic behavior. In reality, it is not found often for typical structural systems. It represents a pure rocking response. Virtually all structures exhibit some hysteretic damping that tends to reduce response from that predicted for pure rocking.

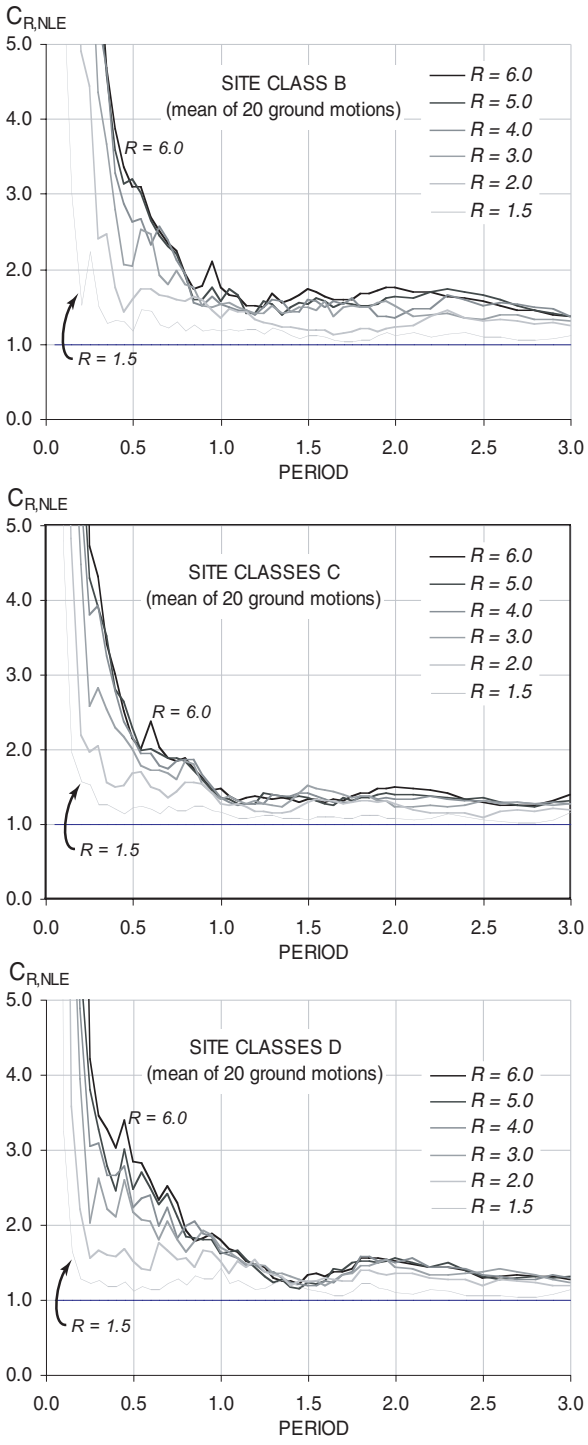

Figure 3-27 Ratio of maximum displacement for a nonlinear elastic (NE) oscillator to elastic response for site classes B, C, and D.

4. Strength Degradation

Loss of lateral strength in structures during an earthquake is an issue of concern for engineers. In general, the nonlinear hysteretic characteristics of most buildings include both stiffness degradation and strength degradation to some extent. Strength degradation, including *P-Δ* effects, can lead to an apparent negative post-elastic stiffness in a force-deformation relationship for a structural model using nonlinear static procedures. The performance implications depend on the type of strength degradation. For structures that are affected by component strength losses, including *P-Δ* effects, occurring in the same cycle as yielding, the negative post-elastic slope can lead to dynamic instability of the structural model. For this reason, a suggestion for a minimum strength for such structures is presented in Section 4.4

4.1 Types of Strength Degradation

Two types of strength degradation during hysteretic response are shown in Figure 4-1. Both oscillators exhibit inelastic stiffness and strength degradation. The oscillator in Figure 4-1a (*cyclic* strength degradation) maintains its strength during a given cycle of deformation, but loses strength in the subsequent cycles. The effective stiffness also decreases in the subsequent cycles. The slope of the post-elastic portion of the curve during any single cycle of deformation is not negative. Figure 4-1b (*in-cycle* strength degradation) illustrates a different type of strength degradation. Note that the degradation occurs during the same cycle of deformation in which yielding occurs, resulting in a negative post-elastic stiffness. This can be due to actual degradation in the properties of the component due to damage. It is also the consequence of *P-Δ* effects that increase demand on components and effectively reduce strength available to resist inertial loads.

4.2 Strength Degradation and SDOF Performance

The strength and stiffness degrading (SSD) oscillators used to evaluate current nonlinear static procedures (see Section 3.2) were similar to those in Figure 4-1a. The results of the evaluation demonstrate that these cyclic strength-degrading oscillators often exhibit maximum displacements that are comparable with those that do not exhibit strength degradation. More importantly, responses are dynamically stable in general, even for relatively weak systems and large ductility.

The in-cycle strength-degrading counterpart discussed in Section 3.4.4, in contrast, can be prone to dynamic instability. Velocity pulses often associated with near-

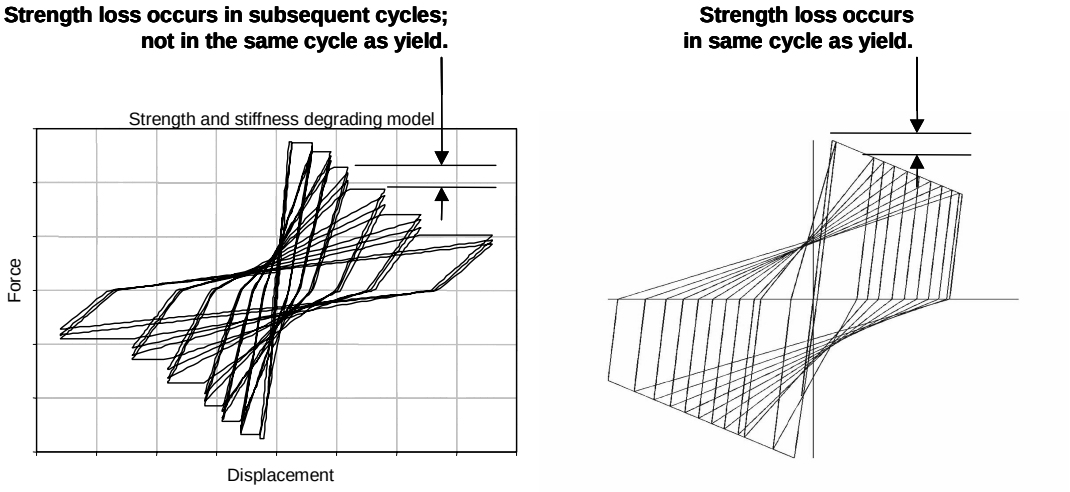

a) Cyclic strength degradation **b) In-cycle strength degradation**

Figure 4-1 Two types of strength degradation.

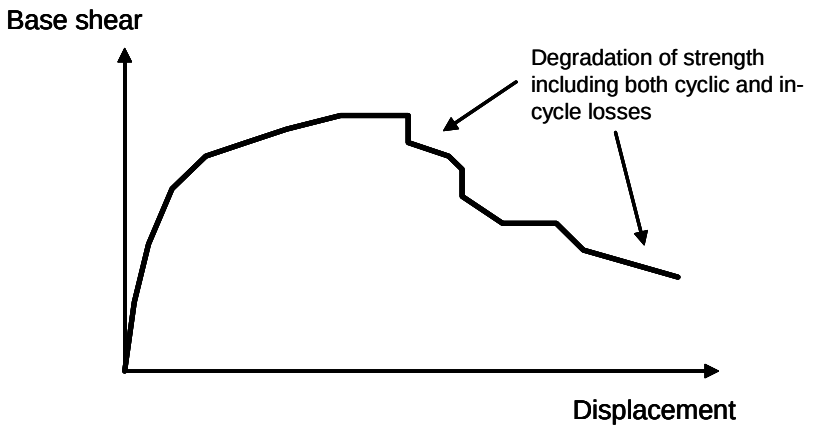

Figure 4-2 Example capacity curve for a medium rise concrete structure

field ground motion records can exacerbate the problem. These pulses can drive the oscillator far into the post-elastic, strength-degrading branch in a single cycle of motion.

4.3 Global Force-Deformation Behavior with Strength Degradation

In many structures, strength degradation is complex. A pushover curve for an example medium-rise reinforced concrete building is shown in Figure 4-2. There is an apparent negative post-elastic stiffness. This might be due to three effects. First, there could be cyclic (that is, from cycle to cycle) strength degradation associated with low-cycle fatigue damage of various components in the lateral-force-resisting system. Interspersed might be in-cycle strength losses due to component damage as deformations increase monotonically. Superimposed on this is the negative slope associated with P-Δ effects, which may or may not be significant. Unfortunately, it is not possible to distinguish between cyclic and in-cycle strength losses solely from information normally available from a nonlinear static analysis. The P-Δ effects are always present and contribute to real negative post-elastic stiffness. The P-Δ effects are simple to separate from the others. Precise separation of the remaining constituents of strength degradation cannot be inferred directly, since the distribution depends on the nature of individual ground motions and the sequence of inelastic behavior among the various components as a lateral mechanism develops.

For purposes of nonlinear static analysis, the calculated relationship between base shear and displacement of a control node (e.g. roof) may be replaced with an idealized relationship to calculate the effective lateral stiffness (K_e), effective yield strength (V_y), and effective positive (α_1) and/or negative (α_2) stiffnesses of the building model, as shown in Figure 4-3. The initial linear portion of the idealized force-displacement curve begins at the origin. A second linear portion ends at a point on the calculated force-displacement curve at the calculated target displacement, or the point of maximum base shear (V_d), whichever is least. The intersection of the two idealized segments defines effective lateral stiffness (K_e), the effective yield strength (V_y), and effective positive post-yield stiffness ($\alpha_1 K_e$). The intersection point is determined by satisfying two constraints. First, the effective stiffness, K_e, must be such that the first segment passes through the calculated curve at a point where the base shear is 60% of the effective yield strength. Second, the areas above and below the calculated curve should be approximately equal. For models that exhibit negative post-elastic stiffness, a third idealized segment can be determined by the point of maximum base shear on the calculated force-displacement curve and the point at which the base shear degrades to 60% of the effective yield strength [the same strength that was used to establish K_e]. This segment defines the maximum negative post-elastic stiffness ($\alpha_2 K_e$). This negative slope approximates the effects of cyclic and in-cycle degradation of strength. Note that the selection of 60% of the yield strength to define this slope is based purely on judgement.

As noted, nonlinear static procedures are not capable of distinguishing completely between cyclic and in-cycle strength losses. However, insight can be gained by separating the in-cycle P-Δ effects from α_2 (see Figure 4-3). An effective post-elastic stiffness can then be determined as

$$\alpha_e = \alpha_{P-\Delta} + \lambda(\alpha_2 - \alpha_{P-\Delta}) \quad (4\text{-}1)$$

where $0 \le \lambda \le 1.0$.

Current knowledge of component behavior as well as unknown characteristics of the future ground motion make it impossible at present to know the correct value of λ. For the present, it is recommended that λ be assigned a value of 0.2 for sites not subject to near field effects and 0.8 for those that are. These values, solely based on judgment, are intended to recognize the potential for dynamic instability that might arise from in-cycle strength losses associated with large impulsive near-field motions while, at the same time, avoid penalizing structures with predominantly cyclic strength loss associated with non-impulsive motions.

4.4 Limitation on Strength for In-Cycle Strength Degradation Including *P-Δ* Effects

When using displacement modification techniques similar to the coefficient method of FEMA 356, it is recommended that the displacement prediction be modified to account for cyclic degradation of stiffness and strength. Chapter 5 presents an improved procedure for calculating the coefficient C_2 for this purpose. It is also suggested that the current coefficient C_3 be eliminated and replaced with a limit on minimum strength (maximum value of R) required to avoid dynamic instability. The same limitation on R_{max} is recommended for the equivalent linearization alternative in ATC-40 as modified in Chapter 6 of this document.

The recommended limitation on the design force reduction, R_{max}, is as follows (see also Figure 4-3 for notation):

$$R_{\max} = \frac{\Delta_d}{\Delta_y} + \frac{|\alpha_e|^{-t}}{4} \quad (4\text{-}2)$$

where

$$t = 1 + 0.15 \ln T \quad (4\text{-}3)$$

If this limitation is not satisfied, then a nonlinear dynamic analysis using representative ground motion records for the site should be implemented to investigate the potential for dynamic instability. The structural model must appropriately model the strength degradation characteristics of the structure and its components.

Equation 4-2 is a simplification of an expression derived by Miranda and Akkar (2003), which was obtained using single-degree-of-freedom systems. It should be noted that significant variability exists in the strength required to avoid dynamic instability; hence, this equation is aimed only at identifying cases where dynamic instability should be further investigated using response history analyses and not as an accurate measure of the lateral strength required to avoid dynamic instability in MDOF structures.

The use of the equivalent linearization techniques (see Chapter 6) can provide initial insight into whether the

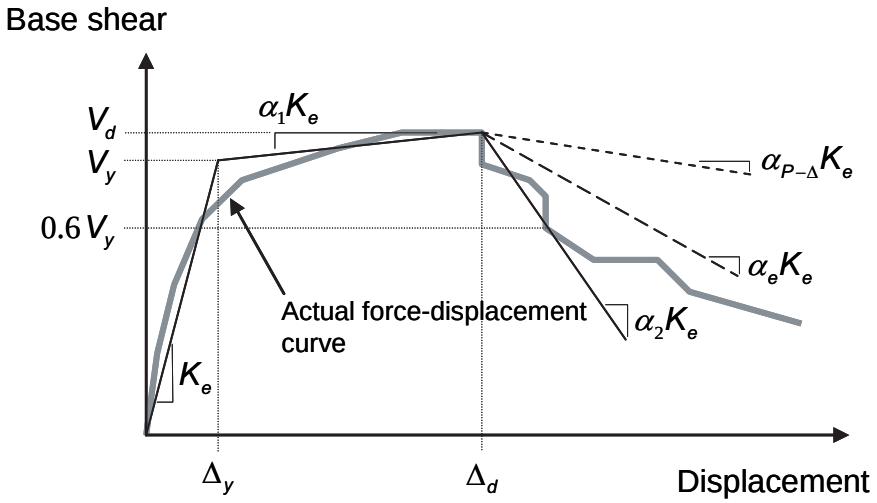

Figure 4-3 Idealized force-displacement curve for nonlinear static analysis

nonlinear dynamic analysis is worthwhile. In particular, solution procedure C produces a locus of potential performance points. If this locus tends to be parallel to and above the capacity curve, then dynamic instability is indicated according to that procedure. However, if the locus intersects the capacity curve, instability is not indicated; nonlinear dynamic analysis may be fruitful in demonstrating this stability.

5. Improved Procedures for Displacement Modification

5.1 Introduction

Based on the evaluation summarized in Chapter 3 and available research data, suggested improvements to the Coefficient Method of FEMA 356 have been developed and are presented in this chapter. Recommendations include several improved alternatives for the basic ratio of the maximum displacement (elastic plus inelastic) for an elastic perfectly plastic SDOF oscillator to the maximum displacement for a completely linear elastic oscillator that is designated as the coefficient C_1 in FEMA 356. This chapter also recommends that the current limitations (capping) allowed by FEMA 356 to the coefficient C_1 be abandoned. In addition, a distinction is recognized between two different types of strength degradation that have different effects on system response and performance, as discussed in Chapter 4. This distinction leads to recommendations for the coefficient C_2 to account for cyclic degradation in strength and stiffness. It is also suggested that the coefficient C_3 be eliminated and replaced with a limitation on strength in accordance with Section 4.4.

The proposed expressions for coefficients in this section are based on empirical data. They have been formulated to provide estimates of expected values based on available analytical results on the response of SDOF oscillators subjected to ground motion records. As noted in the subsequent text, there is dispersion, at times large, in the data. The user should be cognizant of this when applying these procedures in practice.

5.2 Maximum Displacement Ratio (Coefficient C_1)

The coefficient C_1 in FEMA 356 is used along with other coefficients in a nonlinear static procedure known as the Coefficient Method. This form of displacement modification is described in more detail in Section 3.4.1 of this document and in Chapter 3 of FEMA 356. As a result of the work summarized in Chapter 3 and a review of available pertinent research, improvements to the coefficient C_1 can be made. A relatively simple expression is proposed here. As noted in Section 3.4.1, FEMA 356 currently allows the coefficient C_1 to be limited (capped) for relatively short-period structures. It is suggested that this limitation not be used. This may increase estimates of displacement for some structures. However, Chapter 8 presents rational procedures to account for some of the characteristics of short-period structures that may reduce their response to ground motions in lieu of the current limitations on the coefficient C_1.

5.2.1 Simplified Expression

For most structures the following simplified expression may be used for the coefficient C_1:

$$C_1 = 1 + \frac{R-1}{a T_e^2} \tag{5-1}$$

where T_e is the effective fundamental period of the SDOF model of the structure in seconds and R is the strength ratio computed with Equation 3-16 of the FEMA 356 document. The constant a is equal to 130, 90, and 60 for site classes B, C, and D, respectively. For periods less than 0.2 s, the value of the coefficient C_1 for 0.2 s may be used. For periods greater than 1.0 s, C_1 may be assumed to be 1.0.

This expression provides improved estimation of the ratio of peak deformations of inelastic SDOF systems with elasto-plastic behavior to peak deformations of linear single-degree-of-freedom systems. Equation 5-1 is plotted in Figure 5-1. This equation estimates mean values of this ratio. Considerable dispersion (scatter) exists about the mean. For information and discussion of the dispersion of C_1 see Ruiz-Garcia and Miranda (2003). When interpreting results and assessing structural performance, engineers should consider the implications of these uncertainties. For example, the expression can be used with a = 60 for softer sites (class E and F) to estimate displacements, but it is less reliable due to very high dispersion of results in studies of SDOF oscillators for soft sites. Similarly, this equation may not provide completely adequate results for ground motions strongly influenced by forward directivity effects, for the same reason.

Systems with nonlinear elastic hysteretic behavior (e.g. rocking) can have deformation ratios larger than those computed with Equation 5-1. Results of the studies for nonlinear elastic systems (NE) summarized in Section 3.5 indicate that these oscillators can exhibit displacements up to 40% larger than their elasto-plastic counterparts. However, most systems that exhibit rocking also have some hysteretic energy dissipation (as

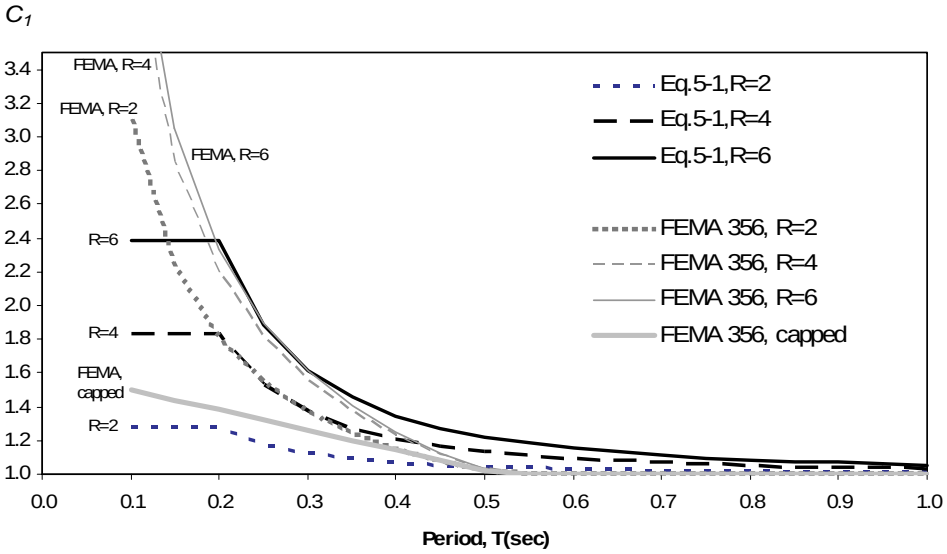

Figure 5-1 Expression for coefficient C_1 (Eqn.5-1 with $a = 90$ for site class C) and current FEMA 356 expression.

opposed to the "pure" rocking of the NE oscillator) that would likely reduce this tendency. Specific recommendations cannot be made at this point and further study is warranted.

Recently, various studies have proposed simplified expressions for C_1. Figure 5-2 compares the C_1 computed with Equation 5-1 assuming site class C to that proposed by other investigators (Aydinoglu and Kacmaz, 2002; Ramirez et al., 2002; Ruiz-Garcia and Miranda, 2003; Chopra and Chintanapakdee, 2003). With exception of the study by Ramirez et al., all deformation ratios plotted in Figure 5-2 are for EPP hysteretic behavior. Deformation ratios by Ramirez et al. shown in Figure 5-2 were computed using constants recommended for systems with post-elastic stiffnesses of 5% of the elastic. The simplified equation proposed here leads to results that are similar to those of previous investigations.

5.2.2 *Limits on Maximum Displacements for Short Periods*

FEMA 356 currently contains a limitation (cap) on the maximum value of the coefficient C_1 as described in Section 3.4.1. As noted in Appendix B, the limitation is used by many engineers. The evaluation of the Coefficient Method in Chapter 3 demonstrates that the limitation contributes to inaccuracy in the prediction of maximum displacements. The authors of FEMA 356 included the limitations for two related reasons. First, there is a belief in the practicing engineering community that short, stiff buildings do not respond to seismic shaking as adversely as might be predicted using simplified analytical models. Indeed, there may be logical explanations for this phenomenon, including various aspects of soil-structure interaction. These factors are often cited qualitatively, along with the observed good performance of such buildings in past earthquakes, as justification for less onerous demand parameters in codes and analytical procedures. Traditional design procedures have evolved accordingly, giving rise to a second reason. The authors of FEMA 356 felt that the required use of the empirical equation without relief in the short-period range would motivate practitioners to revert to the more traditional, and apparently less conservative, linear procedures. FEMA 357, *Global Topics Report on the Prestandard and Commentary for the Seismic Rehabilitation of Buildings* (ASCE, 2000b), has a discussion of the issue and addresses the concern about the limitations (capping) on C_1 and the potential for underestimating the displacement response of weak structures.

In an effort to deal more logically with the characteristics of short-period structures that may reduce their response to strong ground motions from that predicted by current analysis procedures, this document includes the development of rational procedures in Chapter 8. It is suggested that these be used in lieu of the limitation in FEMA 356 to estimate the response of short-period structures.

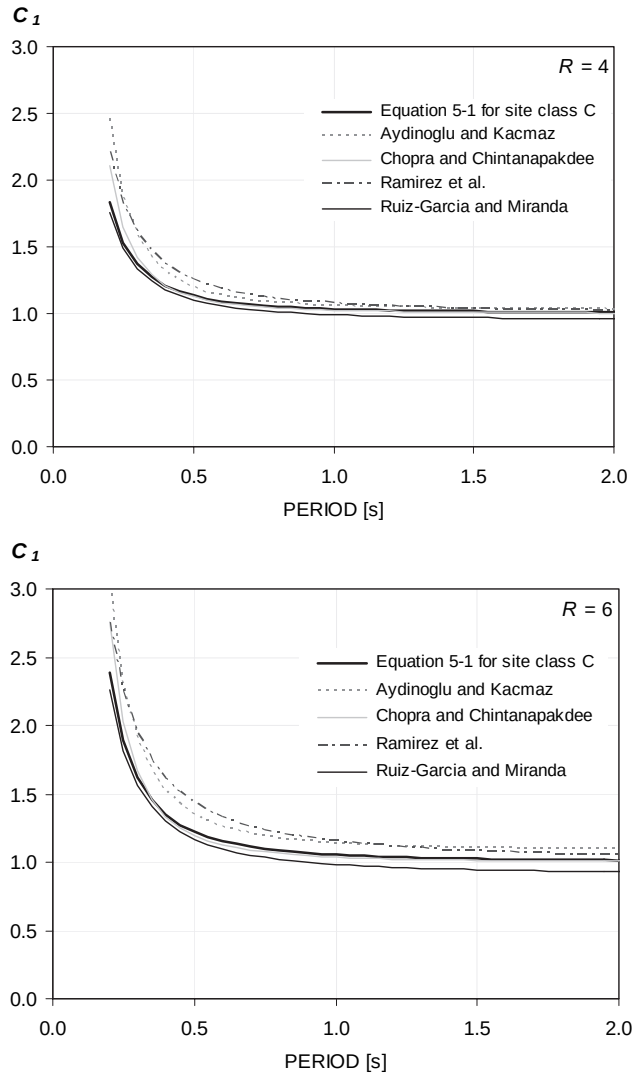

Figure 5-2 Comparison of alternative expressions for the coefficient C_1 for $R = 4$ and $R = 6$ for site class C.

5.3 Adjustment for Cyclic Degradation (Coefficient C_2)

As discussed in Chapter 4, two types of degradation of stiffness and/or strength can affect response. Also, the effects of each type differ from one another. For the purposes of displacement modification procedures in accordance with FEMA 356, it is suggested that the C_2 coefficient represent the effects of stiffness degradation only. The effects of strength degradation are addressed by the suggested limitation presented in Chapter 4. It is recommended that the C_2 coefficient be as follows:

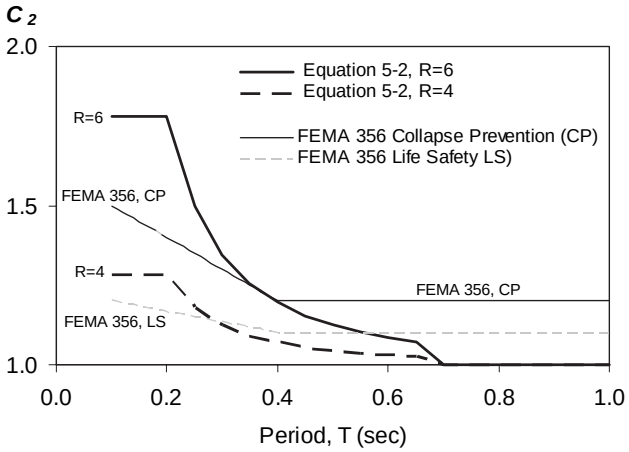

Figure 5-3 Coefficient C_2 from Eq. 4-2 and FEMA 356 for site classes B, C, and D.

$$C_2 = 1 + \frac{1}{800}\left(\frac{R-1}{T}\right)^2 \qquad (5\text{-}2)$$

For periods less than 0.2 s, the value of the coefficient C_2 for 0.2 s may be used. For periods greater than 0.7 sec, C_2 may be assumed equal to 1.0. The expression is plotted in Figure 5-3. The coefficient C_2 need only be applied to structures that exhibit significant stiffness and/or strength degradation.

The degree by which deformation demands are increased by cyclic degradation depends on the characteristics of the hysteretic behavior, which are very sensitive to the structural material, detailing, and ground motion characteristics. Because of the many parameters involved, it is difficult to capture the effects of all possible types of cyclic degradation with a single modifying factor. Equation 5-2 represents a simplification and interpretation of many statistical results with various kinds of cyclically degrading systems. The dispersion of results of SDOF oscillator studies used to formulate the C_2 factor is larger than that of the C_1 factor. It is important to consider this large dispersion when interpreting the results obtained from simplified procedures recommended in this document, particularly for structures with periods of vibration smaller than 0.5s.

5.4 Limitation on Strength to Avoid Dynamic Instability for Nonlinear Static Procedures

The studies of the Coefficient Method in Chapter 3 indicate that global displacement demand is not significantly amplified by degrading strength until a critical point at which dynamic instability may occur. This point is related to the initial strength and period of the oscillator as well as the magnitude of the negative post-elastic stiffness caused by in-cycle strength degradation.

It is suggested that the current coefficient C_3 be eliminated and replaced with a limit on minimum strength (maximum R) required to avoid dynamic instability. The proposed limitation is presented in Section 4.4.

6. Improved Procedures for Equivalent Linearization

6.1 Introduction

This chapter presents an improved equivalent linearization procedure as a modification to the Capacity-Spectrum Method (CSM) of ATC-40. The CSM is a form of equivalent linearization briefly summarized in Sections 2.4 and 3.3.1. Detailed information on equivalent linearization in general and the derivation of the improved procedures are included in Appendix D.

When equivalent linearization is used as a part of a nonlinear static procedure that models the nonlinear response of a building with a SDOF oscillator, the objective is to estimate the maximum displacement response of the nonlinear system with an "equivalent" linear system using an effective period, T_{eff}, and effective damping, β_{eff} (see Figure 6-1). The global force-deformation relationship shown in Figure 6-1 for a SDOF oscillator in acceleration-displacement response spectrum (ADRS) format is termed a capacity curve. The capacity curve shown in Figure 6-1 is developed using the conventional procedures of FEMA 356 or ATC-40. The effective linear parameters are functions of the characteristics of the capacity curve, the corresponding initial period and damping, and the ductility demand, μ, as specified in the following sections.

Recommendations for the improved equivalent linearization procedures rely on the previous procedures in ATC-40, and much of the process remains the same. This chapter focuses on the parts that change. The following section presents new expressions to determine effective period and effective damping. It also includes a technique to modify the resulting demand spectrum to coincide with the familiar CSM technique of using the intersection of the modified demand with the capacity curve to generate a performance point for the structural model. The reduction in the initial demand spectrum resulting from the effective damping may be determined using conventional techniques outlined in Section 6.3. The previous limits on effective damping of ATC-40 should not be applied to these new procedures. However, the user must recognize that the results are an estimate of median response and imply no factor of safety for structures that may exhibit poor performance and/or large uncertainty in behavior. The effective parameters for equivalent linearization are functions of ductility. Since ductility (the ratio of maximum displacement to yield displacement) is the object of the analysis, the solution must be found using iterative or graphical techniques. Three of these are presented in Section 6.4. They have been developed to be similar to those of ATC-40.

Finally, it should be noted that these procedures may not be reliable for extremely high ductilities (e.g., greater than 10 to 12).

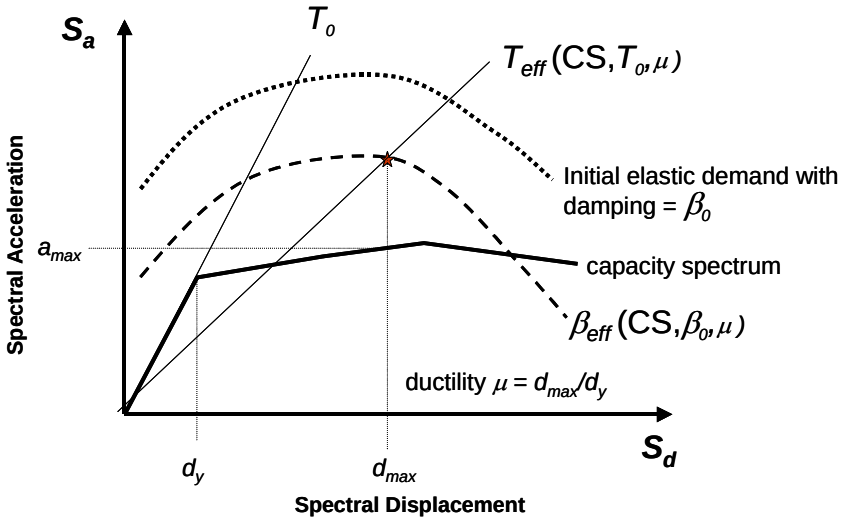

Figure 6-1 Acceleration-displacement response spectrum (ADRS) showing effective period and damping parameters of equivalent linear system, along with a capacity curve.

6.2 Basic Equivalent Linearization Parameters

Optimal equivalent linear parameters (i.e., effective period, T_{eff}, and effective damping, β_{eff}) are determined through a statistical analysis that minimizes, in a rigorous manner, the extreme occurrences of the difference (i.e., error) between the maximum response of an actual inelastic system and its equivalent linear counterpart. Conventionally, the measurement of error has been the mean of the absolute difference between the displacements. Although this seems logical, it might not lead to particularly good results from an engineering standpoint in which the difference between conservative or unconservative estimates is important. This is illustrated in Figure 6-2. It is possible to select linear parameters for which the mean error is zero, as for the broad, flat distribution. However, the narrower curve might represent equivalent linear parameters that provide better results from an engineering standpoint, since the chance of errors outside a –10% to +10% range, for example, are much lower, even accounting for the –5% mean error. This is owing to the smaller standard deviation. See Appendix D for details on the optimization process.

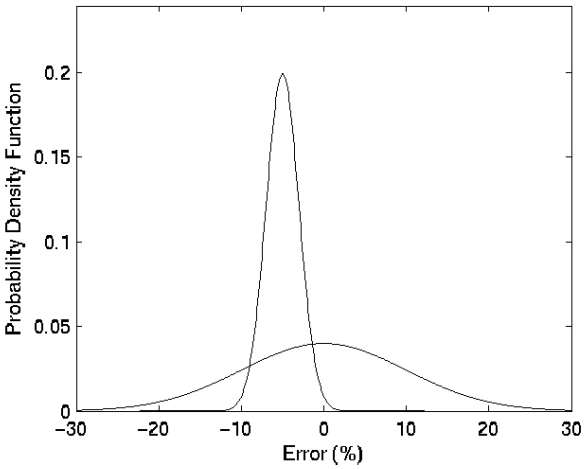

Figure 6-2 Illustration of probability density function of displacement error for a Gaussian distribution.

A variety of different inelastic hysteretic systems have been studied including bilinear hysteretic (BLH), stiffness- degrading (STDG), and strength-degrading behavior as shown in Figure 6-3. Note that the bilinear model (BLH) is the same as the elastic perfectly plastic (EPP) discussed in Chapter 3. Similarly, the stiffness degrading model (STDG) is the same as the SD model in Chapter 3. In contrast, the strength-degrading model (STRDG) differs from the SSD model of Chapter 3. A negative value of the post-elastic stiffness ratio, α, is indicative of in-cycle degradation (see Chapter 4). Also included are parameters that have been optimized for all types of behavior.

6.2.1 Effective Damping

Effective viscous damping values, expressed as a percentage of critical damping, for all hysteretic model types and alpha values have the following form:

For $1.0 < \mu < 4.0$:

$$\beta_{\text{eff}} = A(\mu - 1)^2 + B(\mu - 1)^3 + \beta_0 \qquad (6\text{-}1)$$

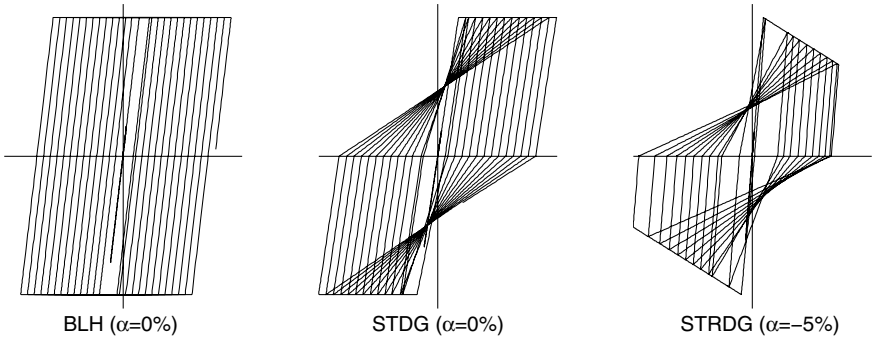

Figure 6-3 Types of inelastic behavior considered. BLH=Bilinear Hysteretic STDG=Stiffness Degrading, and STRDG=Strength Degrading.

For $4.0 \le \mu \le 6.5$:

$$\beta_{\text{eff}} = C + D(\mu - 1) + \beta_0 \qquad (6\text{-}2)$$

For $\mu > 6.5$:

$$\beta_{\text{eff}} = E\left[\frac{F(\mu-1)-1}{[F(\mu-1)]^2}\right]\left(\frac{T_{\text{eff}}}{T_0}\right)^2 + \beta_0 \qquad (6\text{-}3)$$

Values of the coefficients in the equations for effective damping of the model oscillators are tabulated in Table 6-1. Note that these are a function of the characteristics of the capacity curve for the oscillator in terms of basic hysteretic type and post-elastic stiffness, α.

The coefficients in Table 6-1 have been optimized to fit the empirical results for idealized model oscillators having well defined hysteretic behavior designated earlier in this document as Elastic Perfectly Plastic (EPP), Stiffness Degrading (SD) and Strength and Stiffness Degrading (SSD). Real buildings, comprised of a combination of many elements, each of which may have somewhat different strength and stiffness characteristics, will seldom display hysteretic behaviors that match those of the oscillators, exactly. Adaptation of these coefficients to building models with a number of components may be done with caution. If all components exhibit similar behavior (e.g., flexurally controlled concrete with stiffness degradation and strain hardening), then it is reasonable to infer that hysteretic behavior of the overall building will be similar to the behavior of the simple idealized oscillators on which this table is based. For building models in which components exhibit disparate force-deformation behavior, it is less clear which coefficients to use. When in doubt, the practitioner should use the more generally optimized equations presented in the following paragraph.

The following approximate equations for the effective damping value have been optimized for application to any capacity curve, independent of hysteretic model type or alpha value used for the study:

For $1.0 < \mu < 4.0$:

$$\beta_{\text{eff}} = 4.9(\mu - 1)^2 - 1.1(\mu - 1)^3 + \beta_0 \qquad (6\text{-}4)$$

For $4.0 \le \mu \le 6.5$:

$$\beta_{\text{eff}} = 14.0 + 0.32(\mu - 1) + \beta_0 \qquad (6\text{-}5)$$

Table 6-1 Coefficients for use in Equations for Effective Damping

Model	α *(%)*	*A*	*B*	*C*	*D*	*E*	*F*
Bilinear hysteretic	0	3.2	–0.66	11	0.12	19	0.73
Bilinear hysteretic	2	3.3	–0.64	9.4	1.1	19	0.42
Bilinear hysteretic	5	4.2	–0.83	10	1.6	22	0.40
Bilinear hysteretic	10	5.1	–1.1	12	1.6	24	0.36
Bilinear hysteretic	20	4.6	–0.99	12	1.1	25	0.37
Stiffness degrading	0	5.1	–1.1	12	1.4	20	0.62
Stiffness degrading	2	5.3	–1.2	11	1.6	20	0.51
Stiffness degrading	5	5.6	–1.3	10	1.8	20	0.38
Stiffness degrading	10	5.3	–1.2	9.2	1.9	21	0.37
Stiffness degrading	20	4.6	–1.0	9.6	1.3	23	0.34
Strength degrading	-3[a]	5.3	–1.2	14	0.69	24	0.90
Strength degrading	–5[a]	5.6	–1.3	14	0.61	22	0.90

a. Negative values of post-elastic stiffness should be limited to α_e, as discussed in Section 4.3

Table 6-2 Coefficients for use in Equations for Effective Period

Model	α(%)	G	H	I	J	K	L
Bilinear hysteretic	0	0.11	–0.017	0.27	0.090	0.57	0.00
Bilinear hysteretic	2	0.10	–0.014	0.17	0.12	0.67	0.02
Bilinear hysteretic	5	0.11	–0.018	0.09	0.14	0.77	0.05
Bilinear hysteretic	10	0.13	–0.022	0.27	0.10	0.87	0.10
Bilinear hysteretic	20	0.10	–0.015	0.17	0.094	0.98	0.20
Stiffness degrading	0	0.17	–0.032	0.10	0.19	0.85	0.00
Stiffness degrading	2	0.18	–0.034	0.22	0.16	0.88	0.02
Stiffness degrading	5	0.18	–0.037	0.15	0.16	0.92	0.05
Stiffness degrading	10	0.17	–0.034	0.26	0.12	0.97	0.10
Stiffness degrading	20	0.13	–0.027	0.11	0.11	1.0	0.20
Strength degrading	–3[a]	0.18	–0.033	0.17	0.18	0.76	–0.03
Strength degrading	–5[a]	0.20	–0.038	0.25	0.17	0.71	–0.05

a.Negative values of post-elastic stiffness may be limited to α_e, as discussed in Section 4.3

For $\mu > 6.5$:

$$\beta_{\text{eff}} = 19\left[\frac{0.64(\mu-1)-1}{\left[0.64(\mu-1)\right]^2}\right]\left(\frac{T_{\text{eff}}}{T_0}\right)^2 + \beta_0 \qquad (6\text{-}6)$$

6.2.2 Effective Period

Effective period values for all hysteretic model types and alpha values have the following form:

For $1.0 < \mu < 4.0$:

$$T_{\text{eff}} = \left[G(\mu-1)^2 + H(\mu-1)^3 + 1\right]T_0 \qquad (6\text{-}7)$$

For $4.0 \le \mu \le 6.5$:

$$T_{\text{eff}} = \left[I + J(\mu-1) + 1\right]T_0 \qquad (6\text{-}8)$$

For $\mu > 6.5$:

$$T_{eff} = \left\{K\left[\sqrt{\frac{(\mu-1)}{1+L(\mu-2)}} - 1\right] + 1\right\}T_0 \qquad (6\text{-}9)$$

Values of the coefficients in the equations for effective period of the model oscillators are tabulated in Table 6-2. Note that these are a function of the characteristics of the capacity spectrum for the oscillator in terms of basic hysteretic type and post-elastic stiffness, α.

The use of these coefficients in Table 6-2 for actual buildings is subject to the same limitations as for effective damping, as discussed in Section 6.2.1. When in doubt, the practitioner should use the following equations for the effective period value that have been optimized for application to any capacity spectrum, independent of the hysteretic model type or alpha value:

For $1.0 < \mu < 4.0$:

$$T_{\text{eff}} = \left\{0.20(\mu-1)^2 - 0.038(\mu-1)^3 + 1\right\}T_0 \qquad (6\text{-}10)$$

For $4.0 \le \mu \le 6.5$:

$$T_{\text{eff}} = \left[0.28 + 0.13(\mu-1) + 1\right]T_0 \qquad (6\text{-}11)$$

For $\mu > 6.5$:

$$T_{eff} = \left\{0.89\left[\sqrt{\frac{(\mu-1)}{1+0.05(\mu-2)}} - 1\right] + 1\right\}T_0 \qquad (6\text{-}12)$$

Note that these expressions apply only for $T_0 = 0.2$ to 2.0 s.

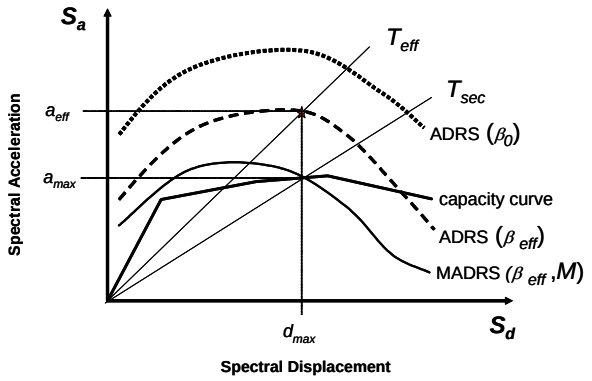

Figure 6-4 Modified acceleration-displacement response spectrum (MADRS) for use with secant period, T_{sec}.

6.2.3 MADRS for Use with Secant Period

The conventional Capacity-Spectrum Method (ATC-40) uses the secant period as the effective linear period in determining the maximum displacement (performance point). This assumption results in the maximum displacement occurring at the intersection of the capacity curve for the structure and a demand curve for the effective damping in ADRS format. This feature is useful for two reasons. First, it provides the engineer with a visualization tool by facilitating a direct graphical comparison of capacity and demand. Second, there are very effective solution strategies for equivalent linearization that rely on a modified ADRS demand curve (MADRS) that intersects the capacity curve at the maximum displacement.

The use of the effective period and damping equations in Sections 6.2.1 and 6.2.2 generate a maximum displacement that coincides with the intersection of the radial effective period line and the ADRS demand for the effective damping (see Figure 6-4). The effective period of the improved procedure, T_{eff}, is generally shorter than the secant period, T_{sec}, defined by the point on the capacity curve corresponding to the maximum displacement, $d_{\max}$. The effective acceleration, a_{eff}, is not meaningful since the actual maximum acceleration, $a_{\max}$, must lie on the capacity curve and coincide with the maximum displacement, $d_{\max}$. Multiplying the ordinates of the ADRS demand corresponding to the effective damping, β_{eff}, by the modification factor

$$M = \frac{a_{\max}}{a_{\text{eff}}} \tag{6-13}$$

results in the modified ADRS demand curve (MADRS) that may now intersect the capacity curve at the performance point. Since the acceleration values are directly related to the corresponding periods, the modification factor can be calculated as:

$$M = \left(\frac{T_{\text{eff}}}{T_{\text{sec}}}\right)^2 = \left(\frac{T_{\text{eff}}}{T_0}\right)^2 \left(\frac{T_0}{T_{\text{sec}}}\right)^2, \tag{6-14}$$

using the equations in Section 6.2.2 for the effective period and recognizing from Equation 3-5 that

$$\left(\frac{T_0}{T_{\text{sec}}}\right)^2 = \frac{1+\alpha(\mu-1)}{\mu} \tag{6-15}$$

where α is the post-elastic stiffness from Equation 6-18.

6.3 Spectral Reduction for Effective Damping

Equivalent linearization procedures applied in practice normally require the use of spectral reduction factors to adjust an initial response spectrum to the appropriate level of effective damping, β_{eff}. They are also a practical way to adjust for foundation damping as presented in Chapter 8. In the case of foundation damping, the initial damping value, β_0, for a flexible-base structural model is modified from the fixed-base linear value, β_i (e.g., 5%). These factors are a function of the effective damping and are termed damping coefficients, $B(\beta_{\text{eff}})$. They are used to adjust spectral acceleration ordinates as follows:

$$(S_a)_\beta = \frac{(S_a)_0}{B(\beta_{\text{eff}})} \tag{6-16}$$

There are a number of options in current procedures for determining $B(\beta_{\text{eff}})$. Some of these are plotted in Figure 6-5. Also shown in the figure is the following expression:

$$B = \frac{4}{5.6 - \ln \beta_{\text{eff}}\,(\text{in } \%)} \tag{6-17}$$

This simple expression is very close to equations specified in both the *NEHRP Recommended Provisions for Seismic Regulations for New Buildings and Other Structures* and the ATC-40 document. It is suggested that Equation 6-17 replace the current specifications.

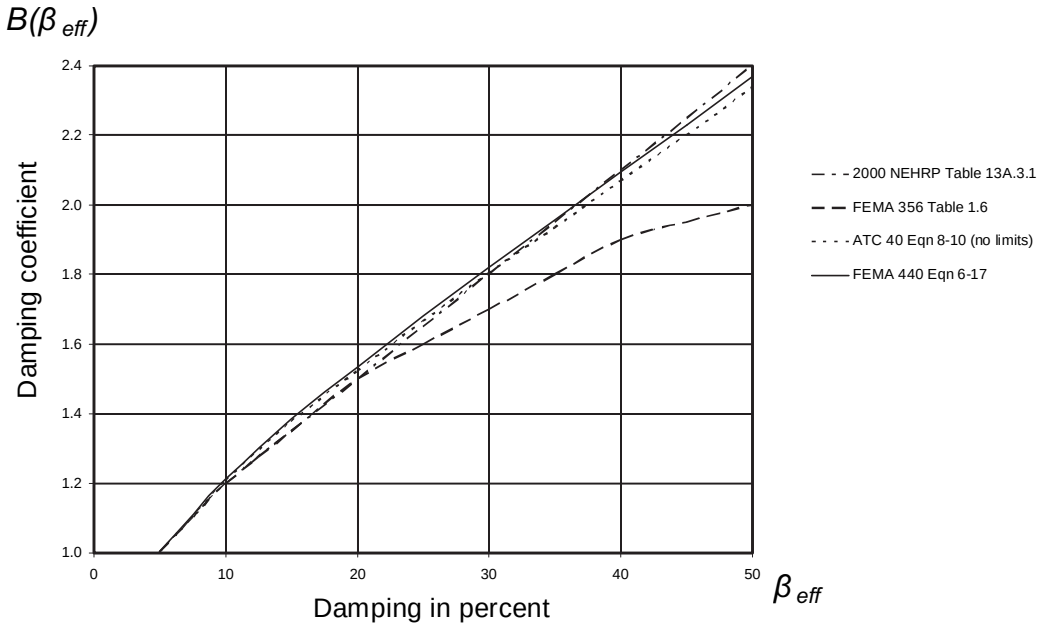

Figure 6-5 Damping coefficients, B, as a function of damping, β_{eff}, from various resource documents.

Note that if the ATC-40 equations are used, then the limits on the reduction should not be applied.

6.4 Solution Procedures

Since the effective period, T_{eff}, and effective damping, β_{eff}, are both functions of ductility demand, the calculation of a maximum displacement using equivalent linearization is not direct and requires an iterative or graphical solution procedure. This is the same as the previous situation with the Capacity-Spectrum Method of ATC-40. This section presents three alternate procedures. Other procedures are possible.

All of the solution procedures presented here require initial steps listed below.

1. Select a spectral representation of the ground motion of interest with an initial damping, β_i (normally 5%). This may be a design spectrum from ATC-40 or FEMA 356, a site-specific deterministic spectrum, or an equal hazard probabilistic spectrum.
2. Modify the selected spectrum, as appropriate, for soil-structure interaction (SSI) in accordance with the procedures in Chapter 9. This involves both potential reduction in spectral ordinates for kinematic interaction and a modification in the system damping from the initial value, β_i to β_0, to account for foundation damping. If foundation damping is ignored, β_0 is equal to β_i.
3. Convert the selected spectrum, modified for SSI when appropriate, to an acceleration-displacement response spectrum format in accordance with the guidance in ATC-40. This spectrum is the initial ADRS demand (see Figure 6-6).
4. Generate a capacity curve for the structure to be analyzed. This is a fundamental relationship for a SDOF model of the structure between spectral acceleration and spectral displacement (see Figure 6-6). Detailed guidance is available in ATC-40 and FEMA 356. Note that the FEMA 356 procedures result in a relationship between base shear and roof displacement. This requires conversion to ADRS format for equivalent linearization procedures (see ATC-40).

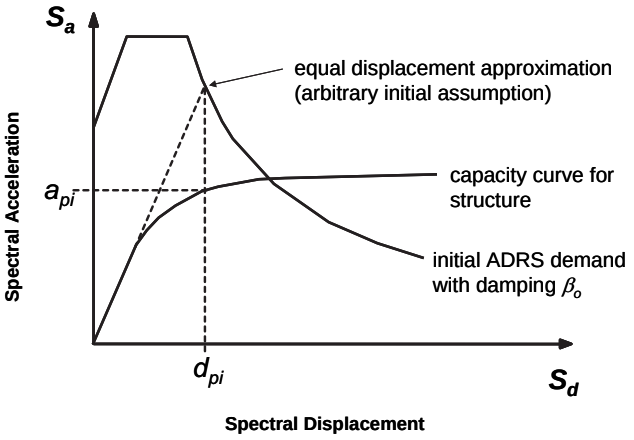

Figure 6-6 Initial ADRS demand and capacity spectrum.

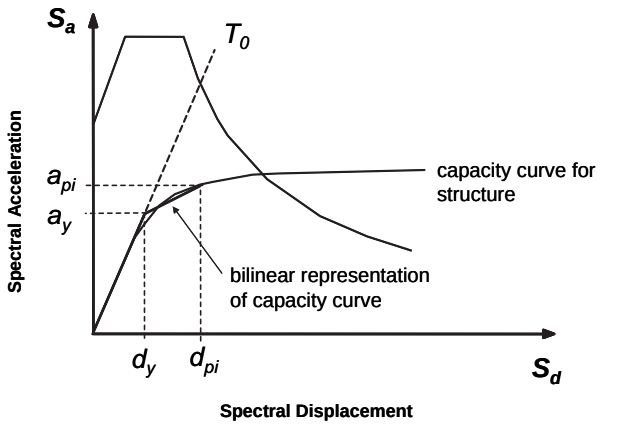

Figure 6-7 Bilinear representation of capacity spectrum.

5. Select an initial performance point (maximum acceleration, a_{pi}, and displacement, d_{pi}). This may be based on an equal-displacement approximation as shown in Figure 6-6 or any other point based on engineering judgment.
6. Develop a bilinear representation of the capacity spectrum in accordance with the procedures in ATC-40. This defines the initial period, T_0, yield displacement, d_y, and yield acceleration, a_y. (see Figure 6-7). Note that these parameters may vary for differing assumptions a_{pi} and d_{pi}
7. For the bilinear representation developed in Step 6, calculate the values of post-elastic stiffness, α, and ductility, μ, as follows:

$$\alpha = \frac{\left(\frac{a_{pi} - a_y}{d_{pi} - d_y}\right)}{\left(\frac{a_y}{d_y}\right)} \tag{6-18}$$

$$\mu = \frac{d_{pi}}{d_y} \tag{6-19}$$

8. Using the calculated values for post-elastic stiffness, α, and ductility, μ, from Step 7, calculate the corresponding effective damping, β_{eff}, (see Section 6.2.1). Similarly calculate the corresponding effective period, T_{eff}, (see Section 6.2.2).

After this step in the procedures, a number of options are available for identifying a single solution. Three possible procedures are described below.

Procedure A (Direct Iteration). In this procedure, the iteration is done to converge directly on a performance point. The ADRS demand spectra generated for the various values of effective damping are not modified to intersect the capacity spectrum, as outlined in Section 6.2.3.

A9. Using the effective damping determined from Step 8, adjust the initial ADRS to β_{eff} (see Section 6.3).

A10. Determine the estimated maximum displacement, d_i, using the intersection of the radial effective period, T_{eff}, with the ADRS for β_{eff}. The estimated maximum acceleration, a_i, is that corresponding to d_i on the capacity curve (see Figure 6-8).

A11. Compare the estimated maximum displacement, d_i, with the initial (or previous) assumption. If it is within acceptable tolerance, the performance point corresponds to a_i and d_i. If it is not within acceptable tolerance, then repeat the process from Step 5 using a_i and d_i, or some other selected assumption (see Section 6.6), as a starting point.

Procedure B (Intersection with MADRS). In this procedure, the performance point is defined as the intersection of the capacity spectrum with the modified ADRS (MADRS). The MADRS demand spectrum is generated by modifying the ADRS for the various values of effective damping, as outlined in Section 6.2.3.

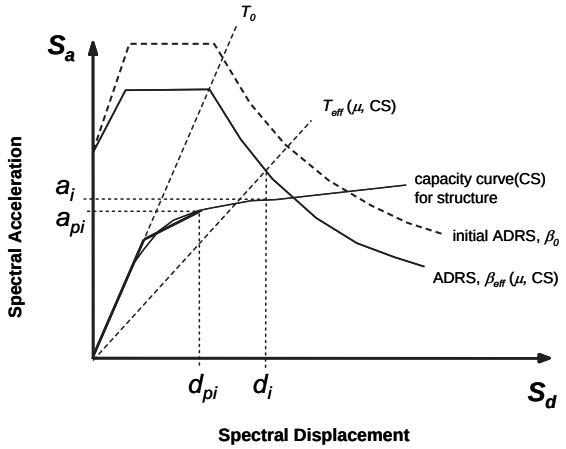

Figure 6-8 Determination of estimated maximum displacement using direct iteration (Procedure A)

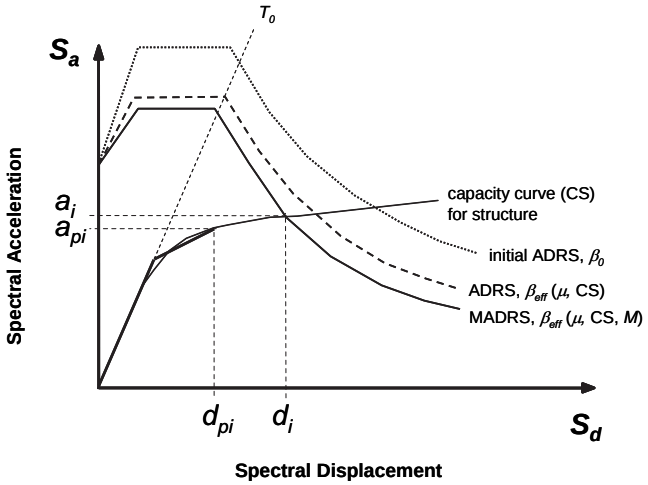

Figure 6-9 Determination of estimated maximum displacement using intersection of capacity spectrum with MADRS (Procedure B)

B9. Using the effective damping determined from Step 8, adjust the initial ADRS to β_{eff} (see Section 6.3).

B10. Multiply the acceleration ordinates only (i.e., not the displacement ordinates) of the ADRS for β_{eff} by the modification factor, M, determined using the calculated effective period, T_{eff}, in accordance with Section 6.2.3 to generate the modified acceleration-displacement response spectrum (MADRS).

B11. Determine the estimate of the maximum acceleration, a_i, and displacement, d_i, as the intersection of the MADRS with the capacity curve (see Figure 6-9).

B12. Compare the estimated maximum displacement, d_i, with the initial (or previous) assumption, d_{pi}. If it is within acceptable tolerance, the performance point corresponds to a_i and d_i. If it is not within acceptable tolerance, then repeat the process from Step 5 using a_i and d_i, or some other selected assumption (see Section 6.6), as a starting point.

Procedure C (MADRS Locus of Possible Performance Points). This approach uses the modified acceleration-response spectrum for multiple assumed solutions (a_{pi}, d_{pi}) and the corresponding ductilities to generate a locus of possible performance points. The actual performance point is located at the intersection of this locus and the capacity spectrum.

C9. Using the effective damping determined from Step 8, adjust the initial ADRS to β_{eff} (see Section 6.3).

C10. Multiply the acceleration ordinates of the ADRS for β_{eff} by the modification factor, M, determined using the calculated effective period, T_{eff}, in accordance with Section 6.2.3 to generate the modified acceleration-displacement response spectrum (MADRS).

C11. A possible performance point is generated by the intersection of the radial secant period, T_{sec}, with the MADRS (see Figure 6-10).

C12. Increase or decrease the assumed performance point and repeat the process to generate a series of possible performance points.

C13. The actual performance point is defined by the intersection of the locus of points from Step 12 and the capacity spectrum.

Note that Procedure C is conducive to an automated process wherein the initial solution is assumed to correspond to a ductility of 1.0 and subsequent trials are set as incrementally greater ductilities (e.g., 2, 3, 4, 5,….).

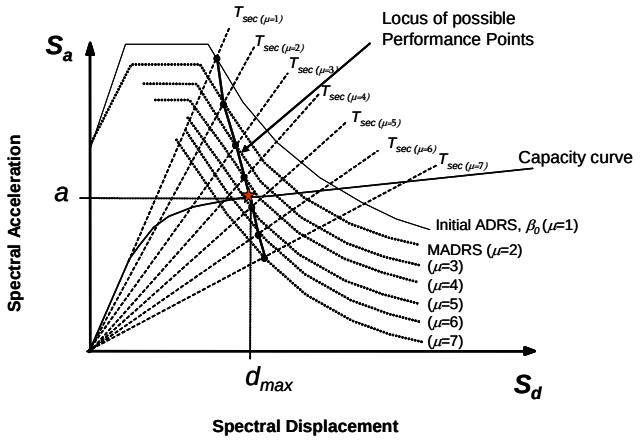

Figure 6-10 Locus of possible performance points using MADRS.

6.5 Approximate Solution Procedure

The following procedure is a simplified MADRS approach based on approximations to the equations in Section 6.2. It uses a MADRS solution procedure similar to that of Section 6.4. The approximations are based upon an EPP single-degree-of freedom system. The results of the approximate procedure are compared to the more rigorous procedures for various types of hysteretic behavior in Figure 6-11. The first seven steps in the procedure are the same as Steps 1 through 7 in the beginning of Section 6.4. The next steps in the approximate procedure are given below.

D8. Using the calculated values for ductility, μ, from Step 7, calculate the corresponding spectral response-reduction factors as

$$\left[\frac{6}{\mu+5}\right] \quad \text{for } 1 \le \mu \le 4 \tag{6-20}$$

$$\left[\frac{75}{\mu+110}\right] \quad \text{for } \mu > 4 \tag{6-21}$$

D9. Using the spectral response-reduction factors from Step 8, multiply both the spectral accelerations and corresponding spectral displacements by the response-reduction factor to generate a reduced ADRS corresponding to the assumed ductility, μ.

D10. Multiply the spectral acceleration ordinates (not the spectral displacement ordinates) of the reduced ADRS by a simplified modification factor

$$M = \frac{1}{\mu} \ge 0.64 \tag{6-22}$$

to generate the approximate modified acceleration-displacement response spectrum (MADRS). It should be noted that for ductilities greater than 1.6 the bounding limit of 0.64 controls this step.

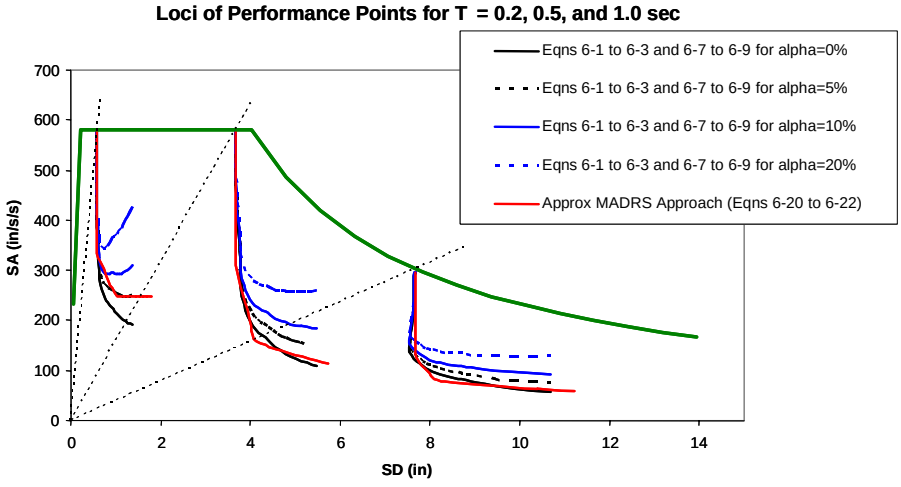

Figure 6-11 Comparison of approximate solution results with results from more detailed procedures.

D11. A possible performance point is generated by the intersection of the radial effective period, T_{eff}, with the MADRS (see Figure 6-9).

D12. Increase or decrease the assumed performance point and repeat the process to generate a series of possible performance points.

D13. The actual performance point is defined by the intersection of the locus of points from Step 12 and the capacity curve. For this approximate procedure, the calculated target displacement must be equal to or greater than the elastic target displacement.

6.6 Iterative Strategy

Subsequent assumptions for the performance point can be calculated by averaging the previous value of the initial assumption d_{pi} and the calculated result d_i, then choosing the corresponding acceleration value from the capacity curve. However, this is not required and some educated guessing and judgment can improve solution time. For example, the initial assumption, d_{pi}, and the resulting estimated maximum displacement, d_i, can be plotted as a point, as shown in Figure 6-12. Note that the actual performance point will fall along the line where the two values are equal. By tracking the subsequent trial point with this type of plot, it is easy to see solution trends. An example with three iterations is shown in Figure 6-12. After the second trial, it is apparent that the performance point is larger than the estimate, as the track of the trial points has not crossed the line of equal displacement. So the third trial assumes a relatively large displacement. The results of the third trial indicate a solution somewhere between the assumptions of Trial 2 and Trial 3.

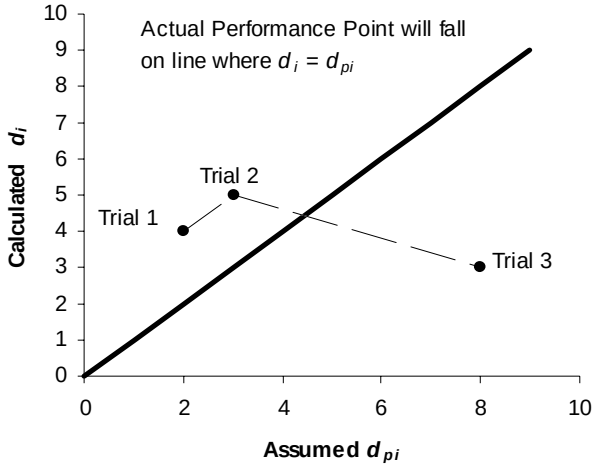

Figure 6-12 Tracking iteration for equivalent linearization by comparing assumed displacement to calculated displacement.

6.7 Limitation on Strength to Avoid Dynamic Instability for Nonlinear Static Procedures

The evaluation of current procedures summarized in Chapter 3 revealed that oscillators that exhibit in-cycle strength degradation can be prone to dynamic instability during strong shaking. The subject is covered in detail in Chapter 4. When using equivalent linearization procedures, the strength of the structural model should be checked in accordance with Section 4.4.

7. Evaluation and Comparison of Improved Nonlinear Static Procedures

7.1 Introduction

Previous chapters have introduced improvements to nonlinear static procedures that are useful for estimating the peak displacement amplitude for a SDOF oscillator subjected to earthquake ground motion. This chapter compares results of those methods with results obtained using nonlinear response-history analyses for ground motion records selected and scaled to be representative of a specific hazard level and site conditions. The ground motion selection and scaling procedures are similar to those specified in the 2000 *NEHRP Recommended Provisions for Seismic Regulations for New Buildings and Other Structures* (BSSC, 2000),[1] and therefore provide an example of the types of results one might obtain in a practice-related application.

Several nonlinear oscillators were selected, having different vibration periods and strengths. The oscillators were assumed to be sited on ground classified as NEHRP Site Class C, with ground motions generated by a fault capable of a strike-slip earthquake of magnitude M_s = 7. Smooth design response spectra were established using the 2000 *NEHRP Recommended Provisions for New Buildings*, scaled for the design-basis earthquake. Furthermore, ground motion records from representative sites and earthquakes were selected and scaled. Displacement amplitudes of the oscillators were calculated by both the nonlinear static procedures and nonlinear dynamic response-history analysis, for comparison purposes.

The scope of the study reported in this chapter is limited by the periods, strengths, and hysteretic behavior of the SDOF oscillators, as well as the number and nature of the ground motions used. The results do not represent a large statistical sample and broad general conclusions should not be drawn solely from these data. Nonetheless, they are illustrative of the types of errors and variations among procedures that should be anticipated when using these simplified analysis techniques.

1.Superseded in 2003 with the FEMA 450 *Recommended Provisions for Seismic Regulations for New Buildings and Other Structures.*

7.2 Summary of Evaluation Procedures

7.2.1 NEHRP Design Response Spectrum

Procedures similar to the 2000 *NEHRP Recommended Provisions for New Buildings* were used to define design response spectra. Values for short- and 1-second period spectral accelerations at the Maximum Considered Earthquake (MCE) level were read from the pertinent maps for 5% damping and site class C, resulting in values S_S = 1.5 g and S_1 = 0.6 g. Following the 2000 NEHRP procedures, the short- and long-period values were modified for site class C to $S_{MS} = F_a S_S$ and $S_{M1} = F_v S_1$, where F_a = 1.0 and F_v = 1.3. Design-basis ordinates then were obtained as $S_{DS} = (2/3)S_{MS}$ and $S_{D1} = (2/3)S_{M1}$. These values were used with the spectral shape defined in the *NEHRP Recommended Provisions for New Buildings* (Figure 7-1) to derive the NEHRP design response spectrum. Note that the acceleration values in Figure 7-1 and in the rest of the document are actually pseudo-acceleration values.

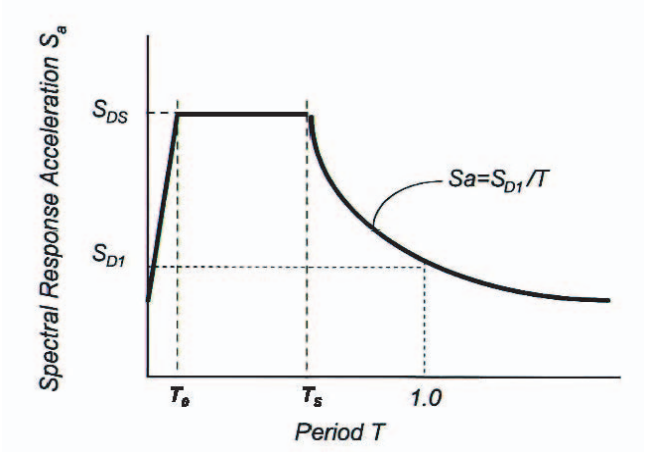

Figure 7-1 NEHRP design response spectrum.

7.2.2 Ground Motions and Ground-Motion Scaling

Ground motions were intended to be representative of design-level motions for a facility located approximately 10 km from a fault rupturing with strike-slip mechanism at magnitude M_s 7. The soil at the site corresponds to NEHRP Site Class C. Ground motions were selected from the Pacific Earthquake Engineering Research (PEER) Center strong ground motion

Table 7-1 Ground Motion Records

Earthquake	*Magnitude*	*Record*	*PGA (g)*	*PGV (cm/s)*	*PGD (cm)*	*Distance closest to fault rupture (km)*
Imperial Valley 1979/ 10/15 23:16	*M* 6.5, M_l 6.6, M_s 6.9	IMPVALL/H-PTS315	0.204	16.1	9.94	14.2
		IMPVALL/H-CPE147	0.169	11.6	4.25	26.5
		IMPVALL/H-CPE237	0.157	18.6	7.95	26.5
Landers 1992/06/28 11:58	*M* 7.3 M_s 7.4	LANDERS/CLW-LN	0.283	25.6	13.74	21.2
		LANDERS/CLW-TR	0.417	42.3	13.76	21.2
		LANDERS/MVH000	0.188	16.6	9.45	19.3
		LANDERS/MVH090	0.14	20.2	6.33	19.3
		LANDERS/DSP000	0.171	20.2	13.87	23.2
		LANDERS/DSP090	0.154	20.9	7.78	23.2
		LANDERS/JOS000	0.274	27.5	9.82	11.6
		LANDERS/JOS090	0.284	43.2	14.51	11.6
		LANDERS/NPS000	0.136	11	4.97	24.2

PGA: peak ground acceleration; PGV: peak ground velocity; PGD: peak ground displacement

database (*http://peer.berkeley.edu*), and were scaled to be representative of design-level motions at the site.

The *NEHRP Recommended Provisions for New Buildings* prescribe a scaling procedure to be used when ground motion records are used directly for time-domain dynamic analysis. According to this procedure, ground motions should be selected that are from similar site conditions, rupture mechanism and magnitude, and epicentral distance. For the present study, the selected records were for sites classified as NEHRP Site Class C, having strike-slip mechanism, magnitude M_s ranging from 6.3 to 7.5, and closest distance to fault rupture ranging from 5 to 25 km.

The SDOF oscillators were to be analyzed as planar structures subjected to a single horizontal component of ground motion. Therefore, records were scaled individually rather than scaling them as pairs as is recommended by the *NEHRP Recommended Provisions for New Buildings* for three-dimensional structures. The *Provisions* stipulate that the ground motions be scaled such that the average of the ordinates of the five-percent-damped linear response spectra does not fall below the design spectrum for the period range $0.2T_i$ to $1.5T_i$, where T_i is the fundamental period of vibration of the structure modeled as a linear system. The period $0.2T_i$ is selected as the lower bound to ensure that important higher modes of vibration are adequately excited. This lower bound is not relevant for the present study because the structure is an oscillator with a single vibration mode. Rather, for the present study, it is more important that the average approximate the design spectrum in the period range just below T_i to values higher than T_i, such that as the oscillator yields, it will, on average, experience ground motion intensities close to that represented by the design spectrum. Also, because this is a study of the procedures, rather than a building design, it is preferable to scale the motions so that the average of the spectral ordinates follows the design spectrum closely, rather than conservatively scaling the motions to be above the design spectrum as might be done for design purposes.

Sixteen ground motion records were selected for consideration. Each was examined to be certain it did not contain obvious near-fault directivity effects. Each motion was scaled so that the five-percent-damped spectral ordinate at the period of the oscillator matched that of the NEHRP response spectrum at the same period. Ground motions were eliminated selectively to avoid motions with unacceptably large scaling factors and motions whose response spectra did not appear consistent with the NEHRP response spectrum. The process of elimination continued until there were ten records available for each oscillator. Note that the oscillators had three different vibration periods (0.2, 0.5, and 1.0 s). Within the criteria stated above, it was not feasible to use the same ten motions for each oscillator. In total, 13 ground motions were used for the study. The ground motion records are identified in Table 7-1. The response spectra of the scaled ground

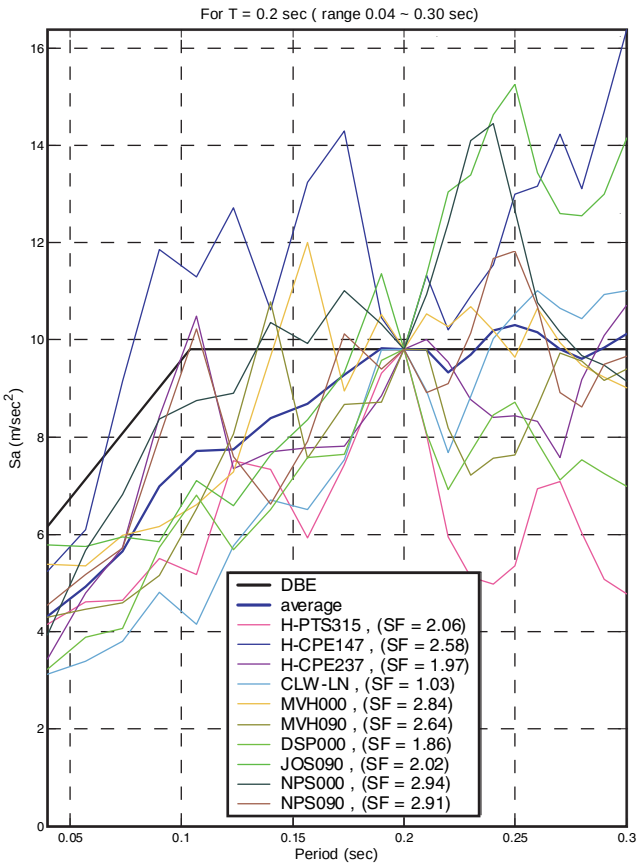

Figure 7-2 NEHRP response spectrum and 5%-damped response spectra of scaled motions, used for oscillators having $T = 0.2$ s.

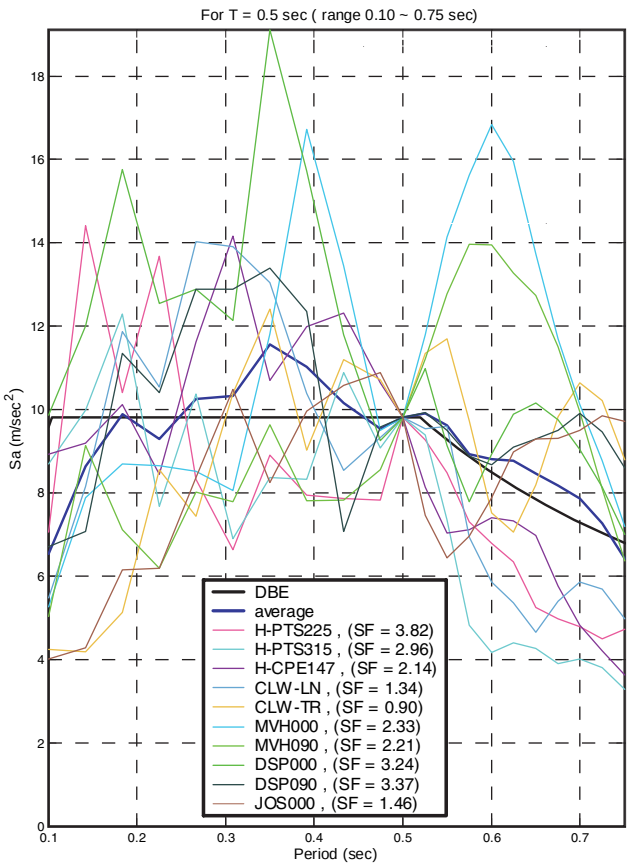

Figure 7-3 NEHRP response spectrum and 5%-damped response spectra of scaled motions, used for oscillators having $T = 0.5$ s.

motions used for oscillators having periods 0.2, 0.5, and 1.0 s are shown in Figures 7-2, 7-3, and 7-4, respectively.

7.2.3 Characteristics of Oscillators

Nine SDOF oscillators were used for this study. The oscillators had bilinear load-displacement relationships with post-elastic stiffness equal to five percent of the initial elastic stiffness. Loading and unloading characteristics are shown in Figure 7-5 without strength or stiffness degradation. Initial damping was five percent of critical damping. The oscillators had three different yield strengths and three different periods. For each period, the spectral acceleration was read from the NEHRP response spectrum. The yield strengths were then defined as the elastic base shear demand (product of the mass and spectral acceleration) divided by a strength reduction factor R. R values of 2, 4, and 8 were considered. Figure 7-6 summarizes the elastic vibration periods and R values selected.

7.2.4 Nonlinear Static Procedure Estimates Using Smoothed or Average Spectra

The improved nonlinear static procedures of Chapters 5 and 6 were applied to the NEHRP response spectra, as well as to the average of the 5%-damped response spectra. The former represents more closely how the procedures would be used with the NEHRP response spectra, whereas the latter represents more closely how the procedures might be used when a site-specific response spectrum is defined by the average of the response spectra for a series of design ground motions selected for a site.

For application of the displacement modification method of Chapter 5, the displacement amplitude was defined as

$$C_1 C_2 S_d = C_1 C_2 S_a \left(\frac{T_i}{2\pi} \right)^2 ,$$

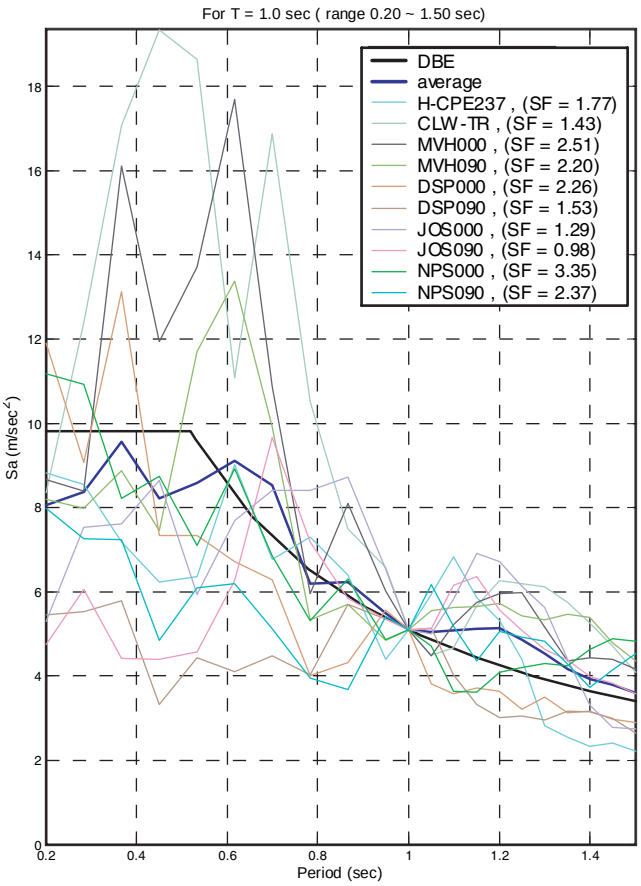

Figure 7-4 NEHRP response spectrum and 5%-damped response spectra of scaled motions, used for oscillators having $T = 1.0$ s.

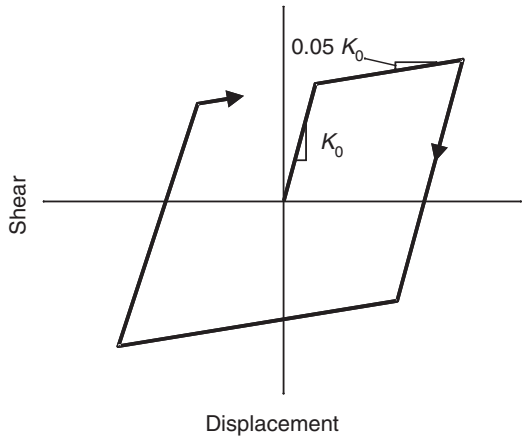

Figure 7-5 Bilinear load-displacement relation of oscillators.

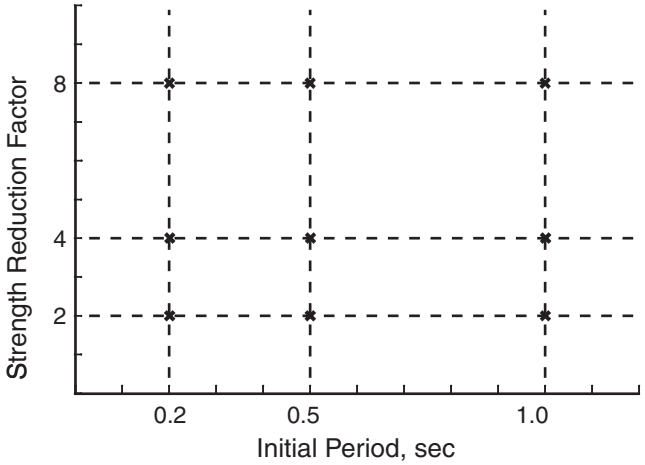

Figure 7-6 Linear vibration periods and strength reduction factors for oscillators.

in which S_a = pseudo-spectral acceleration ordinate at the period of the oscillator T_i. The coefficient C_1 was defined as

$$C_1 = 1 + \frac{R-1}{90T_i^2}.$$

Coefficient C_2 was taken equal to 1.0, as it was assumed that there was no stiffness or strength degradation.

For application of the equivalent linearization procedure of Chapter 6, response spectra were converted to the spectral acceleration-spectral displacement format. In studies using the average response spectra, the spectral ordinates were calculated for each ground motion for each of several different damping ratios. The results for a given damping ratio were averaged for the different ground motions to obtain the average response spectrum for that damping ratio. In studies using the NEHRP smooth design response spectra, spectral ordinates for damping exceeding 5% of critical damping were calculated using the spectral reduction factors of ATC-40; however, the limits on the reductions (ATC-40 Tables 8-1 and 8-2) were not imposed. Damping factors and effective periods were calculated using the equations and tabulated quantities in FEMA 440 Chapter 6, specific to the bilinear oscillator behavior with 5% post-elastic stiffness, rather than the more generally applicable equations. Iteration Procedure A was used with the average spectra, while iteration Procedure B was used for the smooth spectra, in general accordance with Section 6.4. Convergence was assumed when the

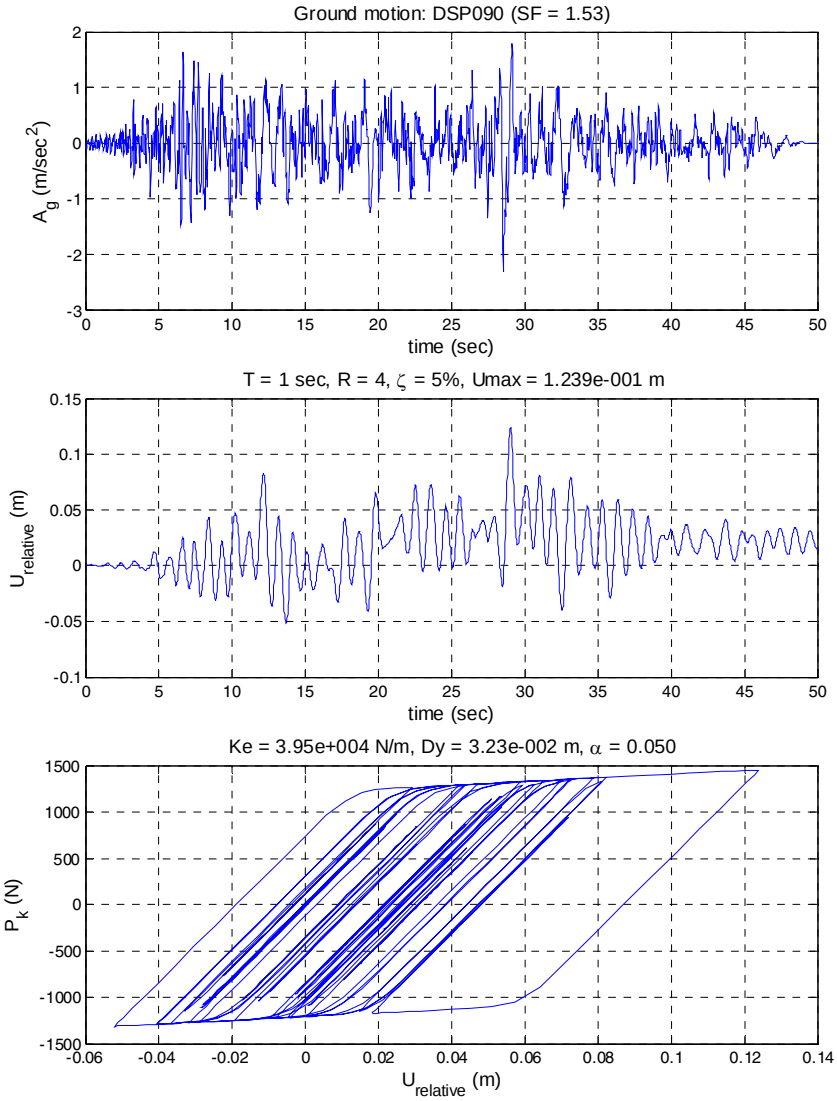

Figure 7-7 Representative nonlinear response-history analysis result (this example is for oscillator period $T = 1$ s, ground motion DSP090 scaled by factor 1.53, and strength-reduction factor $R = 4$).

calculated displacement was not more than 5% different from the assumed displacement. Also, solutions were generated using the approximate MADRS approach of Section 6.5.

Results also are presented using the Coefficient Method of FEMA 356 and the Capacity-Spectrum Method of ATC-40. For the Coefficient Method, the coefficients for the nonlinear static procedure were used with a cap on C_1 equal to 1.5, as permitted, and all other coefficients set equal to 1.0. For the Capacity-Spectrum Method, the procedures of ATC-40 were followed explicitly, using the response spectra in the same manner as for the improved procedure.

7.2.5 Response-History Analyses

Inelastic responses of the single-degree-of-freedom oscillators, with different periods and strength-reduction factors, were calculated for each of the ground motion histories. Figure 7-7 presents a representative result.

7.3 Results of the Study

Figure 7-8 presents results of the study using ground motions scaled to match the NEHRP design response spectrum, with the nonlinear static results calculated for the NEHRP design response spectrum. Data are presented in three sequential graphs, one each for oscillator of the initial periods: 0.2 s 0.5 s, and 1.0 s.

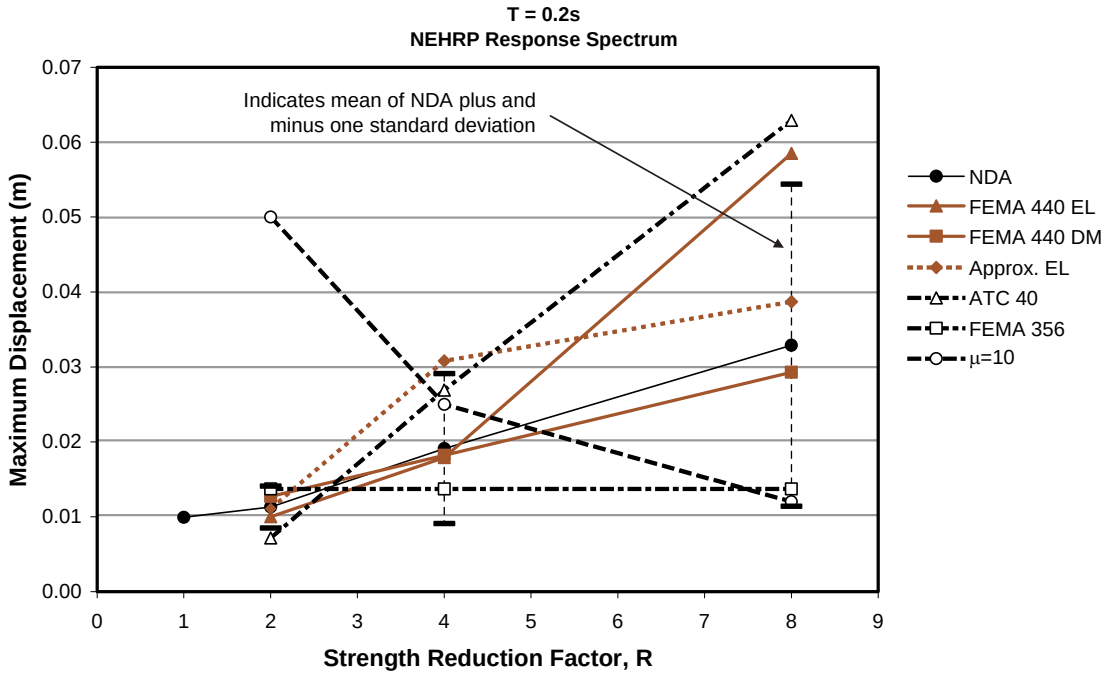

Figure 7-8 Comparison of responses for an oscillator with $T = 0.2$ s calculated using various procedures, response spectra scaled to the NEHRP spectrum, and values calculated for the NEHRP spectrum

Each graph plots maximum relative displacement amplitude as a function of the strength-reduction factor *R*. The legend to the right of each graph identifies the data in the graph, as follows:

1. NDA mean is the mean of the maximum displacement response amplitudes calculated using nonlinear dynamic analysis (time-domain) for the ten ground motions. Each graph also includes a representation of the NDA results for each strength value, consisting of the mean plus and minus one standard deviation.
2. FEMA 440 EL is the result obtained by the improved equivalent linearization method (Section 6.4)
3. FEMA 440 DM is the result obtained by the improved displacement modification method of Chapter 5.
4. Approximate EL is the result obtained by the approach given in Section 6.5.
5. ATC-40 is the result obtained by the Capacity-Spectrum Method of ATC-40.
6. FEMA 356 is the result obtained by the displacement modification method of FEMA 356.
7. $\mu = 10$ plots the displacement corresponding to displacement ductility of 10.

In Figures 7-8, 7-9, and 7-10, the results of primary interest are those for which the actual displacement is less than approximately10 times the yield displacement. Displacements near or beyond this level are unrealistic for most actual structures, because their vertical- and lateral-force-resisting systems are unlikely to be able to sustain such large deformations without failure. The coefficients of the FEMA 440 EL method were optimized for solutions with displacement ductility less than this limit.

The results obtained using nonlinear dynamic analysis (NDA) indicate that for short-period oscillators, the maximum displacement response amplitude increases with decreasing strength (increasing *R*), while for longer-period oscillators the peak displacement response is less sensitive to strength. NDA results reflect wider dispersion for shorter-period oscillators and for lower strength values. This observation is partly because the response spectra (Figures 7-2, 7-3, and 7-4) show increasing dispersion as the period elongates (as occurs for structures with lower strengths). Previous studies, including those summarized in Chapter 3, also have shown that dispersion of response generally

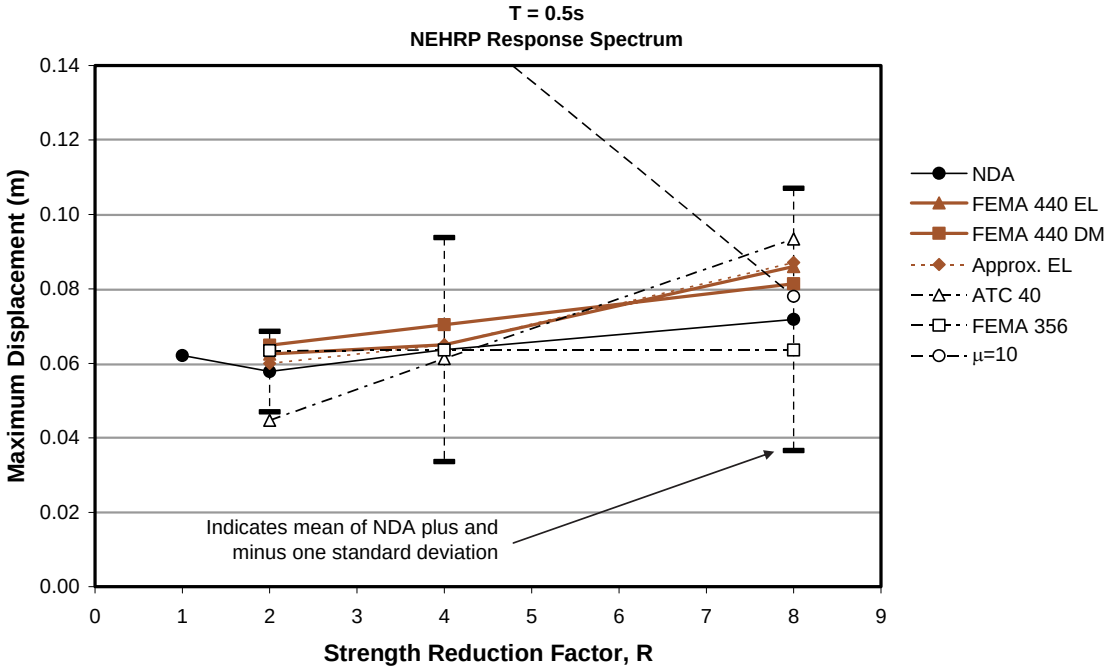

Figure 7-9 Comparison of responses for an oscillator with $T = 0.5$ s calculated using various procedures, response spectra scaled to the NEHRP spectrum, and values calculated for the NEHRP spectrum.

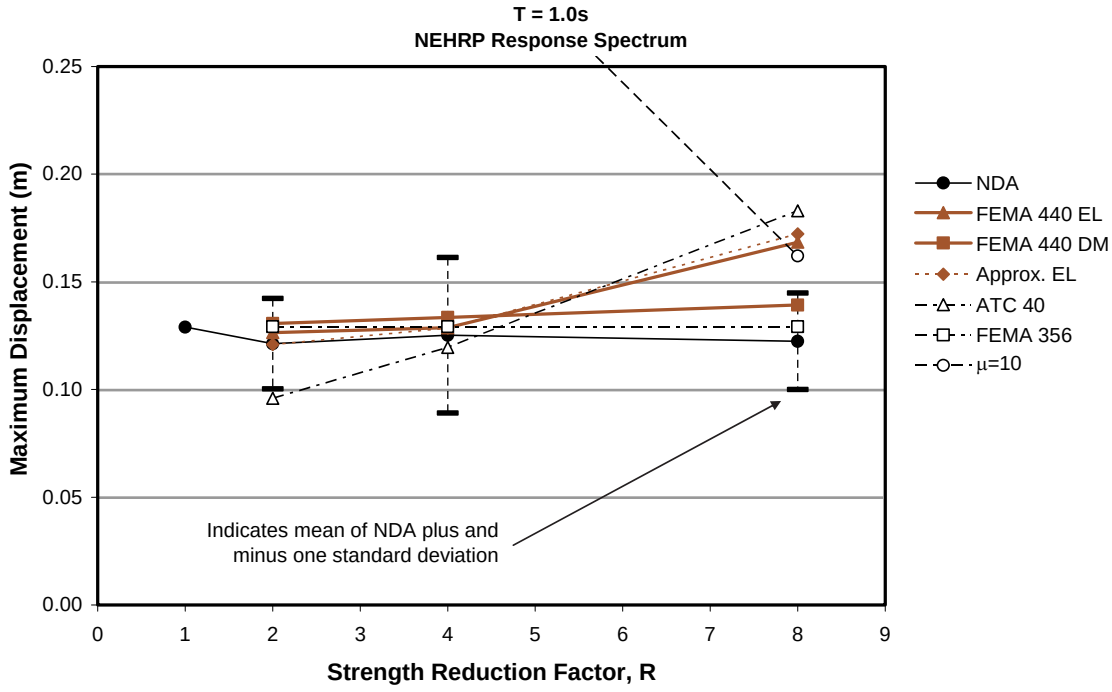

Figure 7-10 Comparison of responses for an oscillator with $T = 1.0$ s calculated using various procedures, response spectra scaled to the NEHRP spectrum, and values calculated for the NEHRP spectrum.

increases for shorter periods and higher *R* values, regardless of the tendency of the response spectra.

The proposed improved procedures generally follow the observed mean trends for the NDA results, provided that the displacement ductilities remain within reasonable bounds. Unreasonable ductility values are the cause of overestimates of displacement in some instances, using the FEMA 440 EL and the approximate EL procedures (e.g., Figure 7-8 with $T = 0.2$ s and $R = 8$, Figure 7-10 with $T = 1.0$ s and $R = 8$). This tendency is not apparent when the average spectrum is used, as noted below.

As expected, the FEMA 356 procedure does not predict the increase in displacement response with increasing *R* for short-period oscillators. The ATC-40 procedure tends to underestimate the displacement response for small *R* and overestimate the response for large *R*. These results are again consistent with the previous studies (Chapter 3).

Figures 7-11, 7-12, and 7-13 present data similar to those of Figures 7-8, 7-9, and 7-10. The ground motions are identical, having been scaled to match the *NEHRP* smooth design response spectrum, and oscillator strengths also are identical. However, the nonlinear static procedures all are applied using the average of the response spectra for the scaled ground motions. For the displacement modification methods, the ordinate of the 5% damped response spectrum at period *T* of the oscillator is unchanged from the previous analyses, so the results shown in Figures 7-11, 7-12, and 7-13 for those methods are the same as those shown in Figures 7-8, 7-9, and 7-10. For the equivalent linearization methods, the analysis required the calculation of the average of the linear response spectra for each scaled ground motion record for each of several different damping values. Results for these methods therefore differ from those presented in Figures 7-8, 7-9, and 7-10. Data are presented in three sequential graphs, separated by the oscillator initial periods of 0.2, 0.5, and 1.0 s. Each graph plots maximum relative displacement amplitude as a function of strength-reduction factor, *R*. The legend to the right of each graph identifies the data in the graph, defined as described above.

Results for the improved equivalent linearization methods using the average spectrum (Figure 7-8) are somewhat improved over those using the NEHRP spectrum (Figures 7-8, 7-9, and 7-10), especially for larger ductilities. This improvement might be expected for two reasons. First, the equivalent linearization methods were derived using response spectra calculated for individual motions for various specific values of

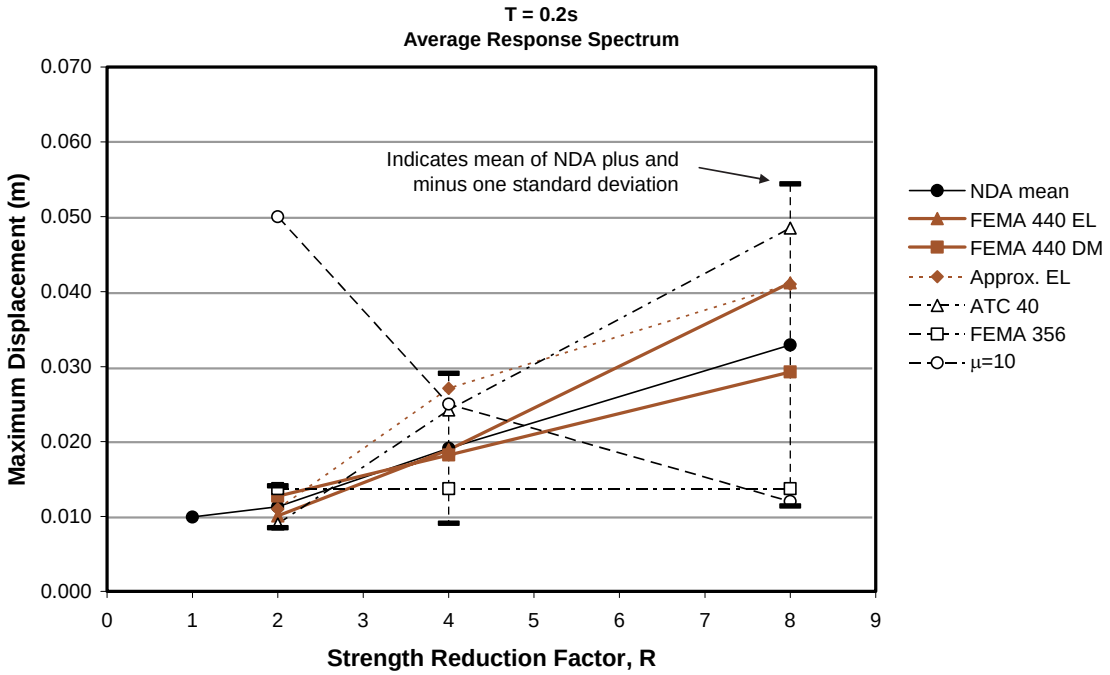

Figure 7-11 Comparison of responses of an oscillator with $T = 0.2$ s calculated using various procedures, response spectra scaled to NEHRP spectrum, and values calculated for the average spectrum.

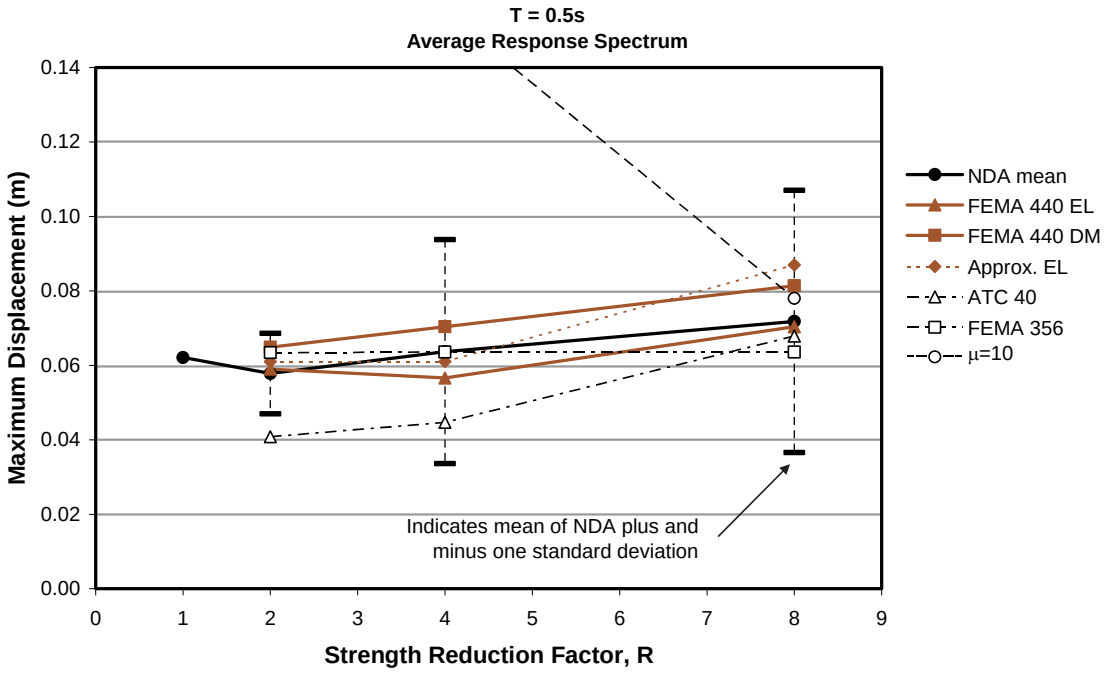

Figure 7-12 Comparison of responses of an oscillator with $T = 0.5$ s calculated using various procedures, response spectra scaled to the NEHRP spectrum, and values calculated for the average spectrum.

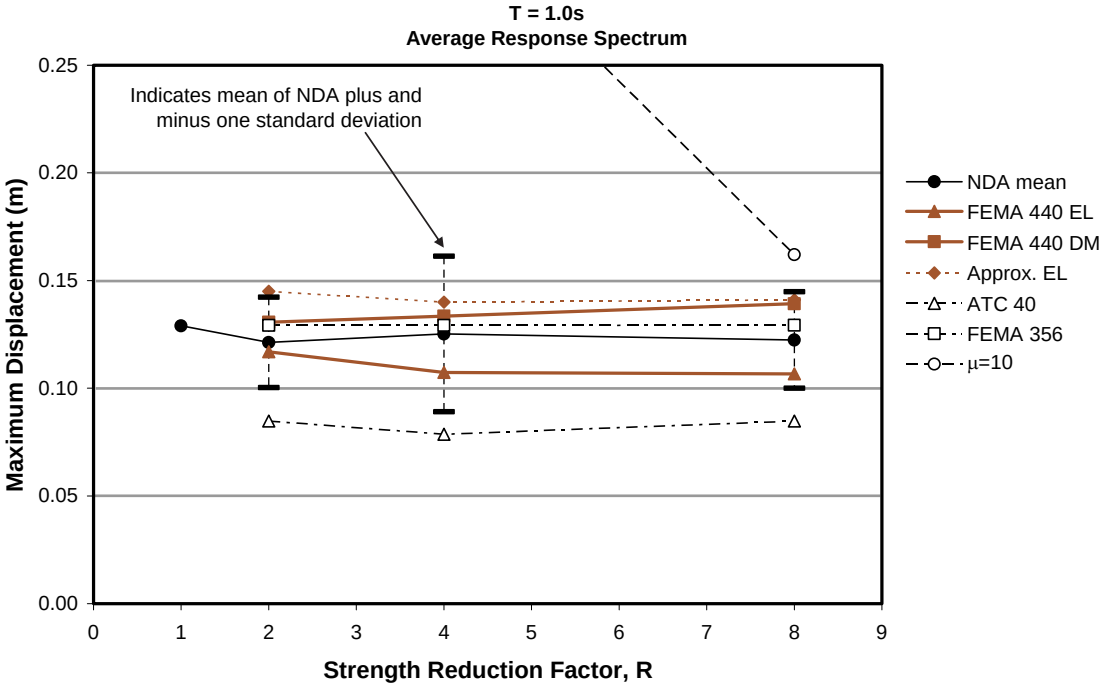

Figure 7-13 Comparison of responses of an oscillator with $T = 1.0$ s calculated using various procedures, response spectra scaled to the NEHRP spectrum, and values calculated for the average spectrum

damping. When used with the NEHRP design spectrum, it was necessary to estimate the effect of damping on spectral ordinates using approximate spectral reduction factors. Additionally, the effective period relationships were optimized from actual spectra as opposed to an assumed shape (e.g., NEHRP spectrum).

7.4 Summary of Implications of the Results of the Study

As noted elsewhere in this document, the dispersion of maximum displacement responses for nonlinear oscillators subjected to earthquake ground motions is relatively large, such that a relatively large number of analyses with different oscillators and ground motions may be required to reach statistically meaningful conclusions regarding response statistics. The results reported in this chapter based on a relatively small number of ground motions and oscillators are insufficient to serve as the basis for broad conclusions for all cases. Nonetheless, some general observations can be made from the results.

Engineers using the Capacity-Spectrum Method of ATC-40 and the Coefficient Method of FEMA 356 have observed that sometimes the two methods give widely different displacement estimates. This observation is evident from the results reported in Section 7.3. In some cases, the results of the methods differ by as much as a factor of two (Figures 7-8 through 7-13). One of the objectives of the effort to develop improved nonlinear static procedures, reported here, was to reduce the discrepancy in the results obtained by the two methods. As shown in Figures 7-8 through 7-13, this objective has been met for the ground motions and oscillators that were studied.

Another objective in developing the improved procedures in the frequency domain was to improve the accuracy of the methods relative to results for maximum global displacements obtained using nonlinear dynamic analysis. For this particular sample of ground motions and oscillators, the improved nonlinear static procedures provide generally better estimates of the mean maximum displacement response than do the current procedures. For displacement ductility less than about 10, which is deemed an excessive value for most structures to which these procedures would be applied, the improved nonlinear static procedures produced results within about one standard deviation of mean responses obtained by nonlinear dynamic analysis.

Another objective was to investigate whether the improved simplified static procedures could be applied to design spectra commonly used in practice, with sufficient accuracy. As shown in Figures 7-8, 7-9, and 7-10, for the ground motions, scaling procedure, and oscillators considered, the improved simplified static procedures effectively estimated the mean of maximum displacement response in conjunction with smooth design spectra. Again, the procedures probably should not be used for excessive displacement ductility values.

Finally, the results reported in this chapter illustrate the dispersion typical of nonlinear dynamic analysis using design-level ground motions. Actual response for a real design-level event may differ significantly from the estimate given by the simplified procedures using a NEHRP-like design spectrum. The same is true even if the spectrum is derived from specific ground motions records and even if the simplified procedures are capable of reasonably matching the median response. When interpreting results and assessing structural performance, engineers must consider the implications of these uncertainties.

8. Procedures for Including Soil-Structure Interaction Effects

8.1 Introduction

This chapter presents simplified procedures for including the effects of interaction between a structure and the supporting soils in a structural model for nonlinear static analysis procedures. There are three primary categories of soil-structure interaction (SSI) effects. These include:

- introduction of flexibility to the soil-foundation system (flexible foundation effects),
- filtering of the ground motions transmitted to the structure (kinematic effects), and
- dissipation of energy from the soil-structure system through radiation and hysteretic soil damping (foundation damping effects).

Current analysis procedures in FEMA 356 and ATC-40 partially address the flexible foundation effect through guidance on including the stiffness and strength of the geotechnical (soil) components of the foundation in the structural analysis model. However, these procedures do not address the reduction of the shaking demand on the structure relative to the free-field motion caused by kinematic interaction or the foundation damping effect. Guidance on including these effects in NSPs is provided in this section. A simple example illustrates the application of these procedures. Appendix E provides detailed information on these soil-structure interaction effects.

Figure 8-1a illustrates the assumption that the structural model is mounted on a rigid base that is excited by the free-field motion. The free-field motion is the theoretical movement of a single point on the surface of the ground, assuming that there is no structure near it. The fixed-base modeling assumption is inappropriate for many structures though. Structural systems that incorporate stiff vertical elements for lateral resistance (e.g., shear walls, braced frames) can be particularly sensitive to even small base rotations and translations that are neglected with a fixed base assumption. Relatively flexible vertical elements (e.g., moment frames) are often not significantly affected by SSI.

Figure 8-1b illustrates the incorporation of foundation flexibility into the structural model directly. ATC-40 and FEMA 356 include provisions for estimating the flexibility and strength of the foundation (i.e., the properties of the springs indicated in Figure 8-1b) in a structural model for inelastic analysis. Those provisions normally use the free-field motion as the seismic demand with 5% damping as the conventional initial value. This approach is capable of modeling both the structural and geotechnical (soil) components of the foundation. The result is that the response of the overall structural system includes deformations (elastic and inelastic) in the structural and geotechnical parts of the foundation system. These deformations are sometimes referred to as an inertial SSI effect. These improvements in modeling can lead to significant departures from fixed-base results and more accurate representation of probable structural response. Compared with the fixed-base modeling approach, the predicted period of the structure lengthens, the distribution of forces among various elements changes, the sequence of inelasticity and the modes of inelastic behavior can change, and foundation mechanisms (e.g., rocking, soil bearing failure, and pier/pile slip) can be directly evaluated and considered. All of these effects result in more realistic evaluation of the probable structural behavior and performance.

Figure 8-1c illustrates the filtering effects that soil-structure interaction can have on the character and intensity of ground motion experienced by the structural model. Kinematic interaction results from the presence of relatively stiff foundation elements on or in soil that cause foundation motions to deviate from free-field motions. Two effects are commonly identified: base-slab averaging and embedment effects. The base-slab averaging effect can be visualized by recognizing that the instantaneous motion that would have occurred in the absence of the structure within and below its footprint is not the same at every point. Placement of a structure and foundation across these spatially variable motions produces an averaging effect in which the overall motion is less than the localized maxima that would have occurred in the free field. The embedment effect is associated with the reduction of ground motion that tends to occur with depth in a soil deposit. Both base-slab averaging and embedment affect the character of the foundation-level motion (sometimes called the foundation input motion, or FIM) in a manner that is independent of the superstructure (i.e., the portion of the structure above the foundation), with one exception. The effects are strongly period-dependent, being maximized at small periods. The effects can be visualized as a filter

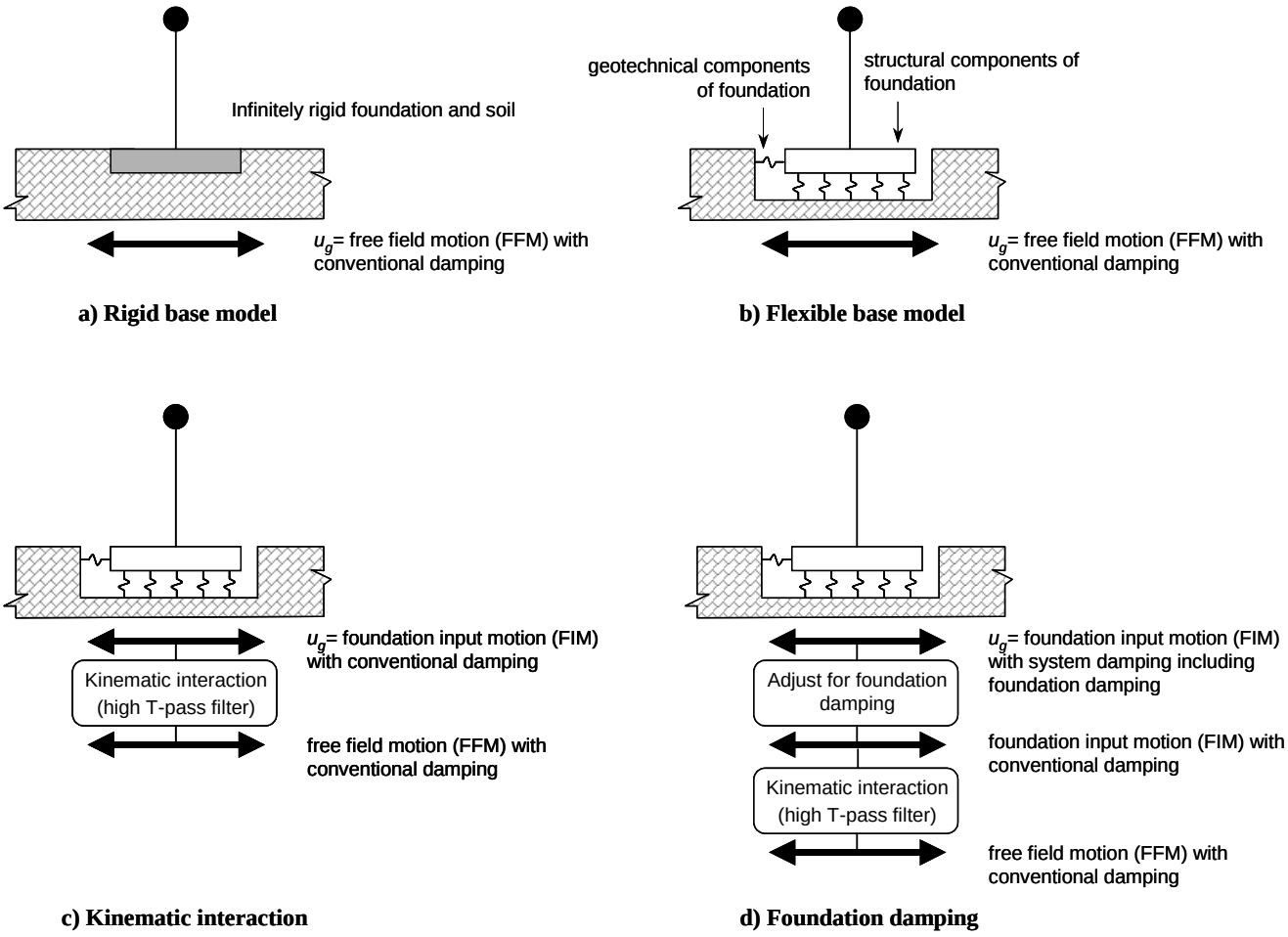

Figure 8-1 Foundation modeling assumptions.

applied to the high-frequency (short-period) components of the free-field ground motion. The impact of those effects on superstructure response will tend to be greatest for short-period buildings. A simplified procedure to apply these principles for reduction of the spectral amplitudes of the free-field motion to generate the FIM spectrum is presented in Section 8.2. The foundation input motion can be applied to a fixed-base model or, as depicted in Figure 8-1c, can be combined with a flexible-base model.

Figure 8-1d illustrates foundation damping effects that are another result of inertial soil-structure interaction in addition to foundation flexibility. Foundation damping results from the relative movements of the foundation and the supporting soil. It is associated with radiation of energy away from the foundation and hysteretic damping within the soil. The result is an effective decrease in the spectral ordinates of ground motion experienced by the structure. Although seldom used in practice the *NEHRP Recommended Provisions for Seismic Regulations for New Buildings and Other Structures* (BSSC, 2000),[1] as well as the ASCE-7 *Standard for Minimum Design Loads for Buildings and Other Structures* (ASCE, 2002) include procedures to account for this effect when using linear analysis procedures. Section 8.3 incorporates similar, although updated, procedures for use with NSPs. In the procedure, the foundation damping is linked to the ratio of the fundamental period of the system on the flexible-foundation to that of a fixed-base model. Other factors affecting foundation damping are the foundation size and embedment. The foundation damping is combined with the conventional initial structural damping to generate a revised damping ratio for the entire system, including the structure, foundation, and soil. This system damping ratio then modifies the foundation

1.Superseded in 2003 with the FEMA 450 *Recommended Provisions for Seismic Regulations for New Buildings and Other Structures.*

input motion imparted to the system model as seismic shaking demand.

8.2 Procedures for Kinematic Effects

The ground motions imposed at the foundation of a structure can differ from those in the free field due to averaging of variable ground motions across the foundation slab, wave scattering, and embedment effects. These effects are referred to here as kinematic interaction effects, and they tend to be important for buildings with relatively short fundamental periods (i.e., periods < ~ 0.5 s), large plan dimensions, or basements embedded 10 feet or more in soil materials. This section presents procedures to account for kinematic effects on building structures.

A ratio of response spectra (RRS) factor can be used to represent kinematic interaction effects. An RRS is simply the ratio of the response spectral ordinates imposed on the foundation (i.e., the foundation input motion, FIM) to the free-field spectral ordinates. Two phenomena should be considered in evaluating RRS: base slab averaging and foundation embedment, both of which are introduced in the preceding section. Base-slab averaging occurs to some extent in virtually all buildings. The slab-averaging effect occurs at the foundation level for mats or spread footings interconnected by either grade beams or reinforced concrete slabs. Even if a laterally stiff foundation system is not present, averaging can occur at the first elevated level of buildings with rigid diaphragms. The only case in which base-slab averaging effects should be neglected is in buildings without a laterally connected foundation system and with flexible floor and roof diaphragms. Foundation embedment effects should be considered for buildings with basements. Such effects should not be considered for buildings without basements, even if the footings are embedded. Embedment effects tend to be significant when the depth of basements is greater than about 10 feet. The following simplified procedure (adapted from Kim and Stewart (2003) and other sources) is recommended for analysis of these two kinematic interaction effects as a function of period, *T*, of the structural model:

1. Evaluate the effective foundation size $b_e = \sqrt{ab}$, where *a* and *b* are the full footprint dimensions (in feet) of the building foundation in plan view.
2. Evaluate the RRS from base-slab averaging (RRS_{bsa}) as a function of period (see Figure 8-2). An approximation to the curves in Figure 8-2 is given by the following:

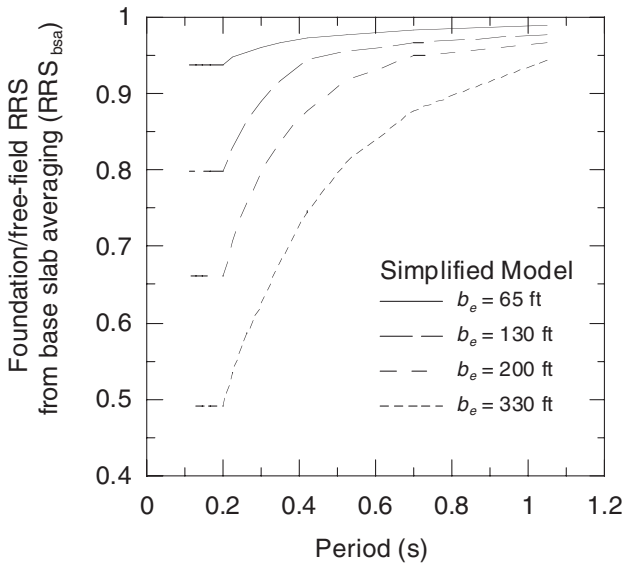

Figure 8-2 Ratio of response spectra for base slab averaging, RRS_{bsa}, as a function of period, *T*, and effective foundation size, b_e.

$$RRS_{bsa} = 1 - \frac{1}{14{,}100}\left(\frac{b_e}{T}\right)^{1.2} \geq \text{the value for } T = 0.2 \text{ s} \quad (8\text{-}1)$$

3. If the structure has a basement embedded a depth *e* from the ground surface, evaluate an additional RRS from embedment (RRS_e) as a function of period (see Figure 8-3). The curves in Figure 8-3 are described by the following:

$$RRS_e = \cos\left(\frac{2\pi e}{T n v_s}\right) \geq \text{ the larger of 0.453 or the } RRS_e \text{ value for } T = 0.2 \text{ s.} \quad (8\text{-}2)$$

where

e = foundation embedment (in feet)

v_s = shear wave velocity for site soil conditions, taken as average value of velocity to a depth of b_e below foundation (ft/s)

n = shear wave velocity reduction factor for the expected PGA as estimated from Table 8-1.

4. Evaluate the product of RRS_{bsa} times RRS_e to obtain the total RRS for each period of interest. The spectral ordinate of the foundation input motion at each period is the product of the free-field spectrum and the total RRS.

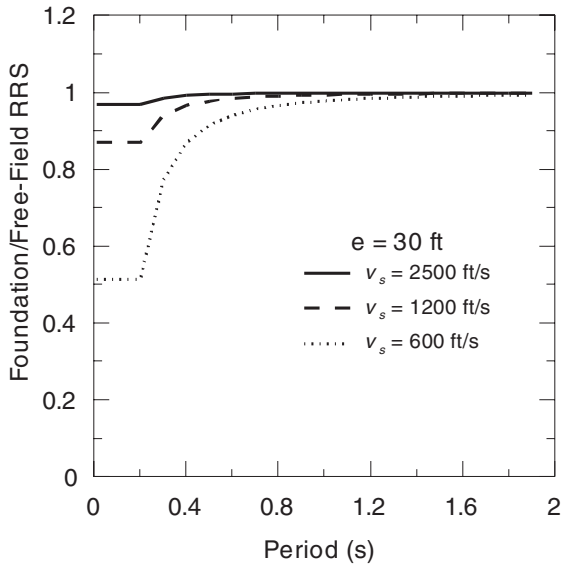

Figure 8-3 Ratio of response spectra for embedment RRS_e, for an embedment, e, of 30 feet as a function of period, *T*, and shear wave velocity, v_s.

Table 8-1 Approximate Values of Shear Wave Velocity Reduction Factor, *n*

	Peak Ground Acceleration (PGA)			
	0.10g	*0.15g*	*0.20g*	*0.30g*
n	0.90	0.80	0.70	0.65

5. Repeat steps 2 through 4 for other periods if desired to generate a complete spectrum for the foundation input motion (FIM).

If desired, more detailed procedures can also be used, which are described in Appendix E.

Limitations associated with application of this approach include the following, each of which is explained in Appendix E:

- Kinematic interaction effects should be neglected for soft clay sites such as Site Class E.
- Embedment effects can be neglected for foundations embedded in firm rock (Site Classes A and B).
- The base-slab averaging model:
  a. underestimates reductions in ground motions for foundation materials that consist of firm rock (Site Classes A and B).
  b. has not been rigorously studied for structures without large in-plane stiffness (continuous mat foundation or footings interconnected with a reinforced slab and/or grade beams); however, it is considered reasonable to extend its application to all structures except those without both an interconnected foundation and rigid floor and roof diaphragms.
  c. has not been rigorously studied for structures with plan dimensions greater than 200 ft.; however, it is considered reasonable to extend the application to these conditions, provided that the foundation elements are laterally connected.
  d. has not been rigorously studied for structures with pile-supported foundations; however it is considered reasonable to extend application to pile-supported structures in which the cap and soil are in contact or in which the caps are laterally connected to one another by a slab or grade beams.

8.3 Procedures for Foundation Damping

Damping related to foundation-soil interaction can significantly supplement damping that occurs in a structure due to inelastic action of structural components. The damping from foundation-soil interaction is associated with hysteretic behavior of soil (not to be confused with hysteretic action in structural components) as well as radiation of energy into the soil from the foundation (i.e., radiation damping). These foundation damping effects tend to be important for stiff structural systems (e.g., shear walls, braced frames), particularly when the foundation soil is relatively soft (i.e., Site Classes D-E).

The effects of foundation damping are represented by a modified system-damping ratio. The initial damping ratio for the structure neglecting foundation damping is referred to as β_i, and is generally taken as 5%. The damping attributed to foundation-soil interaction alone (i.e., the foundation damping) is referred to as β_f. Finally, the damping ratio of the complete structural system, accounting for foundation-soil interaction, as well as structural damping, is referred to as β_0. The change in damping ratio from β_i to β_0 modifies the elastic response spectrum. The spectral ordinates are reduced if $\beta_0 > \beta_i$.

A number of factors influence the foundation damping factor β_f (see Appendix E). Subject to the limitations noted below, the following simplified procedure can be used to estimate β_f and the subsequent spectral ordinate change due to the modified damping ratio of the complete structural system, β_0.

1. Evaluate the linear periods for the structural model assuming a fixed base, T, and a flexible base, $\tilde{T}$ using appropriate foundation modeling assumptions. Guidelines for the evaluation of soil spring stiffnesses are provided in FEMA 356 and ATC-40. In those calculations, the strain-degraded shear modulus should be used to represent the soil stiffness.

2. Calculate the effective structural stiffness of the SDOF oscillator for fixed base conditions as

$$K^*_{\text{fixed}} = M^* \left(\frac{2\pi}{T} \right)^2 \tag{8-3}$$

where M^* is the effective mass for the first mode calculated as the total mass times the effective mass coefficient (see ATC-40 Eqn. 8-21).

3. Determine the equivalent foundation radius for translation as

$$r_x = \sqrt{\frac{A_f}{\pi}} \tag{8-4}$$

where A_f is the area of the foundation footprint if the foundation components are inter-connected laterally.

4. Calculate the translational stiffness of the foundation, K_x. This can be evaluated using the procedures in FEMA 356 (Chapter 4) or ATC-40 (Chapter 10). For many applications, the translational stiffness can be estimated as

$$K_x = \frac{8}{2-\upsilon} G r_x \tag{8-5}$$

where G = effective, strain-degraded soil shear modulus (see FEMA 356, Table 4.7) and υ = soil Poisson's ratio (~0.3 for sand, ~0.45 for clay).

5. Calculate the equivalent foundation radius for rotation, r_θ, by first evaluating the effective rotational stiffness of the foundation, K_θ, as

$$K_\theta = \frac{K^*_{\text{fixed}} \left(h^* \right)^2}{\left(\frac{\tilde{T}}{T} \right)^2 - 1 - \frac{K^*_{\text{fixed}}}{K_x}} \tag{8-6}$$

Where h^* is the effective structure height taken as the full height of the building for one-story structures, and as the vertical distance from the foundation to the centroid of the first mode shape for multi-story structures. In the latter case, h^* can often be well-approximated as 70% of the total structure height. The quantity K_x is often much larger than K^*_{fixed}, in which case an accurate evaluation of K_x is unnecessary and the ratio, K^*_{fixed}/K_x, can be approximated as zero.

The equivalent foundation radius for rotation is then calculated as

$$r_\theta = \left(\frac{3(1-\upsilon) K_\theta}{8G} \right)^{\frac{1}{3}} \tag{8-7}$$

The soil shear modulus, G, and soil Poisson's ratio, υ, should be consistent with those used in the evaluation of foundation spring stiffness.

6. Determine the basement embedment, e, if applicable.

7. Estimate the effective period-lengthening ratio, $\tilde{T}_{\text{eff}} / T_{\text{eff}}$, using the site-specific structural model developed for nonlinear pushover analyses. This period-lengthening ratio is calculated for the structure in its degraded state (i.e., accounting for structural ductility and soil ductility). An expression for the ratio is

$$\frac{\tilde{T}_{\text{eff}}}{T_{\text{eff}}} = \left\{ 1 + \frac{1}{\mu} \left[\left(\frac{\tilde{T}}{T} \right)^2 - 1 \right] \right\}^{0.5} \tag{8-8}$$

where the term μ is the expected ductility demand for the system (i.e., including structure and soil effects). Thus, the ductility must be estimated prior to the actual solution and subsequently verified.

8. Evaluate the initial fixed-base damping ratio for the structure (β_i), which is often taken as 5%.

9. Determine foundation damping due to radiation damping, β_f, based on $\tilde{T}_{\text{eff}} / T_{\text{eff}}$, e/r_x, and h/r_θ, using the plots in Figures 8-4 and 8-5. An approximation to those curves is given by the following:

$$\beta_f = a_1 \left(\frac{\tilde{T}_{\text{eff}}}{T_{\text{eff}}} - 1 \right) + a_2 \left(\frac{\tilde{T}_{\text{eff}}}{T_{\text{eff}}} - 1 \right)^2 \tag{8-9}$$

where β_f is in percent and

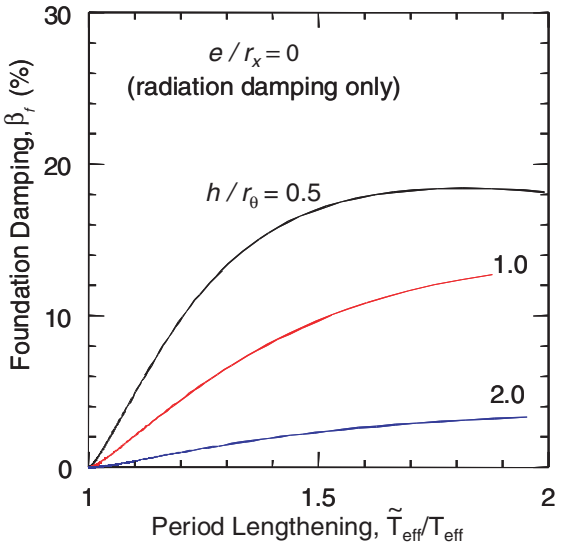

Figure 8-4 Example of foundation damping, β_f, as a function of effective period lengthening ratio, $\tilde{T}_{\text{eff}} / T_{\text{eff}}$, for constant embedment, $e/r_x = 0$, and various values of foundation stiffness rotational stiffness, h/r_θ.

$$a_1 = c_e \exp\left(4.7 - 1.6h / r_\theta\right) \quad \text{(8-9a)}$$

$$a_2 = c_e\left[25\ln\left(h / r_\theta\right) - 16\right] \quad \text{(8-9b)}$$

$$c_e = 1.5\left(e / r_x\right) + 1 \quad \text{(8-9c)}$$

The above equations are most applicable for $\tilde{T}_{\text{eff}} / T_{\text{eff}} < 1.5$, and generally provide conservative (low) damping estimates for higher $\tilde{T}_{\text{eff}} / T_{\text{eff}}$.

10. Evaluate the flexible-base damping ratio (β_0) from β_i, β_f, and $\tilde{T}_{\text{eff}} / T_{\text{eff}}$ as follows:

$$\beta_0 = \beta_f + \frac{\beta_i}{\left(\tilde{T}_{\text{eff}} / T_{\text{eff}}\right)^3} \quad \text{(8-10)}$$

11. Evaluate the effect on spectral ordinates of the change in damping ratio from β_i to β_0 (in accordance with Section 6.3); then modify the spectrum of the foundation input motion (recall that foundation input motion is equal to the free-field motion if kinematic effects are neglected).

From this point, the maximum expected displacement of the nonlinear SDOF oscillator model can be estimated using the displacement modification

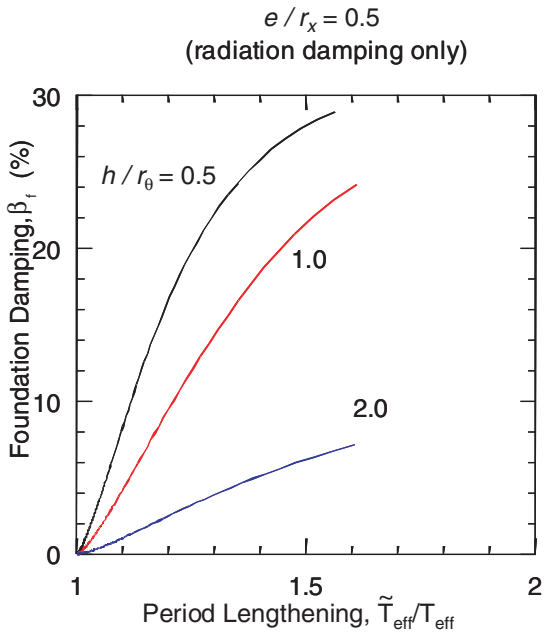

Figure 8-5 Example of foundation damping, β_f, as a function of effective period lengthening ratio, $\tilde{T}_{\text{eff}} / T_{\text{eff}}$, for constant embedment, $e/r_x = 0.5$, and various values of foundation stiffness rotational stiffness, h/r_θ.

procedures of FEMA 356 and Chapter 5 or the equivalent linearization procedures of ATC-40 and Chapter 6. The ductility demand should be checked against the value assumed in Step 7 above.

The damping ratios determined in accordance with this section represent radiation damping effects only. Hysteretic soil damping effects are neglected, since ductility in soil springs is included as part of structural pushover analysis.

Limitations on the damping analysis described above include the following:

- The procedure above should not be used when shear walls or braced frames are spaced sufficiently closely that waves emanating from distinct foundation elements will destructively interfere with each other across the period range of interest. This can effectively decrease the energy dissipated in the soil material, and the above formulation could overestimate the related damping. Unfortunately, this effect has not been investigated sufficiently to justify definitive limits. In the absence of such limits, a reasonable approximation might be to neglect the effect of softly-coupled foundation

components spaced at a distance less than the larger dimension of either component in the corresponding direction. Further discussion is presented in Appendix E, Section E.3.1.5.

- The analysis can be conservative (underpredicting the damping) when foundation aspect ratios exceed about 2:1. Further discussion is presented in Appendix E, Section E.3.1.4.
- The analysis is conservative when foundations are deeply embedded, $e/r_x > 0.5$. Further discussion is presented in Appendix E, Section E.3.1.3.
- The analysis is unconservative (overpredicting the damping) if $v_s T/r_x > 2\pi$ (where v_s = average shear wave velocity to a depth of about r_x) and the foundation soils have significant increases of shear stiffness with depth. Further discussion is presented in Appendix E, Section E.3.1.2.
- The analysis is unconservative if the foundation soil profile consists of a soil layer overlying a very stiff material (i.e., there is a pronounced impedance contrast within the soil profile), and if the system period is greater than the first-mode period of the layer. Further discussion is presented in Appendix E, Section E.3.1.2.

9. Multiple-Degree-of-Freedom Effects

9.1 Introduction

One of the primary assumptions of nonlinear static analysis procedures is that the behavior of a structure with multiple degrees of freedom (MDOF) subject to seismic ground motion can be estimated from the response of an oscillator with a single degree of freedom (SDOF). In order to generate the SDOF model, the engineer generates a global force-deformation relationship for the structure by subjecting a MDOF model to a predetermined lateral load vector. This relationship is then converted to an equivalent SDOF representation to estimate the maximum global displacement of the model using displacement-modification or equivalent linearization techniques. The global displacement is typically monitored at the roof level or center of mass. The magnitude of localized demand in the MDOF model (e.g., story drifts and forces or component deformations) are directly related to the global displacement. The actual maximum global displacement for the MDOF system can differ from the equivalent SDOF approximation. The distribution of localized demand depends on the assumptions associated with the load vector used to generate the equivalent SDOF model. The distribution of forces on the structure changes continuously during an earthquake. In the elastic range, this is attributable to the fact that the response comprises contributions from multiple modes of vibration. The actual distribution is difficult to assess since the dynamic characteristics of the ground motion itself are a major influence. Inelasticity further complicates the situation. The combined deviations of the actual distribution of forces and deformations from those associated with the equivalent SDOF system and the assumed load vector are termed MDOF effects. They can result in maximum inelastic response in components or elements that differ from the SDOF model predictions in nonlinear static analysis.

This section reviews the accuracy and practical implications of the requirements of ATC-40 and FEMA 356 related to MDOF effects including:

1. current options for load vectors, and
2. the conversion of a MDOF pushover curve to an equivalent SDOF system.

The results of a comprehensive study of five example buildings that examines the differences in response predicted using various options compared to a common nonlinear dynamic analyses benchmark are also summarized. Finally, this chapter provides recommendations for practical applications and identifies promising developments for the future.

9.2 Review of Current Simplified Procedures

There are a number of options for the form of the load vector used to generate the SDOF model of a structure. Some are based on a single vector and one uses several vectors applied to comprise a multi-mode pushover approach. In all the options, lateral forces are applied incrementally to a nonlinear structural model to generate a "pushover" or capacity curve representing the relationship between the applied lateral force and the global displacement at the roof or some other control point. The applied lateral force at any level in the structure is proportional to the mass at that level and an acceleration determined from a specific shape vector assumption. The various options are summarized below, as are the specifications of ATC-40 and FEMA 356 related to MDOF effects.

9.2.1 Single-Mode Load Vectors

Concentrated Load. The simplest assumption for a load vector is a single concentrated load located normally at the top of the structure.

Uniform. A uniform load vector assumes that the acceleration in the MDOF model is constant over its height. This alternative is sometimes termed "rectangular."

Triangular. A triangular-shaped vector assumes that the acceleration increases linearly from zero at the base to a maximum at the top of the MDOF model.

Code Distribution. The "code" load pattern appears in many documents. The acceleration pattern varies from the triangular shape for periods less than 0.5 s to a parabolic shape for periods greater than 2.5 s, as a means to account for higher-mode effects.

First Mode. The first-mode technique applies accelerations proportional to the shape of the first mode of the elastic MDOF model.

Adaptive. The adaptive procedure uses the first mode and recognizes that softening of the capacity curve

reflects a reduction in stiffness, which, in turn, causes a change in the mode shape. Thus, lateral forces are applied in proportion to the amplitude of an evolving first-mode shape and the mass at each level within the MDOF model.

SRSS. The square-root-of-the-sum-of-the-squares (SRSS) technique is based on elastic modal responses. The response in each mode has a lateral force pattern, which can be summed to obtain story shears associated with each mode. An SRSS combination of the modal story shears results in a particular shear profile, referred to as the SRSS story shears. The lateral forces required to generate the SRSS story shear profile are applied to the MDOF model in this pushover technique. The elastic spectral amplitudes and modal properties are used even when nonlinear response is anticipated. A sufficient number of modes to represent at least 90% of the mass is generally included.

9.2.2 Multi-Mode Pushover Procedures

Multi-mode pushover analysis procedures consider response in several modes. Approaches have been described by various investigators such as Sasaki et al. (1998), Reinhorn (1997), Chopra and Goel (2002), and Jan et al. (2004). Chopra and Goel (2001b) describe an approach in which pushover analyses are conducted independently in each mode, using lateral-force profiles that represent the response in each of the first several modes. Response values are determined at the target displacement associated with each modal pushover analysis. Response quantities obtained from each modal pushover normally are combined using the SRSS method. Although response in each mode may potentially be nonlinear, the mode shapes and lateral-force profiles are assumed to be invariant in this analysis procedure. Target displacement values may be computed by applying displacement modification or equivalent linearization procedures to an elastic spectrum for an equivalent SDOF system representative of each mode to be considered. Chopra and Goel (2001d) and Yu et al. (2001) illustrate the method using SRSS combinations of floor displacement, interstory drift, and component deformation (plastic hinge rotations).

9.2.3 Summary of Current Provisions

FEMA 356. FEMA 356 (Section 3.3.3.2.3) requires that two separate nonlinear static analyses be done, each using different load vectors. For each response quantity of interest, the larger value of the two analyses is compared to the applicable acceptability criteria.

One load vector is selected from the following list.

- Code distribution—Restricted to the cases in which more than 75% of mass participates in first mode, and the second vector must be the uniform distribution.
- First mode—Restricted to the cases in which more than 75% of mass participates in first mode.
- SRSS of modal story loads – This option must be used if $T_e > 1$ s.

A second load vector is selected from the following options.

- Uniform distribution or
- Adaptive load distribution.

In FEMA 356 (Section 2.4.2.1), the use of NSPs must be supplemented with a linear dynamic analysis if any SRSS story shear from a response-spectrum analysis including modes representing 90% of the mass exceeds 130% of the corresponding story shear from a first-mode response-spectrum analysis.

The yield displacement, Δ_y, of the equivalent SDOF system is effectively determined as

$$\Delta_y = \frac{\Delta_{y,\text{roof}}}{\Gamma_1} \tag{9-1}$$

where $\Delta_{y,\text{roof}}$ = the roof displacement at yield, and Γ_1 = the first-mode participation factor.

In the FEMA 356 approximation, it can be shown that the yield strength coefficient of the equivalent SDOF system is approximated as

$$C_y = \frac{S_a}{g} = \frac{V_{mdof}}{W}\Gamma_1 \tag{9-2}$$

where S_a = the pseudo-acceleration associated with yield of the ESDOF (Equivalent SDOF) system, g = the acceleration of gravity, V_{mdof} = the yield strength of the MDOF system, W = the weight of the MDOF system. This simplification relies on the approximation $\Gamma_1 \approx 1/\alpha_1$, where α_1 is the modal mass coefficient.

ATC-40. The primary recommendation in ATC-40 (Section 8.2.1) for load vectors is to use the first mode. However, the guidelines recognize a hierarchy of other options, arranged here in order of preference.

1. Concentrated load
2. Code distribution
3. First mode
4. Adaptive
5. Multi-mode pushover

The guidelines also note that pushover analyses using the first-mode shape are generally valid for structures with fundamental periods up to about one second. They suggest that the engineer might want to consider multi-mode pushover for structures with longer periods.

In the ATC-40 method, the yield displacement of the equivalent SDOF is the same as that of FEMA 356; however the yield strength coefficient of the equivalent SDOF system is given by

$$C_y = \frac{S_a}{g} = \frac{V_{mdof}/W}{\alpha_1} \quad (9\text{-}3)$$

where S_a = the pseudo-acceleration associated with yield of the ESDOF system, g = the acceleration of gravity, $V_{y,\,mdof}$ = the yield strength of the MDOF system, W = the weight of the MDOF system, and α_1 = the modal mass coefficient.

9.3 Summary of Illustrative Examples

In order to compare and illustrate the effects of the various options with NSPs related to the effects of higher modes, five example buildings were analyzed. Detailed information and results of the analyses are contained in Appendix F. The basic description of the example buildings and the other features of the analysis are listed below.

Example Buildings

- Three-story, steel frame (SAC LA Pre-Northridge M1 Model)
- Three-story, weak-story steel frame (lowest story at 50% of strength)
- Eight-story, shear wall (Escondido Village)
- Nine-story, steel frame (SAC LA Pre-Northridge M1 Model)
- Nine-story, weak-story steel frame (lowest story at 60% of strength)

Ground Motions

- Eleven site Class C motions, 8-20 km from the fault rupture, five events
- Four near-field motions: Erzincan, Northridge (Rinaldi Receiving Station & Sylmar County Hospital), and Landers earthquakes

Global Drift Levels

Ordinary motions (scaled to result in specified global drift)

- 0.5, 2, 4% drift, as a percentage of building height, for frames
- 0.2, 1, 2% drift, as a percentage of building height, for wall

Near-field (unscaled)

- 1.8 to 5.0% for 3-story frames, 1.7-2.1% for 9-story frames
- 0.6 – 2.1% drift, as a percentage of building height, for wall

Load Vectors

- Triangular
- Uniform
- Code
- First mode
- Adaptive
- SRSS
- Multi-mode pushover

Response Parameters

- Floor and roof displacement
- Interstory drift
- Story shear
- Overturning moment

Error Measurements

- Mean over all floors
- Maximum over all floors

9.3.1 Load Vectors

For analyses using the ordinary ground motions, each motion was scaled to result in the pre-determined levels of total drift at the roof for each example building in the

nonlinear response-history analysis of the MDOF models. The resulting response parameters served as the basis for comparison with nonlinear static analyses using the various options for load vectors. Observations from the comparisons are summarized as follows:

- Anomalous capacity curves resulted because the roof displacements reversed in two of the higher-mode pushover analyses. Consequently, the Modal Pushover Analysis procedure described by Chopra and Goel (2001b) could not be applied without modification to the examples. In order to represent higher-mode contributions, a multiple mode calculation procedure was introduced in the ATC-55 project. In this procedure, response quantities for the 2nd and 3rd mode were determined under the assumption that the response in these modes is elastic. A conventional inelastic pushover analysis was used for response in the first mode. Floor displacement, interstory drift, story shear, and overturning moments were determined as an SRSS combination of the modal responses in the first three modes. Motivated by review of early results of these analyses, Chopra et al. (2004) have investigated this approach, described as a "modified MPA," in comparison with the original MPA procedure.
- All the simplified procedures evaluated resulted in good estimates of peak displacements over the height of the five example buildings (Figure 9-1) when compared with nonlinear dynamic response-history analysis results. Estimates made using the first-mode, triangular, and adaptive load vectors were best. A multiple mode procedure may be warranted for structures in which displacement response is suspected to be predominantly in a higher mode.
- The dispersion in the displaced shapes of the weak-story buildings was pronounced at the moderate drift levels. This is likely due to the fact that weak-story mechanisms did not always develop at these levels of roof drift. This is illustrated by comparing the dispersion in floor displacements of the nine-story, weak story frame building at 2% roof drift (Figure 9-2a) that is actually greater than that for the same building at 4% drift (Figure 9-2b).
- Good estimates of interstory drift were obtained over the height of the three-story frames and eight-story wall using the first-mode, triangular, code, adaptive, and SRSS load vectors, as well as with the modified MPA procedure (Figure 9-3).
- Interstory drifts estimates over the height of the nine-story buildings were poor for the single-mode load vectors (see Figure 9-4). The results using the modified MPA procedure were consistently better than those obtained with the single load vectors, although the interstory drift values were still underestimated at some locations in the nine-story frames. Similar results are reported by Goel and Chopra (2004).
- The maximum interstory drift over the height of each building model, determined using the single-mode load vectors (excluding the uniform load vector), was a reasonable estimate of the maximum interstory drift occurring at that particular location in the nonlinear dynamic analyses. This drift was also a reasonable estimate of the maximum interstory drift that developed over the height of each building model in the nonlinear dynamic analyses (Figures 9-3 and 9-4), although these estimates depended to some extent on the load vector selected. Also, drifts at other locations predicted with the load vectors often did not correspond to those from the nonlinear dynamic analyses.
- Estimates of story shear and overturning moment for the three-story frames (Figure 9-5) were not as accurate as the displacement and interstory drift estimates (Figure 9-3a). These quantities typically were underestimated using the single load vectors and overestimated using the modified MPA procedure. The tendency for the modified MPA procedure to overestimate forces and moments is not surprising, as SRSS combinations of these quantities can exceed limits associated with the development of an inelastic mechanism and depend on the number of modes included in the combination.
- Estimates were inconsistent and often poor for story shears and overturning moment for the eight-story wall and nine-story frames (Figure 9-6). Although the overall pattern of overturning moments was often correct, errors in the estimates of overturning moment were often substantial, particularly for the upper floors. Similar results are reported by Krawinkler and Seneviratna (1998) and Gupta and Krawinkler (2003).
- The accuracy of the simplified procedures was similar for the set of Site Class C motions and for the set of near-field motions that was considered.

9.3.2 Equivalent SDOF Estimates of Global Displacement

For each example building, the force-displacement relationship generated with the first-mode vector was converted to an equivalent SDOF system using the

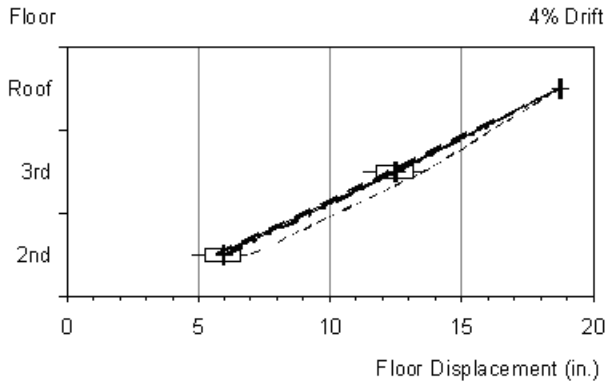

(a) Three-story frame building at 4% drift

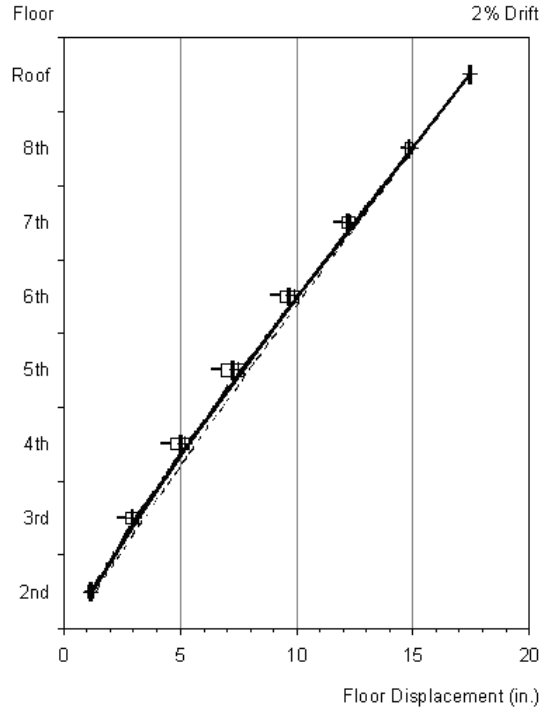

(b) Eight-story wall building at 2% drift

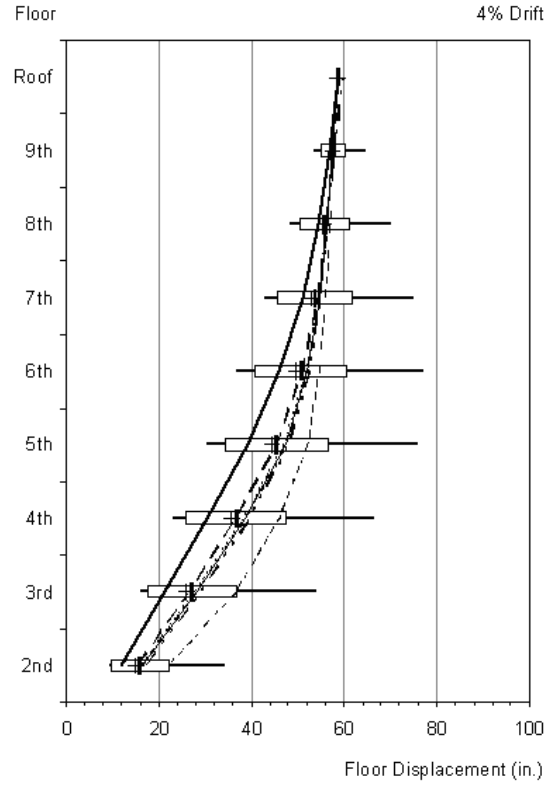

(c) Nine-story frame at 4% drift

NDA **NSP Load Vectors**

Figure 9-1 Example results for displacements predicted by nonlinear static procedures (NSP) compared to nonlinear dynamic response-history analyses (NDA).

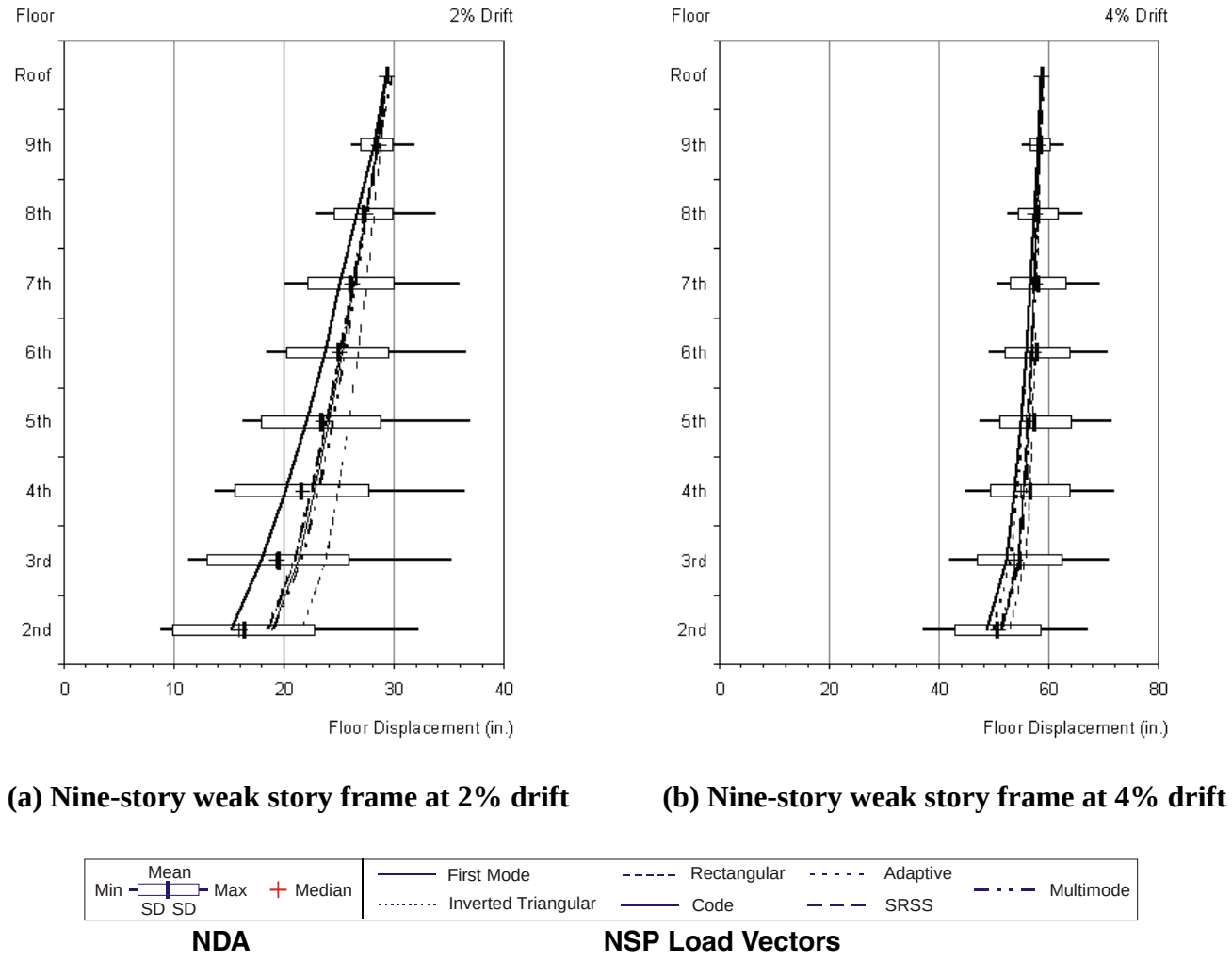

(a) Nine-story weak story frame at 2% drift **(b) Nine-story weak story frame at 4% drift**

Figure 9-2 Dispersion in results for displacement for two levels of global drift.

procedures of both FEMA 356 and ATC-40. These models were then subjected to scaled ground-motion records. A displacement ratio was defined as the ratio of the estimated roof displacement and the peak roof displacement obtained in the nonlinear response-history analysis. Results are reported in detail in Appendix F and summarized below.

- In cases in which the post-yield stiffness of the capacity curve is positive (with or without *P-Δ* effects present), mean displacement ratios obtained using the ATC-40 formulation were between approximately 0.95 and 1.25 for the five buildings. Within this range, mean displacement ratios tended to increase with increasing roof drift.
- Similar mean displacement ratios were obtained with the FEMA 356 formulation, although dispersions were larger for this formulation. Accuracy was similar for the near-field motions.
- In cases in which the post-yield stiffness of the capacity curve is negative (due to *P-Δ* effects), equivalent SDOF systems can have excessive displacement response, leading to overestimates of the peak roof displacement. For such cases, nonlinear dynamic analysis of the MDOF structure may be more accurate.

9.4 Practical Implications

NSPs can provide reliable estimates of maximum displacement. They are also capable of providing reasonable estimates of the largest interstory drift that may occur at any location over the height, but are

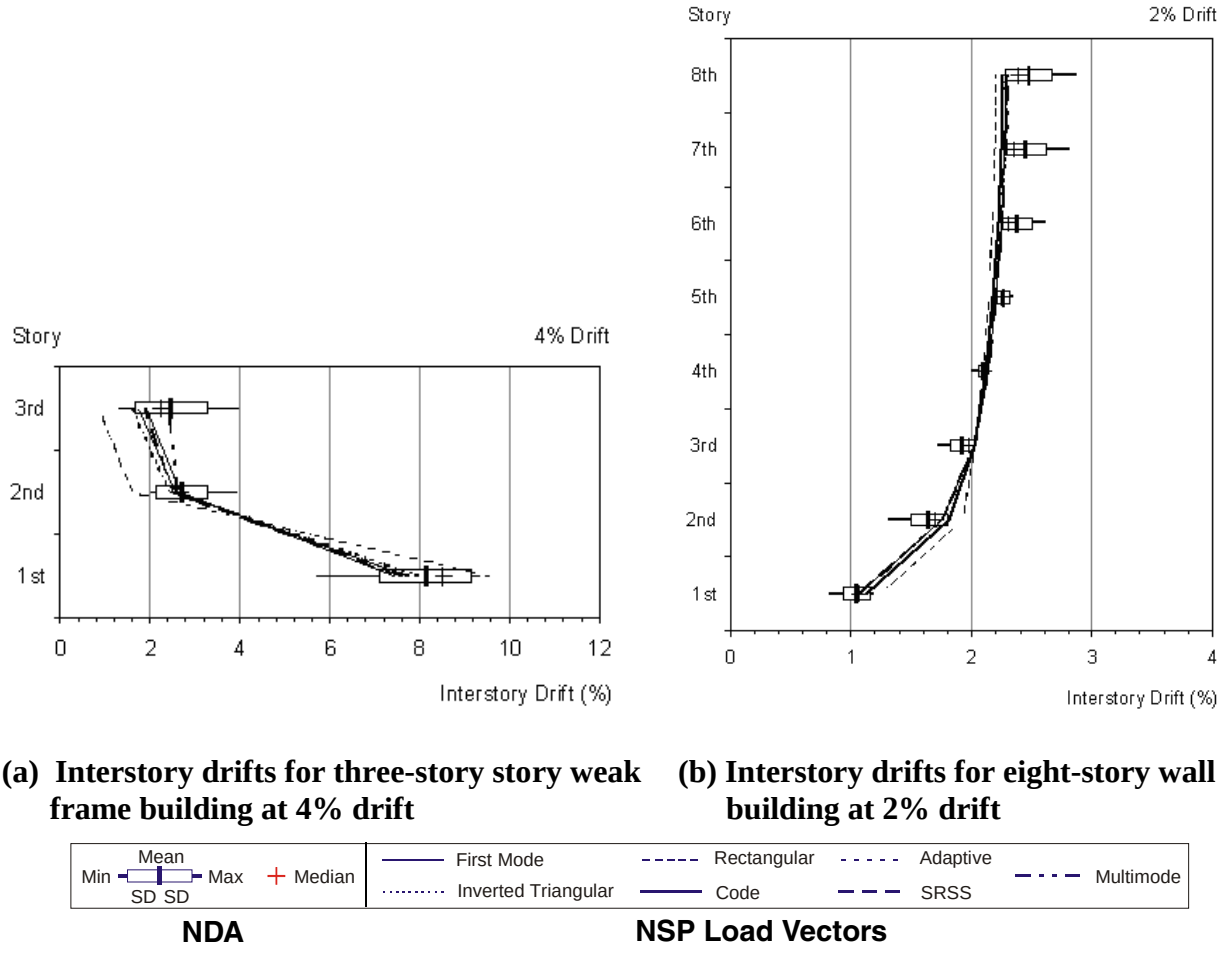

(a) Interstory drifts for three-story story weak frame building at 4% drift

(b) Interstory drifts for eight-story wall building at 2% drift

Figure 9-3 Relatively good results for interstory drift predicted using nonlinear static procedures (NSP), as compared to nonlinear dynamic response-history analyses (NDA).

limited in the capability to predict drift accurately over the full height of relatively tall, flexible MDOF structures. In contrast, interstory drift over the height of the three-story frames and eight-story shear wall example buildings were estimated well. Nonlinear static procedures that combine contributions from independent modal analyses appear to be poor predictors of story shear and overturning moment. These observations are consistent with the results of a number of other research efforts (Seneviratna and Krawinkler, 1994; Krawinkler and Seneviratna, 1998; Kunnath and Gupta, 2000; Lew and Kunnath, 2000; Yu et al., 2001; Chopra and Goel, 2001b; Gupta and Krawinkler, 2003; Goel and Chopra, 2004; and Jan et al., 2004). This situation raises a number of questions with regard to the practical application of NSPs in cases in which MDOF effects are important. First, is there any preference for any one load vector over the others? Second, when should results of NSPs not be relied upon for MDOF effects? Finally, what should be done now and in the future?

9.4.1 Single Load Vectors

The first-mode load vector is recommended because of the low error obtained for displacement estimates made with this assumption and to maintain consistency with the derivations of equivalent SDOF systems. The code distribution and the triangular vectors may be used as alternatives, typically with little increase in error.

Mean and maximum errors were sometimes smaller and sometimes larger using the adaptive load vector. The adaptive method requires more computational effort and fails for systems exhibiting a negative tangent stiffness.

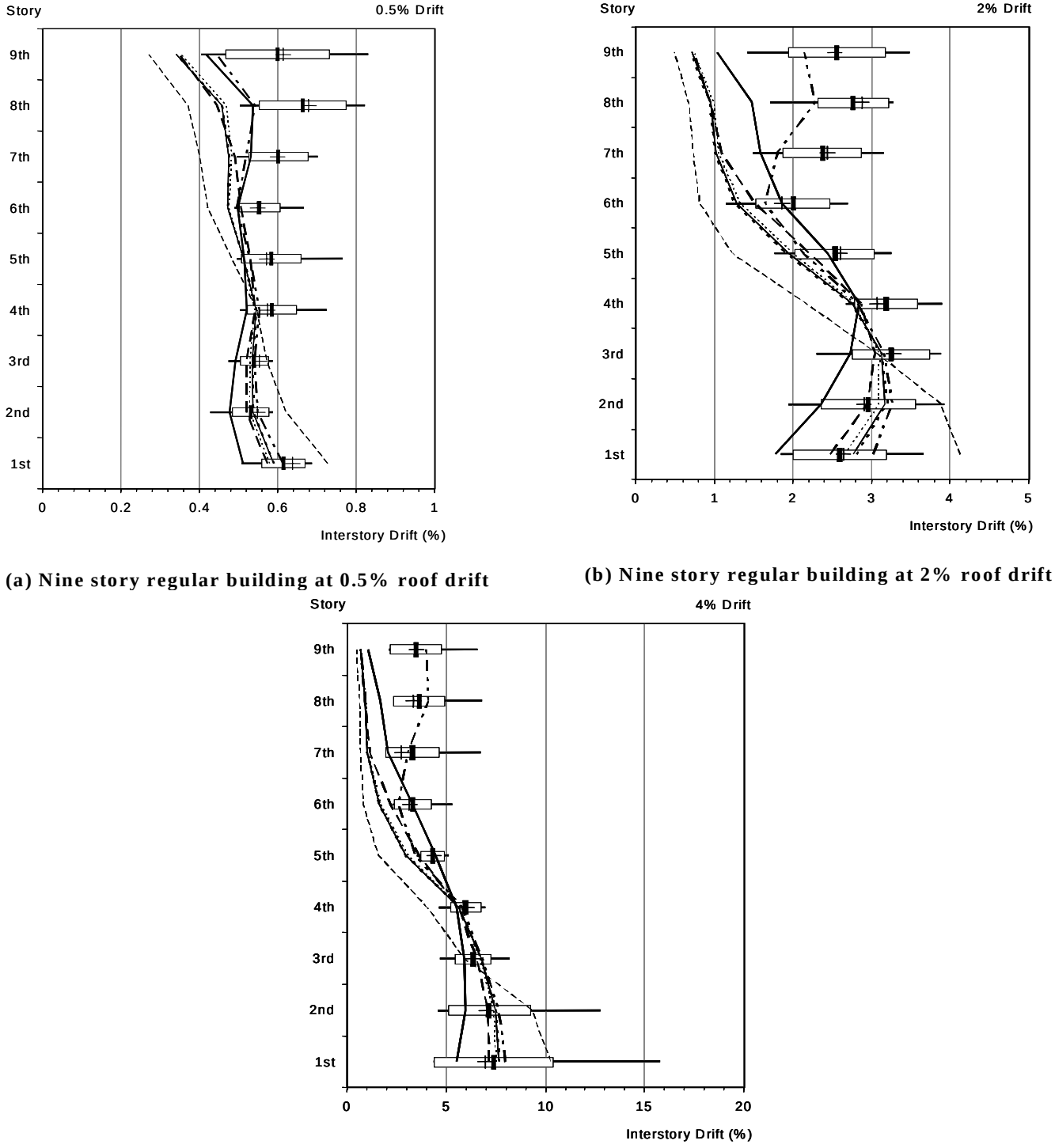

(a) Nine story regular building at 0.5% roof drift

(b) Nine story regular building at 2% roof drift

(c) Nine story regular building at 4% roof drift

Figure 9-4 Relatively poor results for interstory drift predicted using nonlinear static procedures (NSP) compared to nonlinear dynamic response-history analyses (NDA).

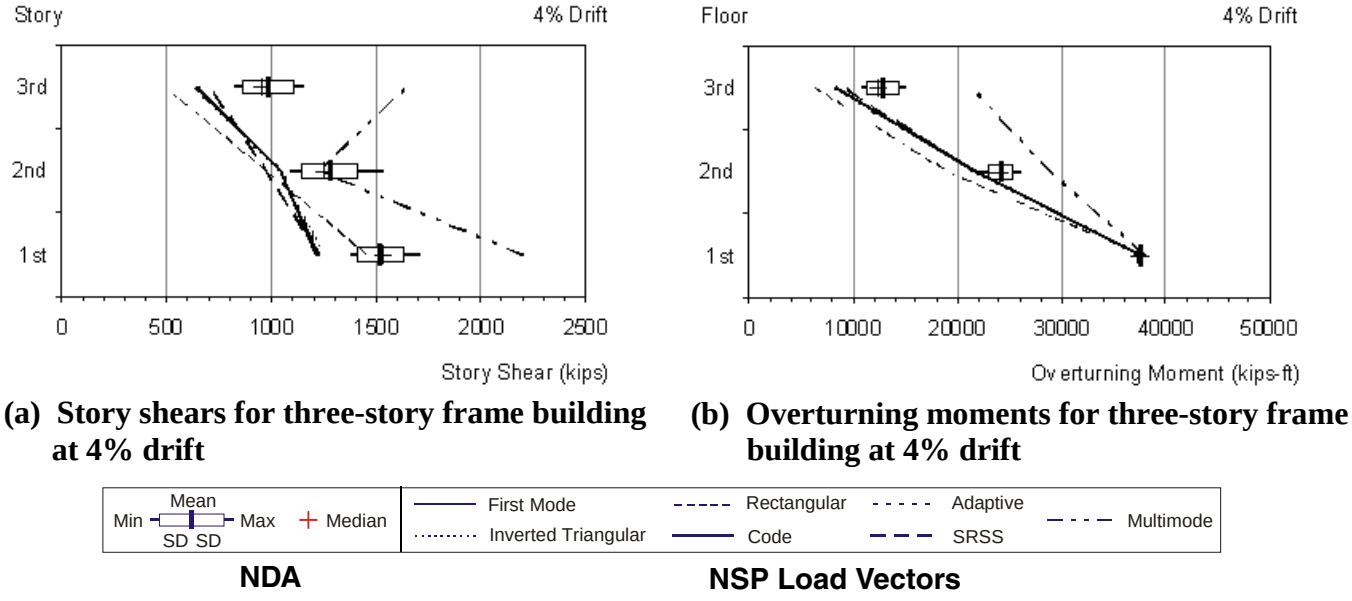

(a) Story shears for three-story frame building at 4% drift

(b) Overturning moments for three-story frame building at 4% drift

Figure 9-5 Story forces and overturning moments in the example three-story frame building when different load vectors are used.

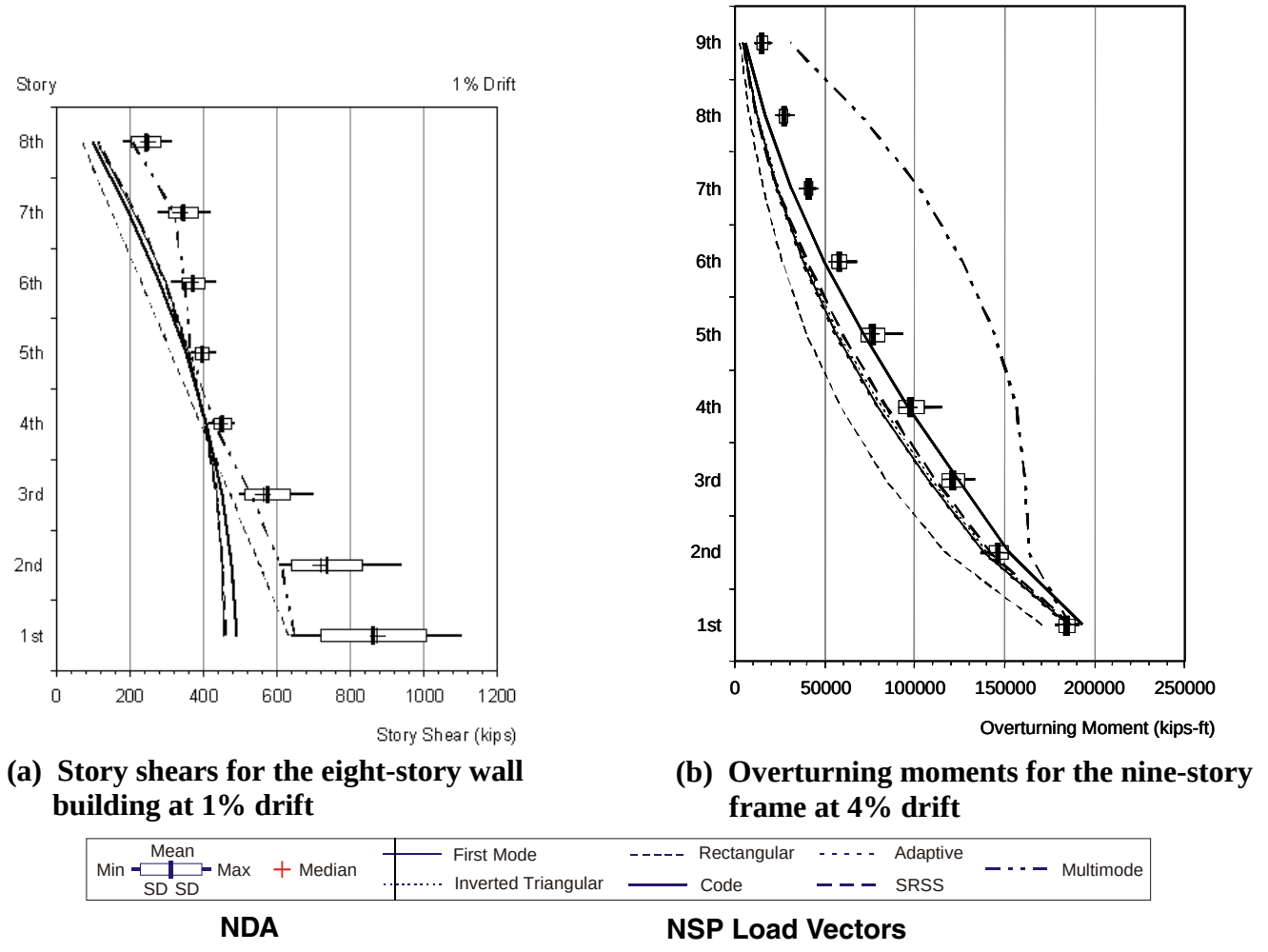

(a) Story shears for the eight-story wall building at 1% drift

(b) Overturning moments for the nine-story frame at 4% drift

Figure 9-6 Story forces and overturning moments in eight-story wall and nine-story frame example buildings, using various load vectors.

The SRSS load vector led to small improvements in story shear and overturning moment for the example frames, had minor and mixed effects for interstory drift, and sometimes was worse for estimates of displacement, when compared to the first-mode load vector. It requires greater computational effort for inconsistent improvements.

The uniform load vector led to notably worse errors for all four response quantities in the example buildings, relative to the first-mode load vector. Thus, it is not recommended as a stand-alone option. Although the use of the uniform load vector in conjunction with another vector as a bounding function (e.g., in the case of a shear wall building to ensure flexurally controlled behavior) is appealing, peak response quantities often exceeded the estimates made with the uniform vector.

The use of multiple load vectors in FEMA 356 implies unwarranted accuracy and does not provide reliable results. A single first-mode vector is sufficient for displacement estimates and for the estimate of response quantities that are not significantly affected by higher modes.

9.4.2 Multi-Mode Pushover Analysis

It is apparent and logical that the use of multiple mode pushover techniques (MPA) should produce generally better estimates of interstory drift than single load vectors. Although higher modes typically contribute little to displacement, multiple mode pushover analyses may be useful for identifying cases in which displacement responses are dominated by a higher mode.

The application of the multi-mode pushover analysis (MPA) procedure in the ATC-55 project was encumbered by the reversals observed in two of the higher-mode pushover curves. Seeking a single approach capable of representing higher-mode contributions, a modified MPA procedure was introduced in these studies. Although often improved over the single-mode vectors, estimates of interstory drift over the full height of buildings made with the modified MPA procedure may not be consistently reliable. However, it is important to note that researchers are devoting significant effort to the further development of MPA procedures. Some of these are briefly described below.

- Chopra and Goel (2001b) found the original MPA provided good estimates of floor displacement and story drift, but did not estimate plastic hinge rotations with acceptable accuracy for a nine-story steel moment-frame building.
- Chintanapakdee and Chopra (2003) applied the MPA procedure to estimate interstory drift for so-called "generic" frames having 3, 6, 9, 12, 15, and 18 stories. They found that the accuracy of interstory drift estimates depend on the story level and degree of inelasticity. Accuracy was best for shorter buildings and for the lower and middle stories of taller buildings. For the upper stories of tall frames, the MPA procedure was not able to provide a reasonable estimate of interstory drift for many ground motions. The procedure was not used to determine shear, bending moment, axial force, or component deformation.
- Yu et al. (2002) applied the original MPA and two modified versions of MPA to estimate the interstory drift and plastic hinge rotation for an instrumented 13-story steel frame building. When target displacements were estimated by applying the displacement Coefficient Method to the median elastic response spectrum, the MPA method tended to underestimate story drifts in the upper stories and to overestimate drifts in the lower stories; beam and column plastic hinge rotations were often overestimated, while panel zone deformations were estimated reasonably well.
- Chopra et al. (2004) compared interstory drift estimates obtained using the original and modified MPA methods for a set of "generic" frames and SAC frames and found the modified MPA method is an attractive alternative to the original MPA, because it leads to a larger estimate of seismic demand, thereby improving the accuracy of the MPA results in some cases and increasing their conservatism in others.
- Goel and Chopra (2004) describe an "improved" version of the MPA, which considers P-Δ effects in all modes considered and which adds a specialized step for estimating plastic hinge rotation on the basis of the estimated interstory drift and an assumed inelastic mechanism. The "improved" MPA procedure, although better than single-mode estimates, is found to lack accuracy for estimating plastic hinge rotation, overestimating the rotation in the lower stories and underestimating it in the upper stories of the 9- and 20-story moment-resisting frames that were studied.
- Jan et al. (2004) propose an alternative technique in which potentially inelastic contributions from the first two modal pushover analyses are added together. Estimates of displacement, interstory drift,

and plastic hinge rotation were compared with those made using a triangular load profile and the original MPA procedure for a set of 2-, 5-, 10-, 20-, and 30-story moment-resisting frames. The triangular load profile and the original MPA produced very good estimates of interstory drift for the 2- and 5-story frames. The proposed technique provided better estimates of interstory drift for the 20- and 30-story frames, and it was the only technique of those considered it that could provide reasonable estimates of the location and severity of plastic hinge rotations in these frames.

- Hernández-Montes et al. (2004) developed an energy-based pushover technique that overcomes the problems observed with reversals of the higher-mode pushover curves that were observed in the application of the original MPA procedure in the ATC-55 studies.

The MPA procedures seem to produce results that are somewhat more reliable than those obtained from single load vectors. However, it is readily apparent from the literature that the adequacy of these results depends upon the parameter of interest (e.g., drift, plastic hinge rotation, force), the characteristics of the structure, and the details of the specific procedure. It is also possible that future development of the basic MPA procedure may improve predictions further. If these improvements can be realized with transparent and computationally efficient procedures, then they may very well be worthwhile. On the other hand, MPA procedures are fundamentally limited, as are NSPs more generally. From a broader perspective, it is important to develop practical versions of nonlinear dynamic response-history analyses of detailed and, perhaps, simplified MDOF models.

Until other practical nonlinear alternatives are available, the recommendation is that experienced practitioners, who interpret results with an appropriate degree of caution, can utilize MPA procedures for comparison with, and possible improvement over, the static load vector procedures.

9.4.3 Roof Displacement Estimation

The results for the estimate of maximum global displacement of the example building models are consistent with the results of other studies (e.g., Miranda, 1991; Collins et al., 1995; Seneviratna and Krawinkler, 1997; Cuesta and Aschheim, 2001; Chopra et al., 2003). The ATC-40 formulation for the yield strength coefficient of an equivalent SDOF (Equation 9-3) is recommended, because it resulted in smaller dispersions, accurately reflected the frequency content of the excitation for elastic response, and maintains consistency with derivations of "equivalent" SDOF systems. Where the hazard is described by smoothed elastic design spectra, displacement estimates should make use of the improved procedures that are described in Chapters 5 and 6.

9.4.4 Limitation of Simplified Procedures

Nonlinear static pushover procedures appear to be reliable for the design and evaluation of low-rise buildings. However, MDOF effects associated with the presence of significant higher-mode response in relatively tall frame buildings, can cause interstory drift, story shear, overturning moment, and other response quantities to deviate significantly from estimates made on the basis of single-mode pushover analyses. Multi-mode pushover procedures appear capable of more reliable estimates than do single-mode procedures; however, they cannot be deemed completely reliable based on currently available data. The dividing line between buildings for which reliable results can be obtained using NSPs and those for which the results cannot be relied upon is nebulous. The sufficiency of nonlinear static procedures and the need for nonlinear dynamic analysis depend on a number of related considerations.

- *Response quantity of interest.* As illustrated in the examples, current simplified procedures are often adequate for estimating displacements. They seem to produce reasonable estimates of interstory drift for low-rise frame buildings and wall buildings. However, for virtually all cases, the simplified procedures produce unreliable estimates of story shear and overturning moments. If required for evaluation or design, accurate estimates of these parameters require more detailed analyses.
- *Degree of inelasticity.* The example buildings indicate that the importance of MDOF effects increases with the amount of inelasticity in the structure. NSPs may be adequate for situations in which the performance goals for a structure are such that only slight or moderate levels of inelasticity are expected.
- *Periods of vibration of the fundamental and higher modes relative to the spectral demands at these periods.* Higher-mode contributions become more significant for structures with fundamental periods that fall in the constant-velocity portion of the response spectrum. It appears that accurate estimates of the distribution of interstory drift over the height of moment-resisting frames cannot be obtained with

NSPs alone when the fundamental period of the structure exceeds approximately twice the characteristic site period, T_S. A significantly lower limit applies to the determination of story forces in both wall and frame structures, however.

- *Structural system type.* Shear walls and frames have different higher-mode periods relative to their fundamental modal periods. These systems have characteristically different percentages of mass participating in the first and higher modes and develop characteristically different types of mechanisms. As noted previously, NSPs do not predict story forces reliably, and more sophisticated analytical techniques may be required for systems sensitive to these parameters.
- *Post-elastic strength.* Both the studies on the response of SDOF oscillators (Chapter 3) and the SDOF examples (Appendix F) demonstrate that systems with a critical level of negative post-elastic strength degradation are prone to dynamic instability. This has been documented in other recent research as well. As discussed in Chapter 4, the critical post-elastic stiffness should be based on P-Δ effects and other types of in-cycle degradation. Systems with strength values less than those specified in Chapter 4 require nonlinear response-history analysis.
- *Inelastic mechanism*. Forces associated with response in other modes may influence the development of an inelastic mechanism, and thus, pushover analyses may not always identify the governing mechanism (Krawinkler and Seneviratna, 1998).
- *Multi-mode pushover analysis procedures.* SRSS combinations of force quantities can exaggerate the effects of gravity loads and can exceed the limits associated with the development of an inelastic mechanism. Typically, algebraic signs of the modes can be expected to influence the intensity of component demands. The use of uniform hazard spectra presents inconsistencies, because different portions of the spectrum may be driven by vastly different events, rather than representing a single event.
- *FEMA 356 provisions.* This document requires supplementary linear dynamic analysis if higher-mode effects are significant. Higher modes are considered significant if the SRSS of story shears from modes that incorporate at least 90% of the mass exceeds 130% of story shear from a first-mode response-spectrum analysis. It is important to note that all the example buildings, with the minor exception of the upper floor of the 9-story frame, would have qualified for the nonlinear static procedure alone without the linear dynamic procedure (LDP) for a NEHRP design spectrum in an area of high seismicity and Site Class C site conditions. The potential for the NSP to significantly underestimate response quantities for structures that satisfy this limitation indicates that the current limitation is not adequate.

9.5 Potential Future Improvements

Based on the studies conducted in conjunction with this document and results from current research, it is apparent that there is a need for improved inelastic analysis techniques that can be used to reliably address MDOF effects. As noted previously, research on multi-mode pushover analysis procedures is ongoing. There are two examples of potential improvements that have not been discussed earlier and that warrant mention here.

9.5.1 Incremental Response-Spectrum Analysis

Aydinoglu (2003) describes a multi-modal incremental response-spectrum analysis method, in which contributions of multiple modes are considered in an incremental pushover analysis. The incremental nature of the analysis allows the effects of softening due to inelasticity in one mode to be reflected in the properties of the other modes. An example was used to illustrate application of the method to a generic frame model of the nine-story SAC building (neglecting gravity loads and P-Δ effects), comparing estimates based on four modes with those determined by nonlinear dynamic analysis. Very good agreement is shown for floor displacement, interstory drift, story shear, floor overturning moment, and beam plastic hinge rotation. Further study is required to establish the generality of the findings and potential limitations of the approach.

9.5.2 Nonlinear Dynamic Procedure Using Scaled Response Histories

The MDOF example studies summarized in Section 9.3 revealed that the estimates of response quantities obtained by nonlinear static pushover analyses often were less accurate than the results obtained by any single nonlinear dynamic analysis when comparing both to the mean results for all ground motions. This observation suggests the possibility of an analytical procedure in which response quantities are determined by nonlinear dynamic analysis using ground motion records that are scaled so that the peak roof

displacement matches a predetermined target displacement. In effect, the seismic hazard would be characterized by the maximum inelastic displacement at the roof level. This displacement could be estimated for a structure using nonlinear static procedures in conjunction with the NEHRP maps, for example. Thus, nonlinear response-history analyses would be used to investigate MDOF effects through nonlinear dynamic analyses using a relatively small number of ground motion records scaled to give the same roof displacement. Such a procedure could avoid both the necessity of generating a series of spectrum-compatible records and the difficulty of combining the results of the analyses for practical use. This potential method, termed the "Scaled NDP" method, is summarized here, with supporting information provided in Appendix F

The basic suggested procedure is outlined below.

Step 1. Given a spectrum representative of the site hazard of interest, estimate the peak displacement of the roof (or more generally, a "control point") using the displacement modification or equivalent linearization procedures, described in Chapters 5 and 6, respectively.

Step 2. Select n ground motion records that reflect the characteristics of the hazard (e.g., magnitude, distance, and site class) and for each record, conduct a nonlinear dynamic analysis, with the record scaled iteratively until the peak displacement of the control point is equal to the estimate determined in Step 1. Extract peak values of the response quantities of interest from the results of each analysis and compute the sample mean, $\overline{x_n}$, of each peak quantity of interest. At least three analyses ($n \geq 3$) are suggested.

Step 3. Although the sample mean is the best estimate of the true mean, sampling error may be present. Furthermore, estimates of some response quantities may be desired at the mean plus κ standard deviation level. Thus, the sample mean could be multiplied by a coefficient that depends on the coefficient of variation of the sample, in order to estimate a response quantity at the mean plus κ standard deviation level with a desired level of confidence. A derivation of such a coefficient is provided in Appendix F

Discussion

The proposed analysis method retains the benefits of the pushover method, in that the engineer can use the pushover to quickly identify the likely nonlinear mechanism of the system and the expected peak displacement response. The method makes use of currently available spectral descriptions of seismic hazard as well as the improvements described in Chapters 5 and 6 of this document. The dynamic analyses indicate the variability in response quantities associated with the randomness in the higher mode amplitudes and timing relative to the first mode. In effect, the static load vector of traditional pushover analysis, used to determine the peak of global displacement demand, is augmented by a dynamic load, represented by the scaled ground motion record.

Within the limitations of the nonlinear model, each analysis faithfully represents the influence of higher modes on response quantities such as interstory drift, story shear, and overturning moment, and does so in a manner that accounts for capacity limits on force and moment quantities. Any single dynamic analysis is a valid representation of actual response of the model, and each analysis helps to establish the central tendency and range of peak response quantities.

Refinements and improvements may potentially be made in the areas of (1) characterizing and selecting site-specific ground motions, (2) determining the confidence levels and numbers of standard deviations above the mean that should be used in the estimation of various response quantities, and (3) improvement of the precision of the NSP estimates of peak roof displacement. The conservatism of current pushover techniques, in their tendency to overestimate the peak roof displacements of structures responding inelastically, may provide a desirable level of conservatism to the method at this stage in its development.